

STRUCTURAL OPTIMIZATION OF A TRAINER AIRCRAFT WING
BY USING GENETIC ALGORITHM

MUSTAFA KAĞAN ÇAKIR

SEPTEMBER 2008

STRUCTURAL OPTIMIZATION OF A TRAINER AIRCRAFT WING
BY USING GENETIC ALGORITHM

A THESIS SUBMITTED TO
THE GRADUATE SCHOOL OF NATURAL AND APPLIED SCIENCES
OF
MIDDLE EAST TECHNICAL UNIVERSITY

BY

MUSTAFA KAĞAN ÇAKIR

IN PARTIAL FULFILLMENT OF THE REQUIREMENTS
FOR
THE DEGREE OF MASTER OF SCIENCE
IN
MECHANICAL ENGINEERING

SEPTEMBER 2008

Approval of the Thesis:

**STRUCTURAL OPTIMIZATION OF A TRAINER AIRCRAFT WING BY
USING GENETIC ALGORITHM**

submitted by **MUSTAFA KAĞAN ÇAKIR** in partial fulfillment of the requirements
for the degree of **Master of Science in Mechanical Engineering, Middle East
Technical University** by,

Prof. Dr. Canan Özgen

Dean, Graduate School of **Natural and Applied Sciences**

Prof Dr. Kemal İder

Head of department, **Mechanical Engineering**

Prof. Dr. Eres Söylemez

Supervisor, **Mechanical Engineering Dept., METU**

Examining Committee Members:

Prof. Dr. Haluk Darendeliler (*)

Mechanical Engineering Dept., METU

Prof. Dr. Eres Söylemez (**)

Mechanical Engineering Dept., METU

Prof. Dr. Suat Kadioğlu

Mechanical Engineering Dept., METU

Prof. Dr. Yavuz Yaman

Aerospace Engineering Dept., METU

Dr. Gürsel Erarslanoğlu

Structural Technologies Manager, TAI

Date: 01/09/2008

* Head of the examining committee

** Thesis supervisor

I hereby declare that all information in this document has been obtained and presented in accordance with academic rules and ethical conduct. I also declare that, as required by these rules and conduct, I have fully cited and referenced all material and results that are not original to this work.

Name, Last Name: Mustafa Kağan ÇAKIR

Signature :

ABSTRACT

STRUCTURAL OPTIMIZATION OF A TRAINER AIRCRAFT WING BY USING GENETIC ALGORITHM

Çakır, Mustafa Kağan

M.Sc., Department of Mechanical Engineering

Supervisor: Prof. Dr. Eres Söylemez

September 2008, 148 Pages

In this study, a design procedure incorporating a genetic algorithm (GA) is developed for optimization of the wing structure of a two seated trainer aircraft with single turboprop engine. The objective function considered is the total weight of the structure. The objective function is minimized subjected to certain strength requirements. In order to evaluate the design constraints and model the wing structure, finite element analysis is performed by using a conventional finite element solver (i.e. MSC/NASTRAN[®]). In addition, MSC/PATRAN[®] commercial package program is used as preprocessor and postprocessor tool. VISUAL FORTRAN programming language is also utilized as the genetic algorithm implementation tool. Several conclusions drawn from the optimization results are presented.

Keywords: Genetic Algorithm, Structural Optimization, Aircraft Wing, Finite Element Modeling.

ÖZ

BİR EĞİTİM UÇAĞI KANADININ GENETİK ALGORİTMA KULLANILARAK YAPISAL OPTİMİZASYONU

Çakır, Mustafa Kağan

Yüksek Lisans, Makina Mühendisliği Bölümü

Tez Yöneticisi: Prof. Dr. Eres Söylemez

Eylül 2008, 148 Sayfa

Bu çalışmada, turboprop motora sahip, iki kişilik bir eğitim uçağının kanat yapısı, genetik algoritma (GA) içeren bir tasarım prosedürü ile optimize edilmiştir. Optimizasyon probleminde esas alınan hedef fonksiyon yapının toplam ağırlığıdır. Hedef fonksiyon çeşitli mukavemet gereksinimleri dikkate alınarak minimize edilmiştir. Tasarım koşullarını çözebilmek için MSC/NASTRAN[®] paket program olarak kullanılmıştır. Uçak kanadının sonlu elemanlar modelini hazırlayabilmek ve sonuçları gözlemleyebilmek için ön işlemci ve son işlemci program olarak MSC/PATRAN[®] ticari paket programı, genetik algoritma uygulaması için ise VISUAL FORTRAN programlama dili kullanılmıştır. Araştırma sonuçlarından çıkarılan bir çok yargı çalışmada sunulmuştur.

Anahtar kelimeler: Genetik Algoritma, Yapısal Optimizasyon, Uçak Kanadı Sonlu Elemanlar Metodu.

To my family

ACKNOWLEDGEMENTS

I would like to express my sincere appreciation to my supervisor Prof. Dr. Eres Söylemez for his guidance and support throughout this thesis study. I consider myself fortunate to have a mentor with the strong work ethic, unyielding patience and tolerance of Prof. Dr. Eres Söylemez.

I would also like to thank to my colleagues Evren Taşkınođlu, Kerem Adıgüzel and Barıř Gider for their technical support. I would also like to thank to Dr. Gürsel Erarslanođlu and Aylin Ararat for their understanding and tolerance.

TABLE OF CONTENTS

| | |
|--|------|
| ABSTRACT..... | iv |
| ÖZ..... | v |
| ACKNOWLEDGEMENTS..... | vii |
| TABLE OF CONTENTS..... | viii |
| LIST OF FIGURES..... | xiii |
| ABBREVIATIONS..... | xix |
| CHAPTERS | |
| 1. INTRODUCTION..... | 1 |
| 1.1 Objective and Scope of the Study..... | 1 |
| 1.2 Literature survey..... | 2 |
| 2. OPTIMIZATION & GENETIC ALGORITHM..... | 6 |
| 2.1 Objective function..... | 7 |
| 2.2 Design variables..... | 8 |
| 2.3 Design constraints..... | 9 |
| 2.4 Classification of optimization problems..... | 10 |
| 2.5 Genetic Algorithm..... | 11 |
| 2.5.1 Genetic algorithm description..... | 11 |
| 2.5.2 Basic structure of genetic algorithm..... | 12 |

| | |
|---|----|
| 2.5.3 Chromosome encoding | 14 |
| 2.5.4 Fitness evaluation..... | 15 |
| 2.5.5 Selection..... | 16 |
| 2.5.6 Crossover and mutation | 18 |
| 2.5.7 Termination criteria | 21 |
| 2.5.8 GA Implimentation | 21 |
| 3. WING DESIGN..... | 23 |
| 3.1 Typical Airplane Wing Box Design Considerations | 23 |
| 3.2 Brief Summary of Wing Loads..... | 27 |
| 3.2.1 General | 27 |
| 3.2.2 Spar conditions..... | 28 |
| 3.2.3 Rib conditions | 28 |
| 3.2.4 Leading edge conditions | 28 |
| 3.2.5 Trailing edge and fairing load conditions | 29 |
| 3.3 Wing Box Design..... | 29 |
| 3.4 Wing Covers | 33 |
| 3.5 Skin-Stringer Panels..... | 38 |
| 3.6 Spars..... | 40 |
| 3.7 Ribs and Bulkheads..... | 44 |
| 3.7.1 Rib Spacing | 48 |
| 4. CASE STUDY | 50 |
| 4.1 Problem definition..... | 50 |
| 4.2 Wing Structural Members..... | 51 |

| | |
|---|-----|
| 4.3 Systems Located in the Wing | 55 |
| 4.3.1 Fuel System..... | 56 |
| 4.3.2 Landing Gear System..... | 57 |
| 4.3.3 Flight control system..... | 58 |
| 4.4 Wing Finite Element Modeling | 59 |
| 4.5 Parametrization of Wing Structure | 65 |
| 4.3 Stress and Instability Analyses for Structural Members..... | 71 |
| 4.3.1 Instability Analyses for Spar Webs..... | 73 |
| 4.3.2 Instability Analyses for Upper Skin..... | 76 |
| 4.3.3 Instability Analyses for Rib Webs | 79 |
| 4.3.4 Instability Analyses for Stringers and Spar Caps on the Upper Skin | 81 |
| 4.3.5 Stress Analyses for Stringers and Spar Caps on the Lower Skin | 85 |
| 4.3.5 Stress Analyses for Lower Skin..... | 86 |
| 4.3.6 Reserve Factors of Wing Elements..... | 87 |
| 4.4 Interrelation of Genetic Algorithm and FEM Tools | 89 |
| 5. DISCUSSION & CONCLUSION | 100 |
| REFERENCES | 104 |
| APPENDICES | |
| A. MODELING TOOLS USED IN THE STUDY..... | 107 |
| A.1 Introduction | 107 |
| A.2 MSC/PATRAN [®] and MSC/NASTRAN [®] Package Programs | 107 |
| A.3 Structural Elements Used in the Study | 109 |

| | |
|--|-----|
| A.3.1 1-D Elements..... | 109 |
| A.3.2 2-D Elements..... | 111 |
| A.3.3 0-D Elements..... | 114 |
| B. STRUCTURAL ANALYSIS CRITERIA FOR INSTABILITY..... | 115 |
| B.1 Column Buckling | 115 |
| B.1.1 Euler Equation..... | 118 |
| B.2 Buckling of Thin Sheets..... | 127 |
| B.2.1 Loading and Edge Conditions | 133 |
| B.2 Buckling of Flat Plates | 135 |
| B.2.1 Compression Load..... | 135 |
| B.2.2 Shear Load..... | 138 |
| B.2.3 Bending Load | 139 |
| B.2.4 Combined Loadings | 140 |
| B.3 Wing External & Inertial Loads..... | 143 |
| B.3.1 Wing Design Loads | 145 |
| C. FLOW CHARTS..... | 148 |

LIST OF TABLES

TABLES

| | |
|--|-----|
| Table 4.1 - Table of optimization design variables | 66 |
| Table 4.2 - Data sets for design parameters..... | 70 |
| Table 4.3 - Final values of the parameters in optimized model..... | 92 |
| Table B.1 - Column End-Fixity Coefficients..... | 120 |
| Table B.2 - Interaction equations for shear, compression and bending loads | 142 |
| | 142 |

LIST OF FIGURES

FIGURES

| | |
|--|----|
| Figure 1.1 - Wing box structure of the turboprop aircraft | 2 |
| Figure 2.1 - Outline of a basic genetic algorithm | 13 |
| Figure 2.2 - A binary encoded chromosome..... | 14 |
| Figure 2.3 - Roulette Wheel..... | 17 |
| Figure 2.4 - One-Point Crossover | 19 |
| Figure 2.5 - Two-Point Crossover | 19 |
| Figure 2.6 - Uniform Crossover..... | 20 |
| Figure 2.7 - Mutation | 20 |
| Figure 3.1 - Typical Transport and fighter wing | 24 |
| Figure 3.2 - Comparison of rib direction (rectangular box) | 30 |
| Figure 3.3 - Wing plan view layout of a transport..... | 31 |
| Figure 3.4 - Preliminary view of spars and wing maximum thicknesses of a transport | 32 |
| Figure 3.5 - Three spar wing-all bending materials concentrated at the spar cap | 33 |
| Figure 3.6 - Multi-spar skin bending material | 34 |
| Figure 3.7 - Typical wing torque box enclosed area..... | 35 |
| Figure 3.8 - Critical wing cover axial loads at wing surfaces | 36 |
| Figure 3.9 - The wing panel affected by eccentricity | 37 |

| | |
|---|----|
| Figure 3.10 - Typical wing skin-stringer panels | 39 |
| Figure 3.11 - Typical spar cap sections | 41 |
| Figure 3.12 - Typical spar cap construction | 41 |
| Figure 3.13 - Typical spar configurations..... | 42 |
| Figure 3.14 - Sloping spars relieve the spar web shear load..... | 44 |
| Figure 3.16 - Typical rib construction | 45 |
| Figure 3.17 - Wing crushing load | 47 |
| Figure 3.18 - Determination of rib spacing by structural weight comparison.. | 49 |
| Figure 4.1 - Wing structural members and control devices..... | 50 |
| Figure 4.2 - Wing root section and spar locations | 51 |
| Figure 4.3 - Wing tip cross section | 52 |
| Figure 4.4 - Wing plan view | 52 |
| Figure 4.5 - Wing spars & dimensions | 53 |
| Figure 4.6 - Spar locations and initial rib spacing | 54 |
| Figure 4.7 - (a) Typical Z-bulb stringer cross-section and dimensions..... | 55 |
| (b) Stringer locations..... | 55 |
| Figure 4.8 - Fuel in the fuel tank is distributed to 13 cells formed by spar webs and ribs..... | 56 |
| Figure 4.9 - Main Landing Gear Installation on Wing. Main landing gear is installed on the 5th rib of the wing | 57 |
| Figure 4.10 - Flight control system (FCS) installation on wing. | 58 |
| Figure 4.11 - Complete wing FE model and element numbering..... | 60 |
| Figure 4.12 - Introducing the inertia effects of the fuel in the integral fuel tank | 61 |

| | |
|---|----|
| Figure 4.13 - FE model of wing spars | 61 |
| Figure 4.14 - FE model of ribs and stringers | 62 |
| Figure 4.15 - Static boundary conditions on wing root section..... | 63 |
| Figure 4.16 - Load distributions on the lower surface of wing FEM model in +7g load case..... | 64 |
| Figure 4.17 - Stringer geometric dimensions..... | 68 |
| Figure 4.18 - Spar cap geometric dimensions..... | 68 |
| Figure 4.19 - Rib reference planes (wing top view) | 69 |
| Figure 4.20 - Rib spacings shown in 3D model..... | 69 |
| Figure 4.21 - Nodes and centroid of the CQUAD #1 (i.e. front spar web first element)..... | 73 |
| Figure 4.22 - Stress state of spar web element in the wing structure | 74 |
| Figure 4.23 - Element forces of front spar first element..... | 75 |
| Figure 4.24 - Nodes and centroid of the CQUAD #299 | 76 |
| Figure 4.25 - Stress state of upper skin elements in the wing structure | 77 |
| Figure 4.26 - Element forces of upper skin element (CQUAD #299)..... | 78 |
| Figure 4.27 - Upper skin CQUAD element orientation..... | 79 |
| Figure 4.28 - Loading on the first rib element..... | 80 |
| Figure 4.29 - Element forces of rib element (CQUAD #52) | 81 |
| Figure 4.30 - Effective width of a skin stringer panel | 83 |
| Figure 4.31 - Beam section constituting of stringer and effective skin..... | 83 |
| Figure 4.32 - Loads on stringer (CBAR #550) and adjacent skin panels | 84 |
| Figure 4.33 - Primary loads on a stringer on the lower skin is axial tensile force and bending moment..... | 85 |

| | |
|--|----|
| Figure 4.34 - Element forces on CBAR #650..... | 86 |
| Figure 4.35 - Upper skin RF Map calculated according to combined shear and compression loading | 87 |
| Figure 4.36 - Wing lower skin RF map calculated according to maximum stress..... | 87 |
| Figure 4.37 - Wing upper stringer and spar cap RF Map calculated according to axial compression loading | 88 |
| Figure 4.38 - Wing lower stringer and spar cap RF Map calculated according to maximum stress | 88 |
| Figure 4.39 - Rib webs RF Map calculated according to combined in plane shear and axial compression load | 88 |
| Figure 4.40 - Spar webs RF Map calculated according to combined in plane shear and bending load..... | 89 |
| Figure 4.41 - Mass(kg) x C1 vs. generation number graph for optimization ... | 90 |
| Figure 4.42 - Comparison of initial rib planes and final rib planes..... | 91 |
| Figure 4.43 - Refined mesh of the wing according to optimization results..... | 93 |
| Figure 4.44 - Upper skin fine mesh | 93 |
| Figure 4.45 - Ribs and spars FEM model | 94 |
| Figure 4.46 - Von Mises stress distribution of upper skin in optimized model | 95 |
| Figure 4.47 - Von Mises stress distribution of upper skin in initial model | 95 |
| Figure 4.48 - Von Mises stress distribution of lower skin in initial model | 96 |
| Figure 4.49 - Von Mises stress distribution of lower skin in optimized model | 96 |
| Figure 4.50 - Von Mises stress distribution at a section cutting wing structure spanwise looking up in optimized model | 97 |

| | |
|---|-----|
| Figure 4.51 - Von Mises stress distribution at a section cutting wing structure spanwise looking up in initial model | 97 |
| Figure 4.52 - Von Mises stress distribution at a section cutting wing structure chordwise near main spar plane looking forward in initial model | 98 |
| Figure 4.53 - Von Mises stress distribution at a section cutting wing structure chordwise near main spar plane looking forward in optimized model | 98 |
| Figure 4.54 - Von Mises stress distribution at a section cutting wing structure spanwise looking down in initial model | 99 |
| Figure 4.55 - Von Mises stress distribution at a section cutting wing structure spanwise looking down in initial model | 99 |
| Figure 5.1 - An aircraft fuselage skin milled by ECM process | 103 |
| Figure A.1 - The basic MSC/NASTRAN [®] elements..... | 109 |
| Figure A.2 - Demonstration of Beam Orientation | 110 |
| Figure A.3 - CBAR Element Forces | 110 |
| Figure A.4 - QUAD4 element geometry and element coordinate system..... | 112 |
| Figure A.5 - Forces, Moments, and Stresses in Plate Elements | 113 |
| Figure B.1 - Perfect vs. Imperfect Structures of an Column | 116 |
| Figure B.2 - Deflection vs. Load | 121 |
| Figure B.3 - Flange Crippling..... | 122 |
| Figure B.4 - A Cross Section Subjected to Crippling Stress | 123 |
| Figure B.5 - Formed vs. Extruded Sections..... | 124 |
| Figure B.6 - Lip Criteria for Formed Sections..... | 125 |
| Figure B.7 - Crippling Stress of Formed Sections..... | 125 |
| Figure B.8 - Crippling Stress of Extruded Sections..... | 126 |

| | |
|---|-----|
| Figure B.9 - Effect of Poisson's Ratio on a Flat Plate | 128 |
| Figure B.10 - Plates with Various Edge Supports | 131 |
| Figure B.11 - Square Plate with Hinged Support on Four Edges..... | 132 |
| Figure B.12 - Long Rectangular Plate with Four Hinged Support Edges | 133 |
| Figure B.13 - Rectangular Plate with Various Edge Supports | 134 |
| Figure B.14 - K_c Coefficients (Compression)..... | 136 |
| Figure B.15 - K_s Coefficients (Shear)..... | 138 |
| Figure B.16 - K_b Coefficients (Bending)..... | 140 |
| Figure B.17 - Example of an Interaction Curve for Combined Compression (R_c) and Shear (R_s) Loadings..... | 141 |
| Figure B.18 - Interaction Curves For Combined Shear and Compression loading ($R_s^2 + R_c = 1$)..... | 142 |
| Figure B.19 - Interaction Curves For Combined Shear and Bending Loading | 143 |
| Figure B.20 - Airplane weight and lifting air loads..... | 144 |
| Figure B.21 - Critical conditions for wing box structure..... | 145 |
| Figure B.22 - V-n Diagram (Gust Envelope) | 146 |
| Figure B.23 - Wing additional lift distributio | 147 |
| Figure C.1 - Flow chart of interrelation of genetic algorithm and FEM building tools..... | 148 |

ABBREVIATIONS

| | |
|----------------------------|--|
| FEM | Finite Element Modelling |
| FEA | Finite Element Analysis |
| GA | Genetic Algorithm |
| MLG | Main Landing Gear |
| MSC | Macneal-Schwendler Corporation |
| DOF | Degree of Freedom |
| F_{cr} | Critical buckling load |
| P_E | Euler buckling load |
| E | Modulus of Elasticity |
| E_t | Tangent Modulus |
| I | Moment of inertia |
| A | Cross sectional area of the column element |
| ρ | Radius of gyration |
| L | Length of the column element |
| μ | Poisson's ratio |
| e_y | Strain in y direction |
| k | Buckling coefficient |
| c | End fixity factor |
| t | Plate thickness |
| η_p | Plastic reduction factor |

| | |
|----------------------------------|----------------------------------|
| k_c | Compression buckling load factor |
| k_s | Shear buckling load factor |
| k_b | Bending buckling load factor |
| R_c | Compression stress ratio |
| R_s | Shear stress ratio |
| R_b | Bending stress ratio |
| MS | Margin of Safety |
| L' | Effective column length |
| F_{cc} | Allowable crippling stress |
| σ_{all} | Allowable tensile stress |
| RF | Reserve factor |
| ECM | Electrochemical milling |

CHAPTER 1

INTRODUCTION

Structural design optimization is a critical and challenging activity that has received considerable attention in the last two decades. The main purpose in design optimization is to find the best ways so that a designer or a decision maker can derive a maximum benefit from the available resources. Genetic algorithm is one of the most popular optimization algorithms that is known for its robustness and ability to search complex and noisy search spaces.

1.1 Objective and Scope of the Study

The purpose of this study is to optimize the outer wing structure of a two seated trainer aircraft having a turboprop engine. This aircraft has been designed and manufactured by Turkish Aerospace Industries Inc. (TAI) in order to meet the pilot training requirements of Turkish Air Force (TUAF). The study is composed of the following steps. First, finite element model (FEM) of the wing structure is created and the boundary conditions and load cases on the structure are defined by using MSC/PATRAN[®]. In the next step, structure is analyzed by using MSC/NASTRAN[®]. According to the analysis results; the optimization program compiled by using VISUAL FORTRAN updates finite element model. Finally, MSC/NASTRAN[®] solves the resulting structure once more. This loop continues until a satisfying improvement on the objective function (weight of the wing structure) is achieved.

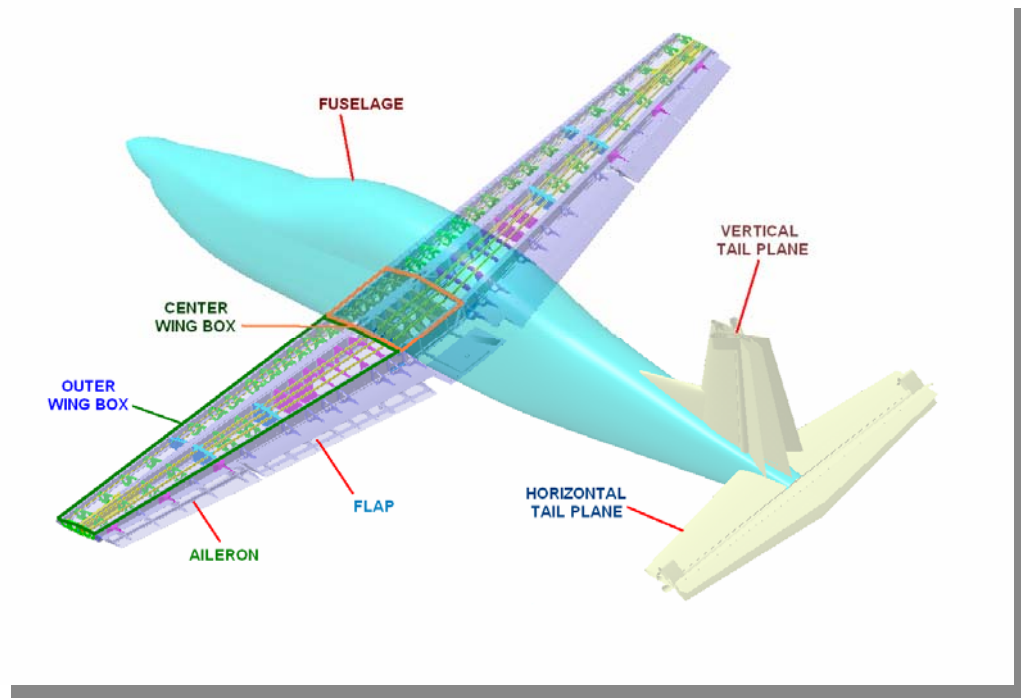


Figure 1.1 *Wing box structure of the turboprop aircraft*

The study also includes development of a code for GA implementation. This code can be used for any kind of structural optimization problem as long as the finite element model of the structure is available. The code uses MSC/NASTRAN[®] as finite element solver.

1.2 Literature survey

A detailed literature survey has been performed in order to get into structural optimization as well as genetic algorithms. The study has started with detailed investigation about optimization concepts and definitions used (objective function, design variable, constraints etc) in optimization. The major characteristics of structural optimization have been identified. The details of

the objective function design and constraint handling have been examined. Several numbers of publications have been read in order to obtain the preliminary background for optimization as well as structural optimization. In addition, a detailed literature survey has been conducted on aircraft wing structural design concepts. Many design approaches for different types of aircraft wing structures have been examined. Furthermore, functions of wing structural elements have been understood in this study.

In 1999, Belegundu and Chandrupatla [1] wrote a book on the implementation of optimization in engineering, offering a strong foundation and coverage of optimization theory.

In 1992, Kamat [2] edited a book written by experts documenting the state of the art in structural optimization with a view to establishing some of the most promising directions for future research in the field.

After forming the necessary structural optimization background, a detailed investigation about Genetic Algorithms has been started. The Genetic Algorithm (GA) concepts, operators and algorithm implementation are the focus points for this part of the survey. The in-depth GA knowledge had been gained by examining the following papers and publications:

Dianati, Song, and Treiber [4] published a paper examining the history, theory and mathematical background, applications, and the current direction of both Genetic Algorithms and Evolution Strategies.

In 2002, Charbonneau [5] published a paper providing a detailed comparison of genetic algorithm based optimization schemes against other optimization schemes and describing in full detail the use of a genetic algorithm.

Said [6] published a paper describing the basic concepts and functionality of Genetic computation.

Gantovnik, Anderson-Cook, Gurdal and Watson [11] published a paper describing a new approach for reducing the number of the fitness function evaluations required by a genetic algorithm for optimization problems with mixed continuous and discrete design variables.

In 2005, McCall [19] published a paper demonstrating the structure of a Genetic Algorithm with simple examples and exploring the key advances that have been made in the theoretical understanding of how Genetic Algorithms operate.

After forming the necessary background for structural optimization and genetic algorithms, a detailed investigation about aircraft wings has been started. The main scope of this part of the study consists of wing structural design approaches, function of wing structural elements and airframe stress analysis and sizing.

In 1973, Bruhn [24] wrote a book called ‘Analysis and Design of Flight Vehicle Structures’ in which he presented a considerable amount of material & data about flight vehicle materials and their properties and practical strength analysis and design of structural components of aircraft

In 1997, Niu [22] published a book on stress analysis and sizing of metallic airframe structures called ‘Airframe Stress Analysis and Sizing’. This book provides a deep knowledge about the procedures and design data for use in the sizing of both airframe and space vehicle structures. The material presented in this book had been compiled largely from the published data of US government agencies such as NACA reports and technical publications.

In 2001 Falco et. al. [25] published a paper on optimization of a wing like structure consisting of spars, ribs, reinforcements and skin in which positioning of spars and ribs as well as dimensions of different parts of the structure are the design variables.

CHAPTER 2

OPTIMIZATION & GENETIC ALGORITHM

The goal of an optimization problem can be formulated as follows: find the combination of parameters (design variables) which optimize a given quantity, possibly subject to some restrictions on the allowed parameter ranges.

The quantity to be optimized (maximized or minimized) is termed as objective function; the parameters, which may be changed in the quest for the optimum, are called design variables; the restrictions on allowed parameter values are known as constraints.

The general optimization problem may be stated mathematically as:

Maximize

$$f(x), \quad x=(x_1, x_2, \dots, x_N) \in R^N \quad (2.1)$$

Subject to

$$g_i(x) \leq 0, \quad i = 1, \dots, K$$

$$h_i(x) \leq 0, \quad i = 1, \dots, P$$

$f(x)$ is the objective function. $g(x)_i$ and $h(x)_i$ are inequality and equality constraints, respectively. They represent constraints, which the design must satisfy, such as stress and displacements limits.

2.1 Objective function

The objective function is a function that returns a single value from which different designs can be compared. It is a scalar quantity that is either minimized or maximized by the optimizer. The optimal design is the design with a minimum (or maximum) value of the objective.

A minimum and maximum formulation may be interchanged by simply changing the sign of the objective. Optimization with more than one objective is generally referred to as multiobjective optimization. For structural optimization problems; weight, displacements, stresses, vibration frequencies, buckling loads and cost or any combination of these can be used as objective functions.

When formulating the design objective, there are a couple of scaling-related issues that should be kept in mind since they affect overall performance. First, the design problem should be posed so that the objective function has sufficient sensitivity with respect to each of the design variables. The second item to consider is the absolute value of the response selected to be the objective function. Care should be taken so that this value is not too close to zero. If it is very close to zero, this will cause numerical difficulties in determination of weighting constants for constraint violations.

2.2 Design variables

Design characteristics that are varied to achieve the objective are called as design variables. Design variables may take continuous or discrete values. Continuous design variables have a range of variation, and can take any value in that range. Discrete design variables can take only discrete values, typically from a list of permissible values.

In structural optimization, there are three types of design variable. These are:

- Size design variables
- Shape design variables
- Topology design variables

The notion of size design variable is related with cross-sectional quantities like area of bars, second moments of area of beams and thickness of plates and shells. The definition of size variable is related to the fact that the modeling domain is not changed. Therefore, the line of the beam, rod or bar is unchanged, just like the reference surface of a plate or a shell is assumed unchanged when the concept of size design variable is used. The orientations of non-isotropic material can also be treated as size design variables.

The notion of shape design variable is related to the reference domain of the actual model. For beams, rods and bars, the length can be thought as a design variable, which is then a shape design variable. For truss structures node coordinates of the truss elements can also be treated as shape design variables. In addition, the curvature of the reference line for these one-dimensional models is a shape design variable. For 2D models likewise the boundary curve or the curvature of the reference surface are shape design variables. For 3D

models the boundary surface (including internal boundaries like holes) is a shape design variable.

Finally, the notion of topology design variable is related to presence or absence of a certain design aspect. The complications in treating topology design variables are due to the fact that a change in topology results in a discontinuous change in the design response, while a continuous change in size or shape design variables normally results in continuous change in the design response.

2.3 Design constraints

In optimization problems, there can be some constraints that have to be satisfied while minimizing (or maximizing) the objective function. Conditions that the designs must meet are called as design constraints.

If there is no constraint imposed on the optimization problem then it is called as unconstrained optimization, otherwise it is called as constrained optimization problem.

In structural optimization problems, a constrained optimization problem arises in finding the minimum weight design of a structure subject to constraints on stress and deflection.

2.4 Classification of optimization problems

There are several classes of optimization problems. Knowing the type of optimization problem in consideration is critical, since the treatments of different class of optimization problems are not the same. The methodology to solve the optimization problem can be defined easily when the class of the problem is known. Optimization problems can be classified as follows:

Stochastic optimization refers to the minimization (or maximization) of a function in the presence of randomness in the optimization process. However, in Deterministic optimization, the process followed to find the minimum (or maximum) for the given function is defined.

An optimization problem can have some constraints defined which have to be satisfied while minimizing (or maximizing) the objective. These types of optimization problems are called Constrained Optimization Problems whereas the problems are called Unconstrained Optimization Problems when there is no condition to be satisfied in the defined problem.

In some optimization problems, it is possible to have more than one objective. These kinds of optimization problems are called Multiobjective optimization problems. However, in Single-objective problems, there is only one objective to be achieved.

2.5 Genetic Algorithm

Several optimization techniques are used in the context of engineering design optimization. Genetic Algorithm (GA) is one such technique that has been gaining substantial attention in recent years.

Genetic algorithm is a search strategy based on the rules of natural genetic evolution. It is well known for its robustness and ability to search complex and noisy search spaces, phenomena that are frequently encountered in design and optimization problems.

Genetic algorithm can be regarded as an expensive optimization tool that sometimes requires thousands of analyses to achieve convergence. However, there is a large amount of research work being done with GAs and it is continuing to grow, with many new ideas aimed at reducing computational cost.

2.5.1 Genetic algorithm description

Genetic Algorithms are nondeterministic stochastic search/optimization methods that utilize the theories of evolution and natural selection to solve a problem within a complex solution space.

A genetic algorithm emulates biological evolution to solve optimization problems. It is formed by a set of individual elements (the population) and a set of biological inspired operators that can change these individuals. It simulates evolution of individual structures via processes of selection, mutation, and reproduction that are referred to as search operators.

Each individual in the population receives a measure of its fitness in the environment. Only the individuals that are the most suited in the population are likely to survive and to generate offsprings, thus transmitting their biological heredity to new generations.

In computing terms, genetic algorithms map strings of numbers to each potential solution. Each solution becomes an individual in the population, and each string becomes a representation of an individual. There should be a way to derive each individual from its string representation. The genetic algorithm then manipulates the most promising strings in its search for an improved solution.

2.5.2 Basic structure of genetic algorithm

In nature, a combination of natural selection and procreation permits the development of living species that are highly adapted to their environments. A GA is an algorithm that operates on a similar principle.

The genetic algorithm (GA) is one of the probabilistic optimization algorithms generated based on the theory of evolution. The optimization process is a model of the law of the survival of the fittest of actual creatures: the fittest adaptable individual can leave offspring. This survival-of-the-fittest process is modeled in a computer program. Those individual with the highest fitness within the given environment are selected at high probability for reproductions of next generation, and the rest of the individuals in the group are curtailed. From the selected elitist group, the genetic information of the next generation is produced by means of crossovers and mutations.

In order to solve the optimization problems by means of GA, design variables must be coded into a list of genes (chromosome) and a design example must correspond to a chromosome or chromosomes that represent an individual. The complexity of an organism can be controlled by the length and number of chromosome and gene strings, and the size and number of gene alphabets.

A group is made from these individuals, and the optimization is performed for the group using genetic procedures like fitness evaluations, selections, crossover and mutation. A genetic algorithm is usually made up of a group of organisms commonly referred to as a population of organisms. Although there are many different algorithms, the basic structure is still the same as shown in Figure 2.1.

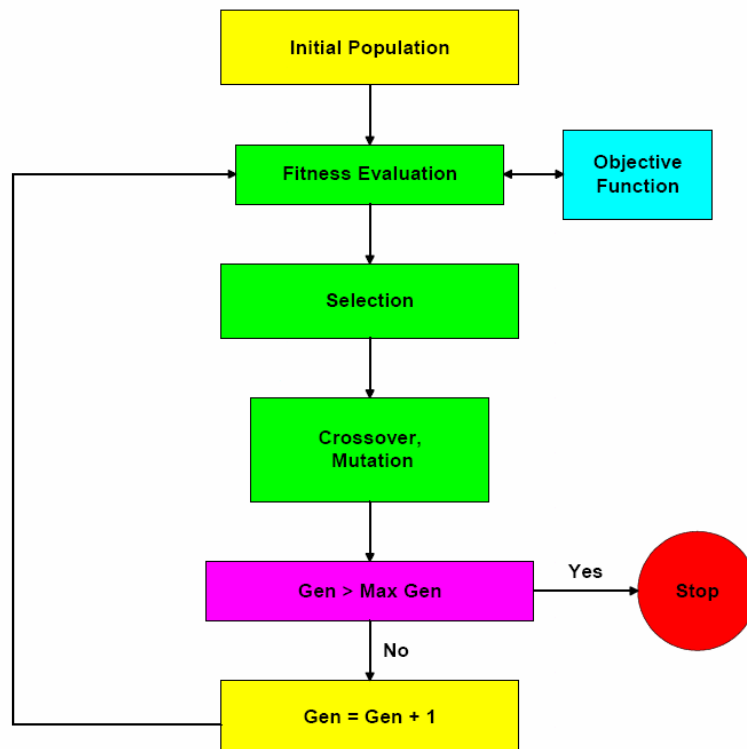


Figure 2.1 Outline of a basic genetic algorithm

The main components of the basic genetic algorithms are the chromosome encoding, fitness evaluation, selection, crossover and mutation.

2.5.3 Chromosome encoding

A GA manipulates populations of chromosomes, which are string representations of solutions to a particular problem. A chromosome is an abstraction of a biological DNA chromosome, which can be thought of as a string of letters from the alphabet {A,C,G,T}. A particular position or locus in a chromosome is referred to as a gene and the letter occurring at that point in the chromosome is referred to as the allele value or simply allele. Any particular representation used for a given problem is referred to as the GA encoding of the problem. The classical GA uses a bit-string representation to encode solutions. In binary encoding, every chromosome is a string of bits, 0 or 1.



Figure 2.2 *A binary encoded chromosome*

Encoding depends on the problem and on the size of instance of the problem. There are many other ways of encoding.

2.5.4 Fitness evaluation

GAs typically work by iteratively generating and evaluating individuals using an evaluation function. The fitness function is a computation that evaluates the quality of the chromosome as a solution to a particular problem

For structural design optimization, x is an N -dimensional vector called the design vector, representing design variables of N structural components to be optimized, and $f(x)$ is the objective function. In addition, $g(x)_i$ and $h(x)_i$ are inequality and equality constraints, respectively. They represent constraints, which the design must satisfy, such as stress and displacements limits. Moreover, $F[f(x)]$ is the fitness function that is defined as a figure of merit.

It is not possible to utilize GAs in order to solve the constrained problems. In GAs, constraints are usually handled by using the concept of penalty functions, which penalize infeasible solutions. If any constraints are violated, a penalty is applied to the objective function, with the value of the penalty related to the degree in which the constraints are violated. The resulting penalized objective function quantitatively represents the extent of the violation of constraints and provides a relatively meaningful measurement of the performance of each solution string. Consider a problem where displacement and stress constraints are imposed. Each element is checked for stress violation, and each model node is checked for displacement violation. If no violation is found, then no penalty is imposed on the objective function. If a constraint is violated then the penalty is defined on the objective function.

There are several penalty methods. These are:

- Death Penalty
- Static Penalties

- Dynamic Penalties
- Annealing Penalties
- Adaptive Penalties
- Segregated GA
- Co-evolutionary Penalties

In this study, static penalty method is used. In this method, penalty parameters do not depend on the current generation number and a constant penalty is applied to unfeasible solutions. The individuals are simply evaluated by using

$$eval(x) = f(x) + \sum_{i=1}^N R_i \times C_i^L \quad (2.2)$$

where R indicates the penalty coefficient, N indicates the number of constraint types in consideration, C is number of constraint violation and L is the proportionality constant.

2.5.5 Selection

A GA uses fitness as a discriminator of the quality of solutions represented by the chromosomes in a GA population. The selection component of a GA is designed to use fitness to guide the evolution of chromosomes by selective pressure. Chromosomes are therefore selected for recombination based on fitness. Those with higher fitness should have a greater chance of selection than those with lower fitness, thus creating a selective pressure towards more highly fit solutions. Selection is usually with replacement, meaning that highly fit chromosomes have a chance of being selected more than once or even recombined with themselves. There are many different selection schemes.

Most common selection schemes are Rank selection and Tournament selection.

In Rank selection, all designs in the population must be ranked from best to worst according to the value of each designs' fitness. A roulette wheel is implemented where the i^{th} ranked design in the population is given an interval $[\Phi_{i-1} ; \Phi_i)$, whose size depends on the population size, P , and its rank, i , in the population:

$$\Phi_i = \Phi_{i-1} + \frac{2 \cdot (P - i + 1)}{P \cdot (P + 1)} \quad (2.3)$$

where $\Phi_0 = 0$; and $i = 1, \dots, P$. A random number is generated between 0 and 1; design i is selected as a parent if the number lies in the interval $[\Phi_{i-1}; \Phi_i)$. When the wheel is spun (simulated by using a random number generator between 0 and 1, where the circumference of the wheel is normalized to be 1), those designs that occupy larger slices of the wheel have a better chance to be chosen as parent designs.

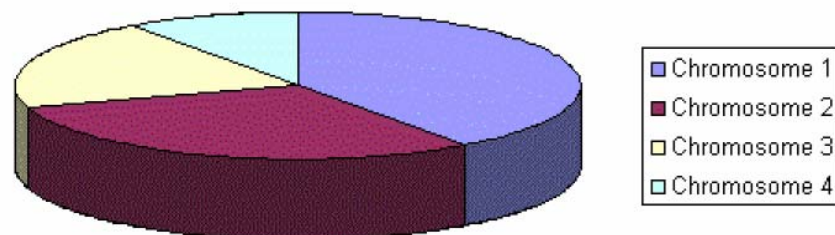


Figure 2.3 *Roulette Wheel*

The Tournament selection is very simple and needs less processes. In this selection scheme, a number of individuals (typically between 2 and 7 individuals) are chosen randomly from the population and the best individual from this group is selected as parent. This process is repeated as often as individuals must be chosen. Tournament Selection is naturally elitist.

2.5.6 Crossover and mutation

Selection alone cannot introduce any new individuals into the population (i.e., it cannot find new points in the search space). These are generated by genetically inspired operators, of which the most well known are crossover and mutation. Crossover is sometimes referred to as recombination.

The crossover and mutation are the most important part of a genetic algorithm. The performance of the algorithm is mainly influenced by these two operators. Usually, there is a predefined probability of procreation via each of these operators. Traditionally, these probability values are selected such that crossover is the most frequently used, with mutation being resorted to only relatively rarely. This is because the mutation operator is a random operator and serves to introduce diversity in the population. The kind of operator to be applied to each member of the gene pool is determined by random choice based on these probabilities.

The crossover operator functions on the breeding pool. Crossover is one of the genetic operators used to recombine the population genetic material. It takes two chromosomes and swaps part of their genetic information to produce new chromosomes. This operation is similar to sexual reproduction in nature. There are several types of crossovers that include single crossover also known as

one-point crossover, two-point crossover, and uniform crossover among others.

In one-point crossover, a crossover point is selected randomly within a chromosome, and then the two parent chromosomes at this point are interchanged to produce two new offspring.

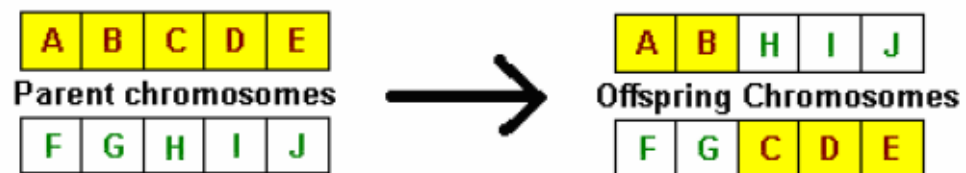


Figure 2.4 One-Point Crossover

Similarly, in two-point crossover, two crossover points are selected randomly within a chromosome, then the two parent chromosomes between these points are interchanged to produce two new offspring.

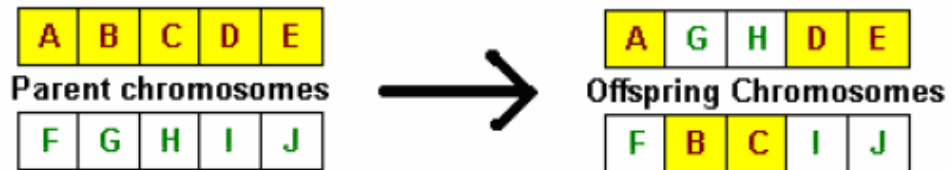


Figure 2.5 Two-Point Crossover

Uniform crossover is a crossover operator that decides (with some probability) which parent will contribute each of the gene values in the offspring chromosomes. This allows the parent chromosomes to be mixed at the gene level rather than the segment level (as with one and two point crossover).

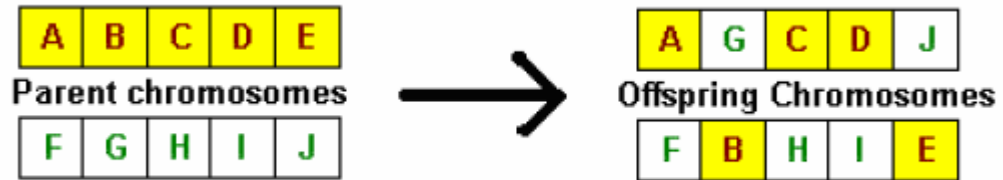


Figure 2.6 Uniform Crossover

In mutation, instead of exchanging cross-sections of a given two strings, the mutation operator randomly alters each gene with a small probability (i.e. 0.001). The main objective of the mutation operator is to produce a variety of different strings. The traditional view is that crossover is more important of the two techniques for rapidly exploring a search space. Mutation provides a small amount of random search, and helps ensure that no point in the search space has a zero probability of being examined.



Figure 2.7 Mutation

2.5.7 Termination criteria

There are several termination criteria used in GA's. The most common termination criteria is to put a limit on the maximum number of generation. When the number of generations reaches to a predefined value then the optimization process stops. Another common criterion is based on the percentage of identical solutions in the population. If the percentage of identical solutions are higher or equal to the predefined percentage value then the optimization process is terminated.

A criterion based on no improvement tolerance can also be used in GA's. This criterion checks for the number of generations with no improvement in the best solution obtained and it terminates the optimization process based on the predefined tolerance.

2.5.8 GA Implementations

The pseudo-code for GA approach is as follows:

- Define the objective function (environment). Objective function is used in evaluating the designs' fitnesses.
- Define the chromosome structure (genetic representation of the system) suitable for the problem in consideration. The characteristics of an organism are provided in the gene strings of each chromosome. All the design variables should be placed somewhere inside chromosome structure.
- Generate a random population of specific size (Initial population). The population size affects the efficiency and performance of GA. GA does poorly for very small size of populations and very large population size

impacts performance of the algorithm. For typical applications, the suggested range is between 10-160 chromosomes.

- Evaluate the fitness of every solution over the objective function. Each organism is then placed into a common environment where it competes and breeds with other members of the population
- Select two parent chromosomes for mating from a population according to their fitness (the better fitness, the bigger chance to be selected) by a random selection method e.g. tournament selection and rank selection. The fittest organisms in the population are given the best opportunity to become parents of a child and may survive into the next generation.
- Apply crossover operation on the selected pairs if they have been chosen for crossover (based on probability of crossover). The main objective of crossover is to take good characteristics from organisms in the parent population and create child organisms which will hopefully be better suited to their environment than their predecessors
- Based on the probability of mutation, mutate new offsprings at each locus (position in chromosome). Once offsprings have been created, they may be exposed to a mutation operator that allows for the introduction of new, random information that may aid the algorithm in creating stronger organisms.
- Replace the initial population with new generated population.
- Go through all the steps until the termination criteria met.

CHAPTER 3

WING DESIGN

3.1 Typical Airplane Wing Box Design Considerations

The purpose of this chapter is to explain the basic principles of wing design that can be applied to conventional airplanes.

It will be noted that any wing requires longitudinal (lengthwise with the wing) members to withstand the bending moment which are greatest during flight and upon landing. This is particularly true of the cantilever wings, which are normally employed for high-performance aircraft. Some of the light aircraft have external struts for wing bracing and these do not require the type of structure needed for the cantilever wing shown in Figure 3.1. the aircraft wing employed in this optimization study does not include any type external bracing since it as a cantilever wing.

The outline of the wing, both in planform and in the cross-sectional shape, must be suitable for housing a structure, which is capable of doing its job. As soon as the basic wing shape has been decided, a preliminary layout of the wing structure must be indicated to a sufficient strength, stiffness, and lightweight structure with a minimum of manufacturing problems. [21]

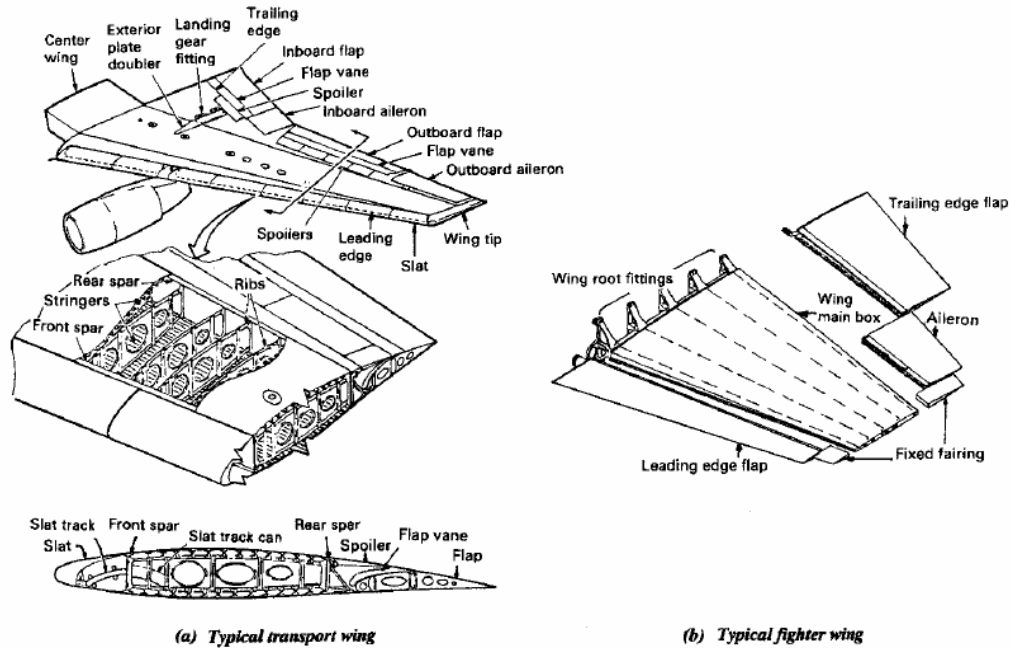


Figure 3.1 Typical Transport and fighter wing [21]

There are several types of wing structure for modern high speed airplanes; thick box beam structure (usually built up with two or three spars for high aspect-ratio wings as shown in Fig. 3.1(a)), multi-spar box structure for lower aspect-ratio wings with thin wing airfoil as shown in Fig. 3.1(b), and delta wing box.

The wing is essentially a beam, which transmits and gathers the entire applied air load to the central attachment to the fuselage. For preliminary structural sizing and load purposes, it is generally assumed that the total wing load equals the weight of the aircraft times the limit load factor times a safety factor of 1.5. In addition to this applied load, other loads that may also be applied to the wing may include:

- Internal fuel pressure (static & dynamic) which may influence the structure design
- Landing gear attachment loads
- Wing leading and trailing loads
- Thrust load

These are generally secondary loads in wing design, the primary loads resulting from the applied air load. The local concentration of these loads may however require a rib to distribute the load to the overall structure. The applied air loads result in increasing shear and bending moments toward the wing root with the shear carried by the wing spar webs and cover and the bending moment by the wing covers and spar caps. In addition, covers together with the spar caps carry normal force. Rather than referring to bending moment what is generally defined as cover load N_x , the load per inch measured along the chord line. If this load is divided by the thickness of the cover skin, the result is the average stress of the cover at that point. [21]

Since the covers typically represent fifty to seventy percent of the structural weight of the wing, it is imperative that the covers be designed as efficiently as possible.

Since the lower cover is loaded primarily in tension, its design is straightforward. It requires careful material selection in order to assure fairly high tensile strength to density ratio combined with good fracture toughness and fatigue life. Certain aluminum alloys such as 2024-T3 and the newer

alloys such as 7475-T7351 are excellent candidates along with most of the titanium alloys such as Ti-6Al-4V. [21]

An additional consideration of tension cover design is improving the fatigue strength by utilizing interference fit fasteners. In this process, a fastener is installed in a hole that is several thousandths of an inch, typically 0.003 inch, smaller than the fastener diameter. This produces radial compression and tangential tension stresses at the edge of the hole. Since the tangential tension stresses are larger than the stress produced by most of the applied loads, the edge of the hole sees less stress cycling and therefore a lower effective stress concentration resulting in increased fatigue life. [21]

The upper cover optimum design is far more complex and configuration dependent. Since the upper cover is loaded primarily in compression, its design efficiency is dictated primarily by how well it can be stabilized, that is, prevented from buckling.

In order to enforce a mode requires that the cover be supported and restrained from moving up or down at the particular location. Many techniques are available to accomplish this and will be discussed in later sections of this chapter. The selection of the optimum cover stabilization technique is very configuration dependent. For thin wings, multi spar and full depth honeycomb tend to be the lowest weight construction. For deeper wings, wing cover with skin-stringer panel become attractive but ribs have to be spaced closely enough to prevent the stiffeners from failing as a column. [21]

3.2 Brief Summary of Wing Loads

3.2.1 General

- Positive high angle of attack (+HAA)
- Negative high angle attack (—HAA)
- Positive low angle of attack (+LAA)
- Negative low angle of attack (—LAA)
- Dive maneuvers
- Flaps down maneuver — takeoff configuration
- Flaps down maneuver — landing configuration
- Taxiing
- Jacking
- Maneuver with certain wing fuel tanks empty
- Flutter
- Control surface reversal
- Roll initiation
- Unsymmetrical spanwise lift distribution
- Fatigue
- Fail-safe
- Fuel vapor or refueling pressures
- Thermal gradients
- Lightning strike

3.2.2 Spar conditions

- Fuel slosh
- Fuel head — crash conditions
- Concentrated shear loads
- Fuselage pressure in center section

3.2.3 Rib conditions

- Rib crushing
- Concentrated load redistribution
- Fuel slosh
- Fuel head
- Wing cover stabilization
- Sonic fatigue

3.2.4 Leading edge conditions

- Hail strike
- Thermal anti-icing
- Duct rupture
- Sonic fatigue — engine reverse thrust

3.2.5 Trailing edge and fairing load conditions

- Sonic fatigue
- Buffet
- Slosh and gravel impact
- Minimum gage
- Positive and negative normal force pressures

3.3 Wing Box Design

It appears that the primary structural design problem is one of general structural layout first, whether a large percentage of the wing bending shall be carried by the spars, or whether the cover should be utilized to a large extent; and second, in which direction should be primary wing ribs run along the flight path, or normal to the rear spar in the wing?

Regarding the first, it is fairly obvious that the cover should be utilized for a large percentage of the bending material. This is true, since it appears that torsional rigidity is required and, since it is, this same torsion material may as well be used for both primary bending and torsion material. Spanwise stiffeners spaces fairly close together are, therefore, required to keep the buckling of the bending material down to a minimum. [21]

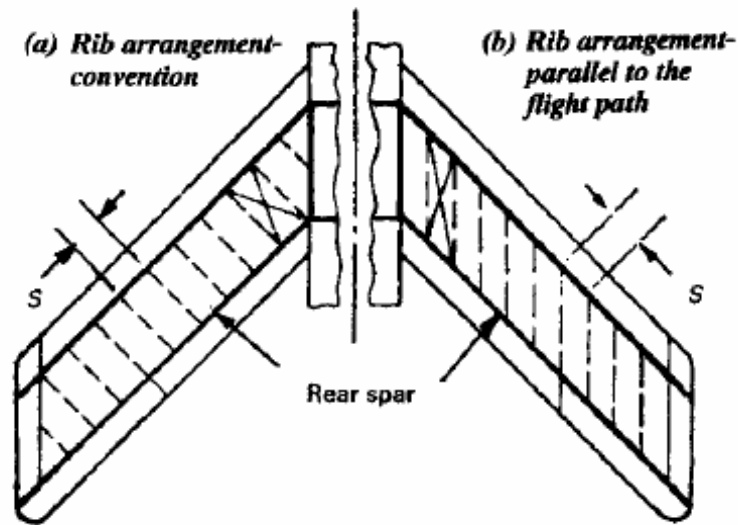


Figure 3.2 Comparison of rib direction (rectangular box) [21]

In consideration of the direction of wing ribs, Fig. 3.2(a) shows the somewhat conventional structure; Fig. 3.2(b) shows the wing ribs parallel to the flight path. It may be noted here that some opinions hold it necessary to have the wing ribs parallel to the flight path in order to insure a smooth aerodynamic shape between the spars (assuming a two-spar wing). This latter arrangement seems to have too many disadvantages to be structurally sound and, further, if spanwise stringers are utilized between the spars, then the rib riveting will not particularly further aggravate the aerodynamic contour because a large amount of riveting is already required for the spanwise stiffeners. For the sample illustration chosen, the total rib length is 28% longer for the wing with the ribs parallel to the flight path, with corresponding weight loss.

The fore and aft spar locations as shown in Fig. 3.3 are approximate locations early in the design during layout of high lift devices. The design of the wing

body joint, and development and sizing of the hydraulic components, control components, and electrical systems may require changing spar locations as design progresses. However, firm spar locations must be established very early in the design and preferably by the time the final mathematically defined loft are available. In any case, both are required before final layouts and drawings can be started. [21]

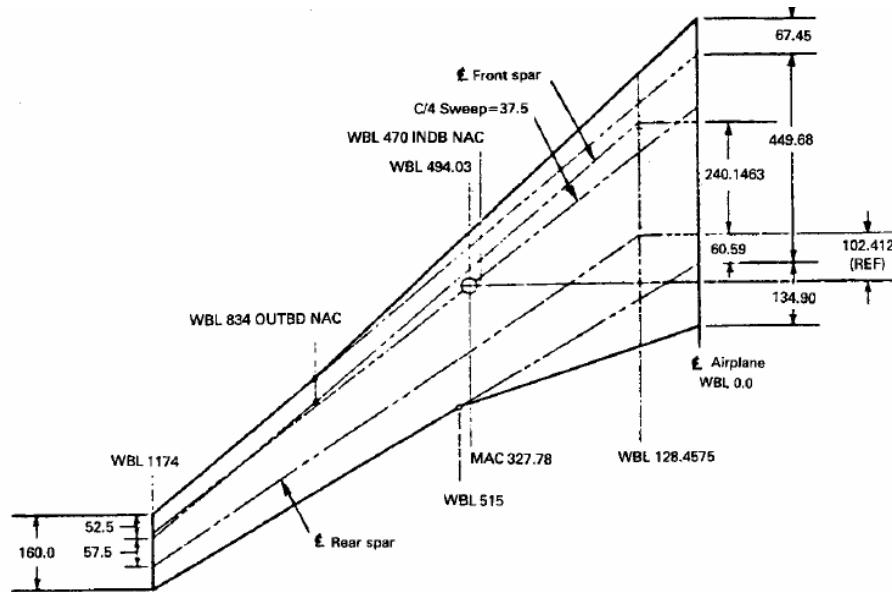


Figure 3.3 *Wing plan view layout of a transport*

The rear spar must be located at a suitable chordwise station, leaving sufficient space for the flaps and for housing the controls to operate the flaps, ailerons and spoilers. A rearward shift of this spar increases the cross-sectional area of the torsion box (and incidentally the fuel storage space) but the reduction in the

sectional height will make it less efficient in bending. Similar criteria apply to the front spar when it is moved forward.

The central part of the wing, bounded by the front and rear spars, takes the loads from the nose and rear sections and carries them to the fuselage, together with its own loads. Primary wing structure of transport aircraft is in effect a leak-proof, integral fuel tank, the arrangement of which in the spanwise direction is dictated by considerations of balancing the aircraft for various fuel loads. Center tanks should be avoided from the outset, although for long-range aircraft they are more or less essential. [21]

Fig. 3.4 shows a preliminary view of spars and maximum wing thicknesses. In conjunction with a preliminary cubic mathematically defined loft, these are used for fuel quantities and management design (locations of end ribs), and to establish the torsional and bending material of the wing box.

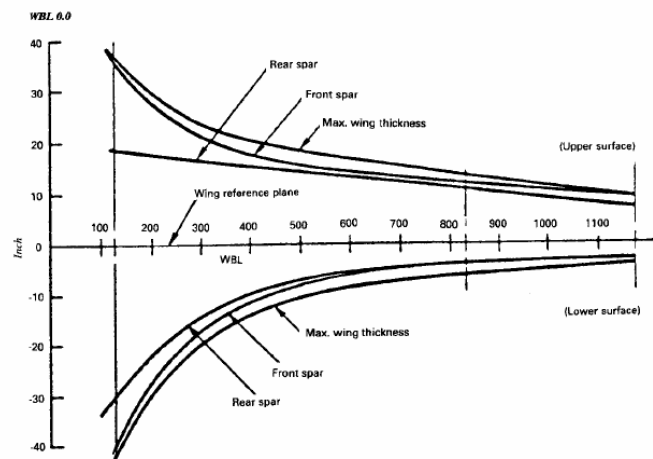


Figure 3.4 Preliminary view of spars and wing maximum thicknesses of a transport

3.4 Wing Covers

In the consideration of bending material, it is convenient to classify wing structure according to the disposition of the bending-load resistant material: (a) all bending material is concentrated in the spar caps; (b) the bending material is distributed around the periphery of the profile; (c) skin is primarily bending material. Typical wing cross-section in which the bending material is concentrated in the spar caps is shown in Fig. 3.5

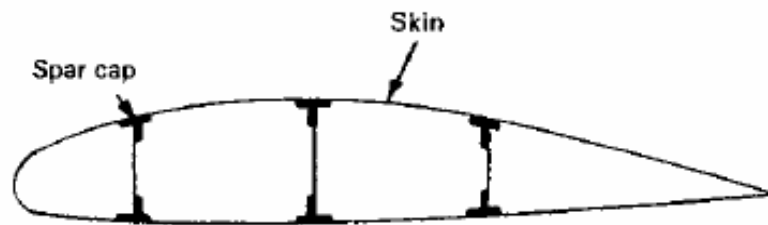


Figure 3.5 *Three spar wing-all bending materials concentrated at the spar cap*
[21]

Some of the main advantages of the concentrated spar cap type:

- Simplicity of construction (mostly used on general aviation aircraft).
- Because of the concentration of material, the spar caps can be so designed that buckling occurs near the ultimate stress of the material; this allows the use of higher allowable stresses.

Whereas concentrated spar cap type has also some disadvantages:

- Skin will buckle at a very low load. The load-carrying ability of the skin, in so far as bending is concerned, is therefore negligible, which means that it has a certain amount of material, which is not being utilized.
- Skin can be in a wave state having relatively large amplitudes, which disturbs the airflow over the wing profile and causes an increase in drag.
- Fatigue failures due to the local bending stress in the buckled sheet.

Typical wing cross sections in which the bending material is distributed around the periphery of the profile. The distributed bending material consists of stiffening elements running in a spanwise direction. In high-speed airplanes, the wing structure is usually made of multiple spars, which are primarily shear material and carry vertical shear. Very little bending material is contributed by the spars. They may be built-up shear webs or channel sections, as shown in Fig. 3.6

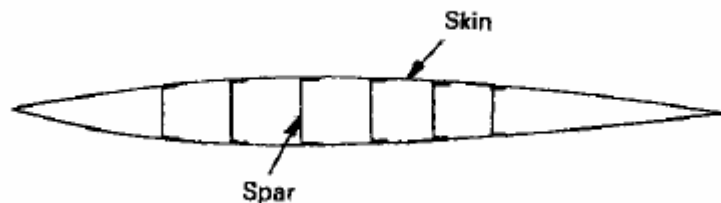


Figure 3.6 *Multi-spar skin bending material* [21]

The wing bending loads, which cause compression at the upper surface of the wing, are generally somewhat higher than those causing compression at the lower surface. This requires that the stiffening elements along the upper surface be more efficient and more closely spaced than those on the lower surface.

The torsional moments are primarily resisted by the skin and the front and rear spars. The portion of the wing aft of the rear spar is usually over the greater portion of the chord for control surfaces, which does not resist any of the torsional loads (see Fig. 3.7).

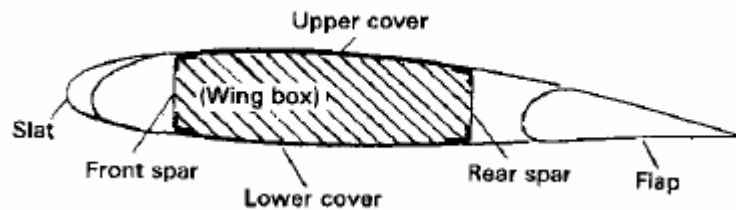


Figure 3.7 Typical wing torque box enclosed area [21]

Since positive flight design load factors are always higher than for negative flight, the wing upper surface is usually critical for compression loads. When large weights (such as tip tanks) are concentrated at the wing tip, the upper surface near the tip may be critical in tension for positive flight conditions. The following loads must be considered in the design of a compression surface:

- (a) Direct compression induced by bending of the entire section.

- (b) Shear flows — Maximum panel shear flows induced by wing box torsion loads.
- (c) Combination of maximum compression panel load with corresponding local shear flow, or maximum shear flow with corresponding local compression load to optimize the least weight structure.
- (d) Local bending effects caused by surface aerodynamic pressure load — consists of air loads normal to the surface of the wings. The summation of the components of these pressures normal to the airplane reference plane over the entire wing surface is equal to the airplane weight times the design load factor plus or minus the effects of tail load. For the conditions critical for the wing upper surface (usually +HAA, +LAA), the air loads normal to the upper surface are negative, i.e. they are suction pressures and act upward. When wing fuel tanks are pressurized, this pressure adds to the external pressures. Inertia loads due to fuel, structure and articles of equipment usually act opposite to the above and must be considered. Fig. 3.8 shows the critical wing cover axial loads at different locations. [21]

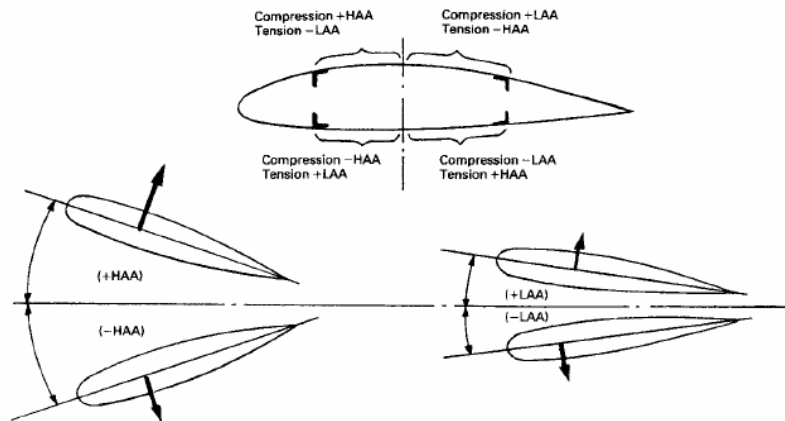


Figure 3.8 *Critical wing cover axial loads at wing surfaces* [21]

(e) Local bending effects caused by wing tank fuel loads which includes fuel vapor pressure, refueling pressure, inertia, etc.

(f) Local bending effects caused by wing bending crushing loads are radial loadings caused by curvature of the wing cover as it bends. As a wing is loaded, it naturally deflects and this load is reacted by ribs. This load always acts inward to compress the ribs. Generally, the crushing and inertia loading are less than the air loading on the compression cover and act in the opposite direction. The effect of these loads on the design of the cover structure is generally small and depends to a good extent on the rib spacing. If skin-stringer panels are used, the entire shear flow is carried by the skin. To properly consider these normal loads the longitudinal members are treated as beam-columns or panel compression.

It is good practice to avoid eccentricities in any structure. Many times eccentricities do occur and they must be accounted for in the design. For example, if a stringer is spliced from two different sections, the centroidal axes of the section may differ in location as shown in Fig. 3.9. This will weaken the strength of the member locally and must be considered at the splice point and in the adjacent bays; therefore, this splice should be made at a rib location.

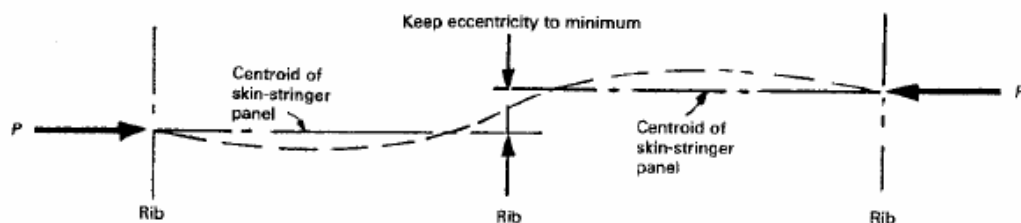


Figure 3.9 *The wing panel affected by eccentricity* [21]

The principal source of eccentricity occurs where stringers end. To properly provide for this eccentricity these stringers should be ended only at ribs where the shear load due to surface pressures and eccentricity or loading can be resisted without over-straining the skin. The stringer should be tapered at the end to prevent a sharp change in section. The stringer will tend to carry the same stress as the skin since they are both tied together. A sharp change of section can overload the rivets near the end and may cause failure. It is good practice to space the rivets near the end reasonably close together and also taper the stringer thickness near the end to reduce relative deflection between the stringer and skin [21]

3.5 Skin-Stringer Panels

The most common wing covers of transports are skin-stringer panels as shown in Fig. 3.10. Wing skins are mostly machined from a thick plate to obtain the required thickness at different locations and then required pads can be integral; otherwise, the pads or doublers have to be riveted or bonded on the basic skin around cutouts. The machined skins combining with machined stringers are the most efficient structures to save weight. This machined skin process has been adopted by modern aircraft structures.

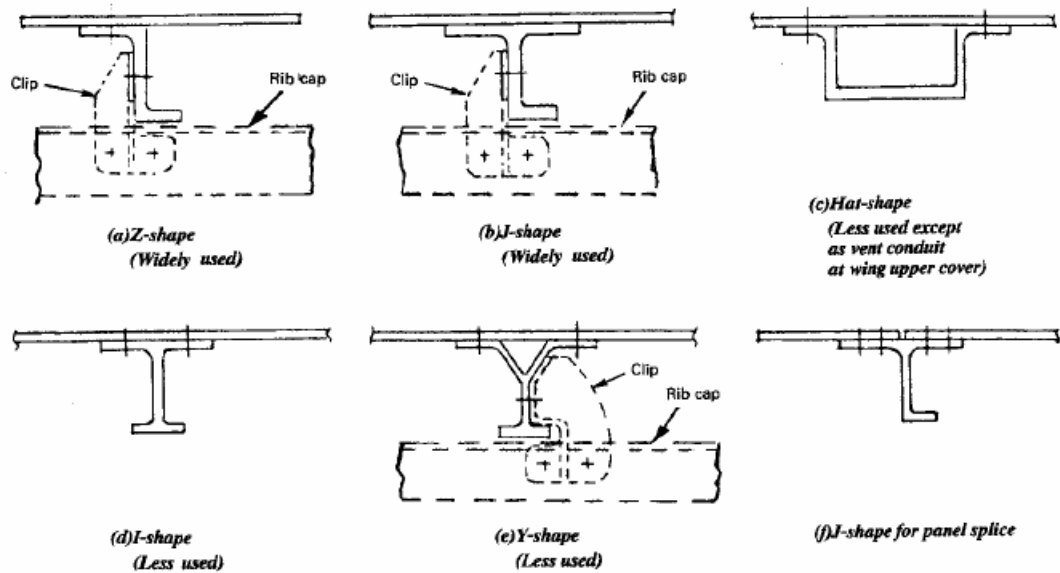


Figure 3.10 Typical wing skin-stringer panels [21]

Optimum distributions of area between skin and stiffener for minimum weight exist. Various studies show that the optimum ratio of stiffener area to skin area is approximately 1.4, assuming equal buckling stress in the skin and stiffener. The optimum design of unflanged integrally stiffened panels and from results obtained therein, the ratio of stiffener area to skin area is 1.7. Based on the equality of Euler column failure stress of the composite section with the initial buckling stress of the skin, the optimum ratio of stiffener area to skin area for Z section stiffeners is obtained to be approximately 1.5; and the ratio of stiffener thickness to skin thickness for minimum weight is 1.05. It should be noted that in a practical design, the skin area would be a higher fraction of the total weight than indicated in this discussion because of interacting shear loads, fatigue, and stiffness considerations. It is recognized that the upper as well as the lower wing cover must be designed to fatigue criteria. [21]

In the design of current transports, the allowable tension stress, based on fatigue considerations on the lower cover, is somewhat lower than the maximum compression stress on the upper cover; however, the average working stresses are of the same order of magnitude, resulting in approximately equal weight for the upper and lower covers. Centroids of sections should be as close to the skin as possible for maximum centroidal depth of the wing box and minimum panel eccentricity.

3.6 Spars

For strength/weight efficiency, the beam (or spar) cap should be designed to make the radius of gyration of the beam section as large as possible and at the same time maintain a cap section, which will have a high local crippling stress. The cap sections for large cantilever beams, which are frequently used in wing design, should be of such shape as to permit efficient tapering or reducing of the section as the beam extends outboard. Fig. 3.11 shows typical beam cap sections for cantilever metal wing cover construction where additional stringers and skins are also used to provide bending resistance. These cap sections are generally of the extruded type although such sections as (c) is made from sheet stock. These cap sections are almost always used with a beam web composed of flat sheet, which is stiffened by vertical stiffeners riveted to the web as shown in Fig. 3.12. [21]

The air loads act directly on the wing cover, which transmits the loads to the ribs. The ribs transmit the loads in shear to the spar webs and distribute the load between them in proportion to the web stiffnesses. In the past, it has been customary to design wings with three or more spars. The use of several spars

permit a reduction in rib stresses and also provides a better support for the spanwise bending material. Another important purpose is so designed for structural failsafe feature.

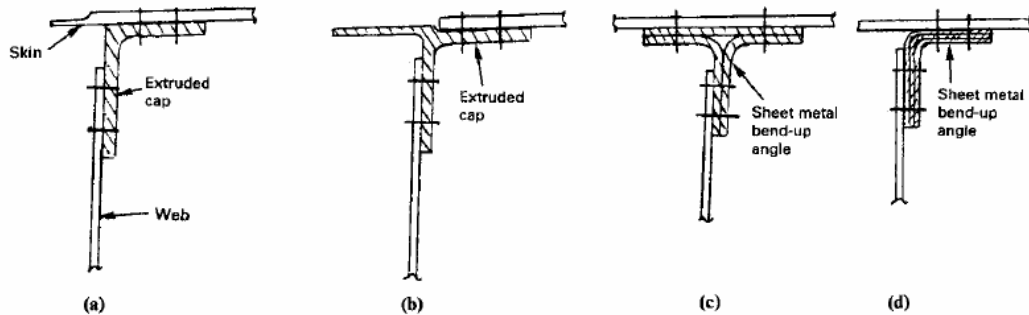


Figure 3.11 Typical spar cap sections [21]

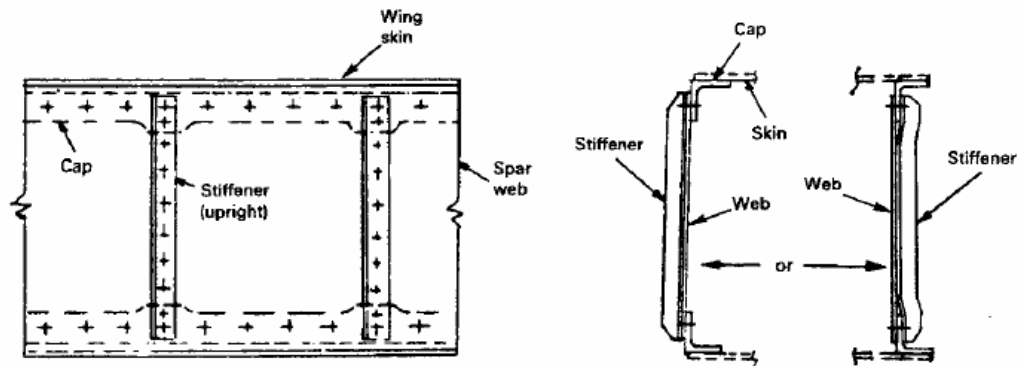


Figure 3.12 Typical spar cap construction [21]

Space requirements for the housing of fuel tank and landing gears (when retracted) is the main reason for the at least two spar wing box construction. A two-spar wing construction usually consists of a front and rear spar, the front

spar located that the wing leading edge slats can be attached to it and the rear spar located that the control surface such as these hinge brackets of flaps, aileron, spoiler, etc, can be attached to it. Furthermore, the front and rear spars combined with wing skin panels form as the closing member of the torsion-resistant box and also serves as integral fuel tank.

Different types of spar beam construction are shown in Fig. 3.13 and spars can be divided into two basic types; shear web type and truss type. The shear web type is widely adapted to design the modern wing spar for its structural efficiency as described later.

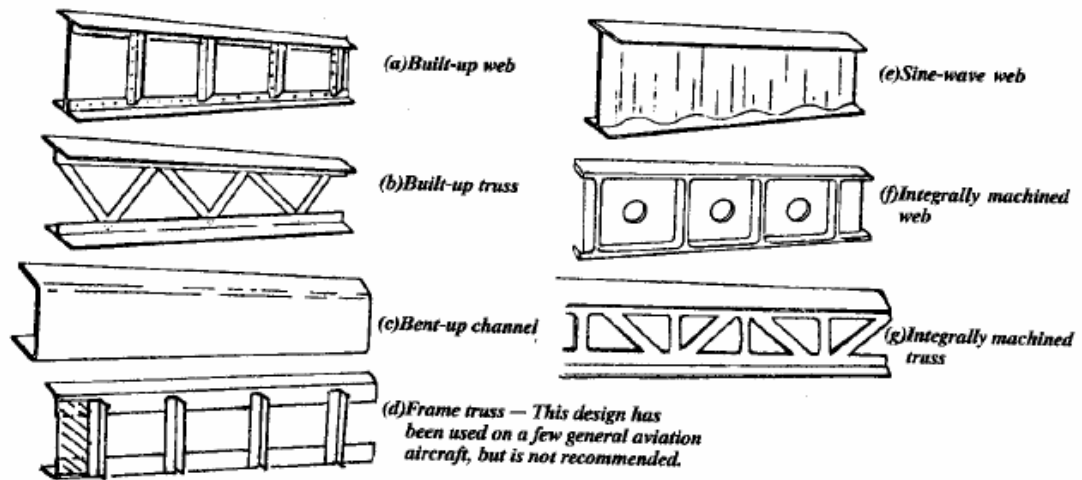


Figure 3.13 Typical spar configurations [21]

The design of a metal beam composed of cap members riveted or spotwelded to web members is a common airplane structural design. In this section, shear resistant (non-buckling) type shear beam construction is discussed.

A shear resistant beam is one that carries its design load without buckling of the web, or, in other words, it remains in its initially flat condition. The design shear stress is not greater than the buckling shear stress for the individual web panels and the web stiffeners have sufficient stiffness to keep the web from buckling as a whole. In built-in or integral fuel tanks, it is often desirable to have the beam webs undergo no buckling or wrinkling under the buckling criteria of 1.0-1.5g of level flight loads in order to give better insurance against leaking along riveted web panel boundaries. It is realized that the buckling web stress is not a failing stress as the web will take more before collapse of the web takes place, thus in general the web is not loaded to its full capacity for taking load and the web stiffeners are only designed for sufficient stiffness to prevent web buckling and sufficient strength to take the full failing strength of the web. [21]

A large majority of the beams in aircraft wing surfaces have sloping spar caps because of the taper of the structure in both planform and box depth. This sloping of the spar caps relieves the beam web of considerable shear load and should not be neglected as illustrated in Fig. 3.14.

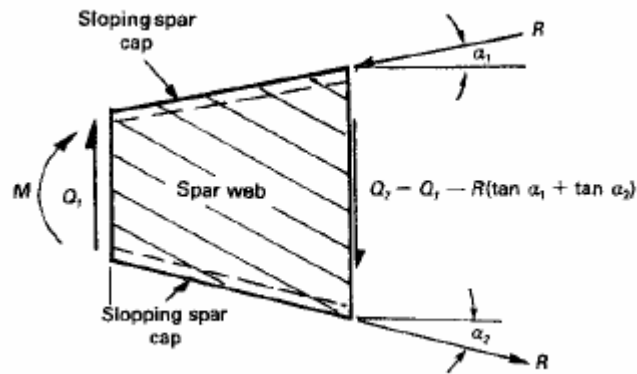


Figure 3.14 *Sloping spars relieve the spar web shear load* [21]

3.7 Ribs and Bulkheads

For aerodynamic reasons the wing contour in the chord direction must be maintained without appreciable distortion. Therefore, ribs are used to hold the cover panel to contour shape and also to limit the length of skin-stringer or integrally stiffened panels to an efficient column compressive strength. The rib also has another major purpose; to act as a transfer or distribution of loads. The applied loads may be only distributed surface air and/or fuel loads, which require relatively light internal ribs to carry through or transfer these loads to main spar structures. [21]

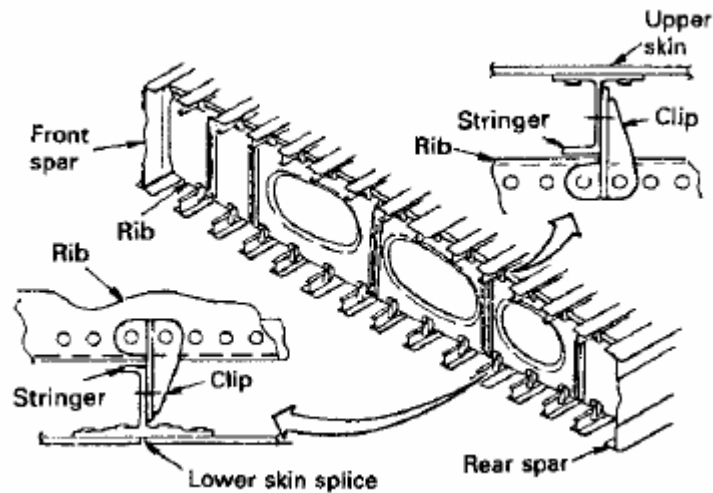


Figure 3.16 *Typical rib construction* [21]

A typical wing rib, illustrated in Fig. 3.16, is composed of caps, stiffeners and webs. Forged or sheet metal folded clips are used for attachment of stringers to ribs in lieu of bolting to stringer and rib cap flanges. Rib bulkheads are also provided for such purposes as flap, aileron, pylon and landing gear support, tank ends and redistribution of loads at the sweep and dihedral break.

Basically, there are many types of rib construction similar to the spar shown in Fig. 3.13. The aircraft industry generally uses shear web rib design due to a number of advantages. Its web acts as a fuel slosh inhibitor. The rib cap members and shear web inherently require gradual cross sectional change, eliminating load concentrations. The web provides continuous support for the wing cover panels for internal integral fuel tank pressures of up to 20-25 psi at the tip of the wing box. [21]

The shear web rib is somewhat forgiving for small changes in load criteria or analysis, and is a distinct original release schedule and eventually has a

"growth airplane" advantage. A truss type rib has none of the above advantages. In addition, it generally will be heavier, particularly on deep ribs where column lengths in compression are a problem. Truss member end design for fixity and concentrated loads of truss members are a distinct disadvantage, particularly where they attach to tension members. [21]

The rib structure in the torque box should be put to double use wherever possible. Flap tracks supported from the same ribs that support the landing gear is the best example. When the airplane is on the ground, the flap has no load and vice versa.

Some of the main function of wing ribs are as follows:

- (1) Wing bulkheads are frequently constructed as solid webs, although webs with access holes or trusses may be used.
- (2) Wing ribs carry the following loads:
 - The primary loads acting on a rib are the external air loads and the transfer of them to the spars.
 - Inertia loads (fuel, structure, equipment, external stores (missiles, rockets, etc.)).
 - Crushing loads due to flexure bending when a wing box is subjected to bending loads, the bending of the box as a whole tends to produce inward acting loads on the wing ribs as shown in Fig. 3.17. Since the inward acting loads are oppositely directed on the tension and compression side, they tend to compress the ribs.

- Redistributes concentrated loads such as nacelle and landing gear loads to wing spars and cover panels.

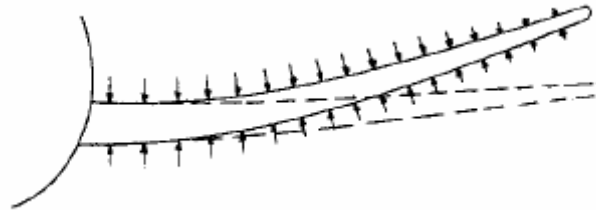


Figure 3.17 *Wing crushing load* [21]

- Supports members such as skin-stringer panels in compression and shear.
- Diagonal tension loads from skin (when the wing skin wrinkles in a diagonal tension field the ribs act as compression members).

(3) The manner in which the rib structure resists external loads and reaction forces acting on the ribs depends on the type of construction.

- Shear web type ribs are usually employed to either distribute the concentrated loads, such as the nacelle and engine or landing gear to the shear beams.
- Webs with lightening holes and stiffeners are applied to resist bending moments by the rib cap members and shear by the web.

(4) Ribs must effect a redistribution of shear flows in a wing where concentrated loads are applied or where there is a change in cross section such as cutouts, dihedral change or taper change, etc.

(5) The analysis of rib is usually similar to that of a simple beam. The items to check are:

- Shear in web, or axial loads in truss members

- Rib caps due to bending loading on ribs
- Shear attachment of rib to spar and wing covers
- Tension attachment of wing covers to rib (usually gives a combined shear and tension loading)
- Effects of crushing loads on rib
- Effects of shear flow distribution on rib if it borders a cutout.
- Effects of loads normal to the plane of the rib from such items as fuel pressure, slosh etc.

3.7.1 Rib Spacing

The spacing of the wing ribs usually has to be established early in the design phase. Since the weight of the ribs is a significant amount of the total box structure, it is important to include the ribs in the overall optimization consideration of the structure. This is illustrated in Fig. 3.18 where the relative weight of ribs and cover panels is presented for a specific span-wise of the wing. It is advantageous to select larger rib spacing; for equal structural weight, it leads to cost savings and less fatigue hazards.

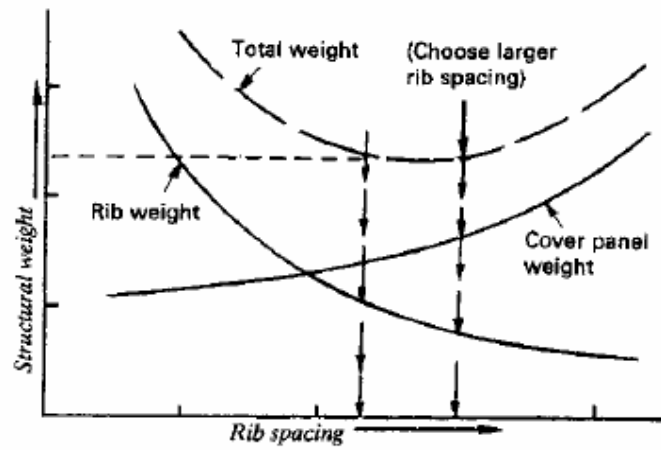


Figure 3.18 *Determination of rib spacing by structural weight comparison*

[21]

CHAPTER 4

CASE STUDY

4.1 Problem definition

A wing structure consisting of spars, ribs, skins and stringers is optimized considering two design constraint: (i) maximum stress, and (ii) instability (panel or column buckling) while the objective function is the weight of the wing. The wing carries an elliptically distributed load along the span. Positions of ribs as well as dimensions and thickness properties of certain parts of the structure are the design variables. Results indicate that significant improvement in terms of objective function has been achieved through the optimization procedures.

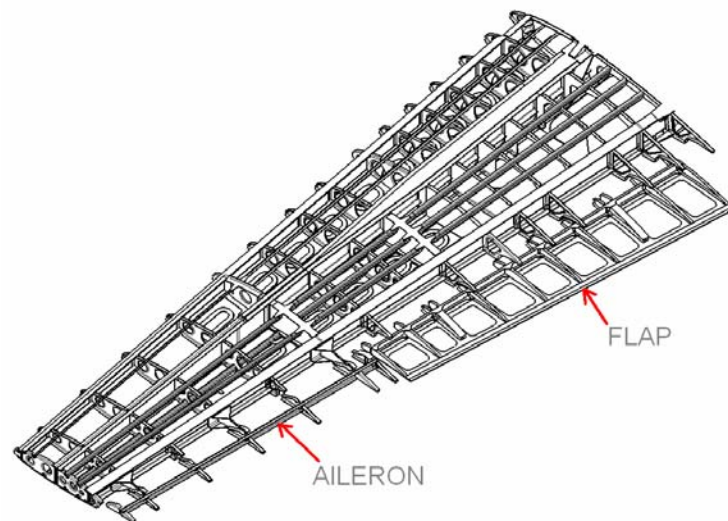


Figure 4.1 *Wing structural members and control devices*

4.2 Wing Structural Members

The outer wing structure to be optimized is assumed to be a cantilever wing (Figure 4.1). The length of the outer wing is 4320 mm. The width of the wing is 2036 mm at the root and 998 mm at the tip. The airfoil profiles at the root section and tip section can be seen in Figure 4.2 through Figure 4.3 respectively. The wing also has a dihedral angle of 5 degrees and a sectional twist angle of 3,5 degrees. The structure involves flight control mechanisms such as aileron and flap at the trailing edge as shown in Figure 4.2 and Figure 4.4. Flaps are used to increase the maximum lift coefficient to shorten airplane take-off and landing distance whereas ailerons are utilized for unsymmetrical maneuvers.

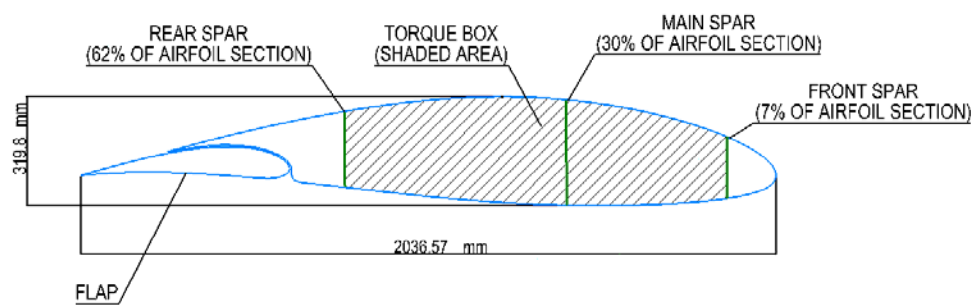


Figure 4.2 Wing root section and spar locations

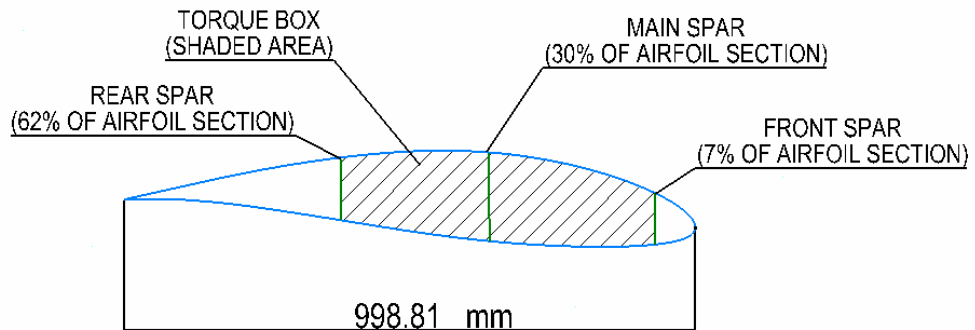


Figure 4.3 *Wing tip cross section*

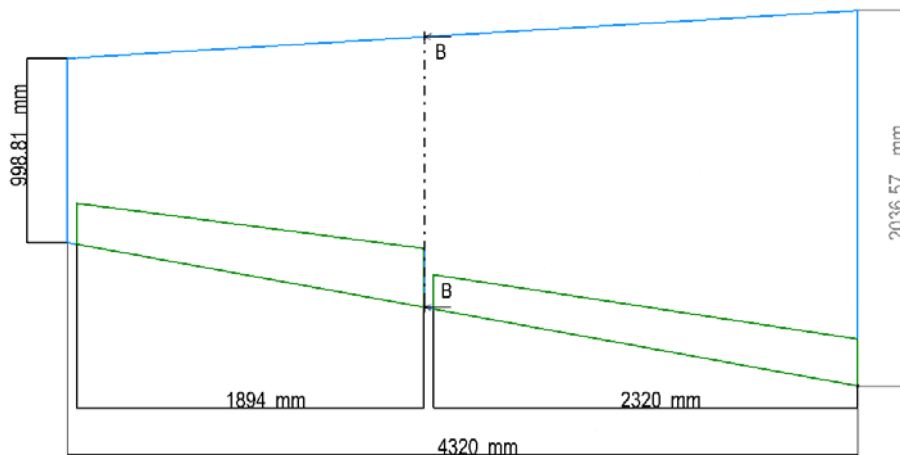


Figure 4.4 *Wing plan view*

The initial wing structural model has 3 spars and 18 ribs, which are parallel to the flight direction in order to insure a smooth aerodynamic shape between the spars. The rear spar is located at 62% chord-wise station, (Figure 4.2) leaving sufficient space for the flaps and for housing the flight control system parts to operate the flaps and ailerons. Main spar, which is the most important bending

member in the wing structure, is located at the 30% of the wing chord to take advantage of the height of the airfoil section and increase the bending stiffness (i.e. I_{xx}) of the main spar since 30% of the wing chord is the highest chord-wise location in the airfoil section. All the three spars in the wing box have I cross sections. The main spar is an NC machined part whereas rear spar and front spars are built-up structures having T caps and sheet metal webs. (Figure 4.5)

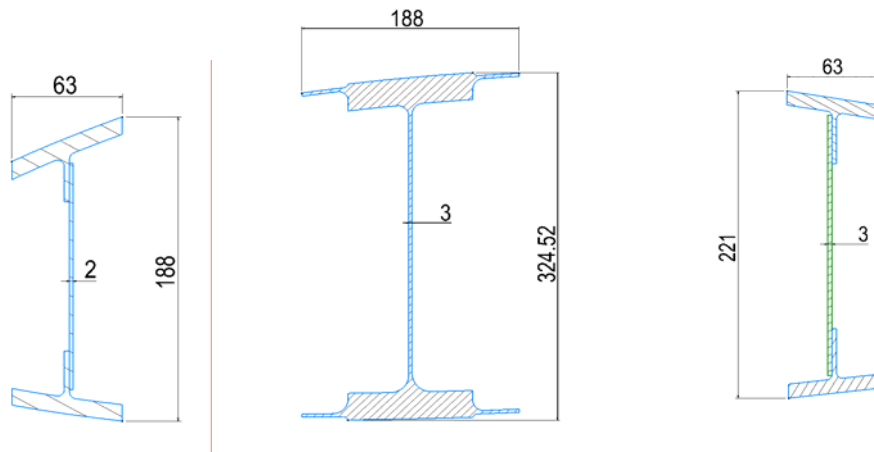


Figure 4.5 *Wing spars & dimensions*

In practice the central part of the wing, bounded by the front and rear spars, takes the loads from the leading edge and trailing edge and carries them to the fuselage, together with its own loads. Whereas in this study the fuselage is not modeled and instead the wing structure is fixed at spar locations representing the end conditions assuming a cantilever wing. Primary wing structure of the aircraft is in fact a leak-proof, integral fuel tank, the arrangement of which in the spanwise direction is dictated by considerations of balancing the aircraft for various fuel loads. The integral fuel tank is located between the rear spar

and front spar. Therefore, in order to leave the fuel tank enough volume the front spar is located at the 7% chord-wise location. (Figure 4.5)

In the initial wing model, there are 18 ribs, which are equally spaced. (Figure 4.5) Since the length of the wing span is 4320 mm, the spacing between each rib is about 255 mm which is to be later determined as a result of optimization. In addition, the leading edge and trailing edge structures are out of the scope of this study. Only the torque box of the wing structure, which is bounded by front and rear spars, is optimized.

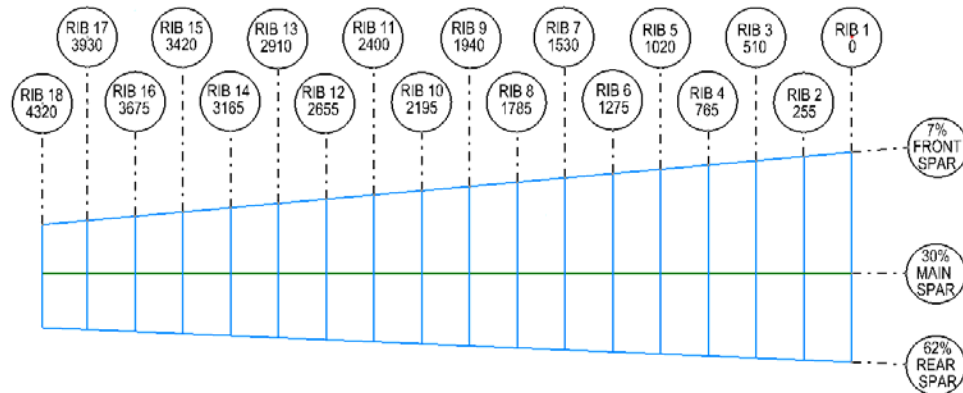
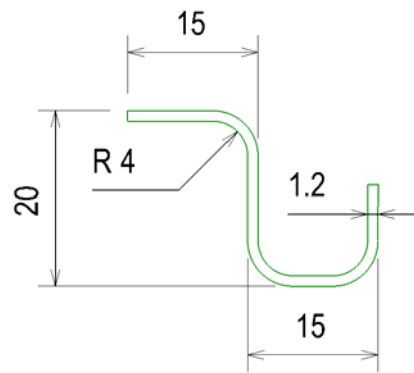
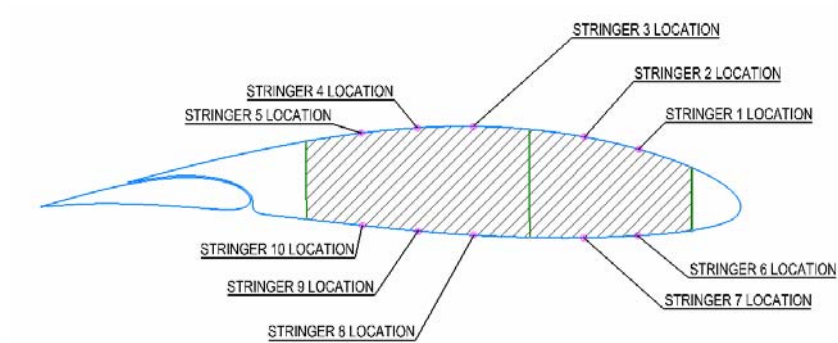


Figure 4.6 Spar locations and initial rib spacing

In the skin stringer panels a total of 10 stringers are utilized. Half of these stringers are on the upper skin panel and half of them are on the lower skin panel. Between front spar and main spar, there are 2 stringers whereas between main spar and rear spar there are 3 stringers. The cross section of stringers utilized in the initial FE model is Z-bulb section. (Figure 4.7)



(a)



(b)

Figure 4.7 (a) Typical Z-bulb stringer cross-section and dimensions

(b) Stringer locations

4.3 Systems Located in the Wing

Some of the systems that have vital importance for the survival of the airplane are located in the wing structure. Among these systems, the most important are fuel system, landing gear system and flight control systems including aileron and flap. Installation of these systems must be taken into consideration in the

optimization process because of space allocation reasons. In addition, the concentrated shear forces and inertia loads produced by these systems must be considered. The systems that are in the scope of this concern are:

- i) Fuel system
- ii) Landing gear system
- iii) Flight control system

4.3.1 Fuel System

Fuel is stored in the integral fuel tank cells in the wing. Integral tanks are areas inside the aircraft structure that have been sealed to allow fuel storage. Natural cells are formed in the wing structure by means of rib and spar webs that cross each other perpendicularly. In this case, fuel is stored in 13 such cells. The total weight of fuel stored in one wing is about 220 kg's. Therefore, the average weight of fuel stored in one cell is about 17 kg's. (Figure 4.8)

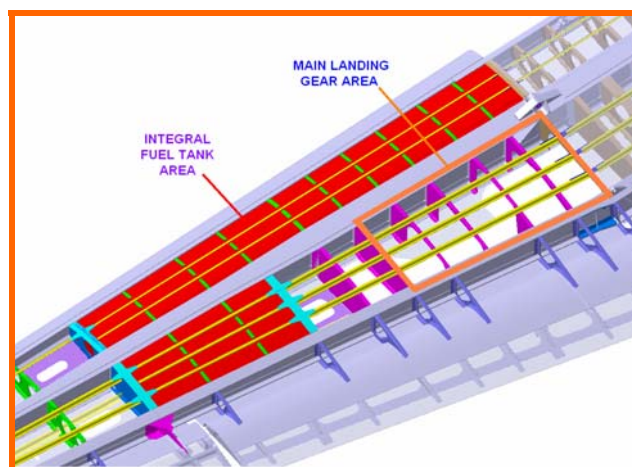


Figure 4.8 Fuel in the fuel tank is distributed to 13 cells formed by spar webs and ribs

4.3.2 Landing Gear System

Main Landing Gear (MLG) is directly connected to the 5th rib in order resist the concentrated shear forces during landing. Therefore, location of the 5th rib (892 mm from the wing root) is fixed and not a design parameter. Rib spacing of the initial model is determined by locating the ribs between first and 5th ribs with equal spacing of 223 mm and the ribs between 5th rib and 18th rib with a spacing of 277.5 mm.

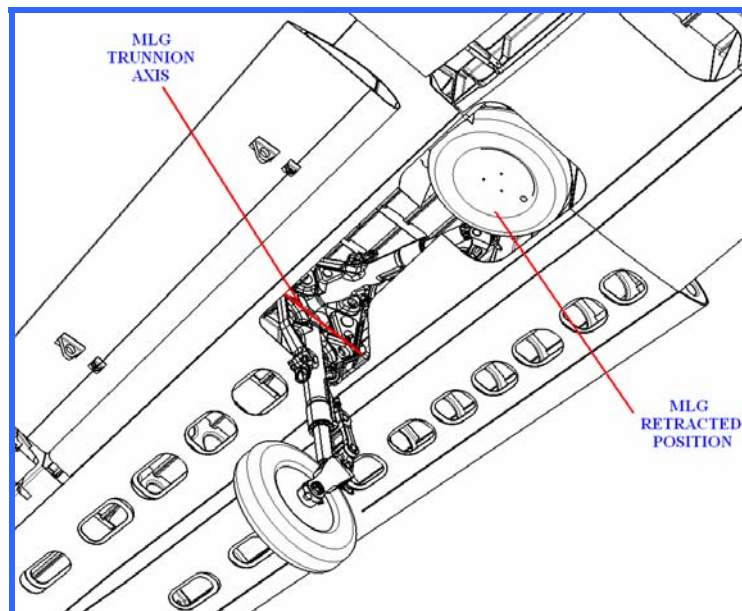


Figure 4.9 *Main Landing Gear Installation on Wing. Main landing gear is installed on the 5th rib of the wing*

4.3.3 Flight control system

Position of the rear spar is located at 62 % of the chord. The driving requirement for the position of the rear spar is flight control system (FCS) fittings. The rear spar plane should be located as to ensure enough space for the FCS installation fittings at the trailing edge. Main spar web is located in such a plane to provide largest possible web height in order to obtain the largest bending stiffness for main spar since moment of inertia of the spar web (i.e. I_{xx}) changes proportional to the 3rd power of the web height. Therefore main spar web is located at 30% of the wing chord. Finally, front spar is located at 7% of the wing chord in order to provide sufficient volume for integral fuel tank. Therefore, spar locations are constant and not design parameters of the optimization problem.

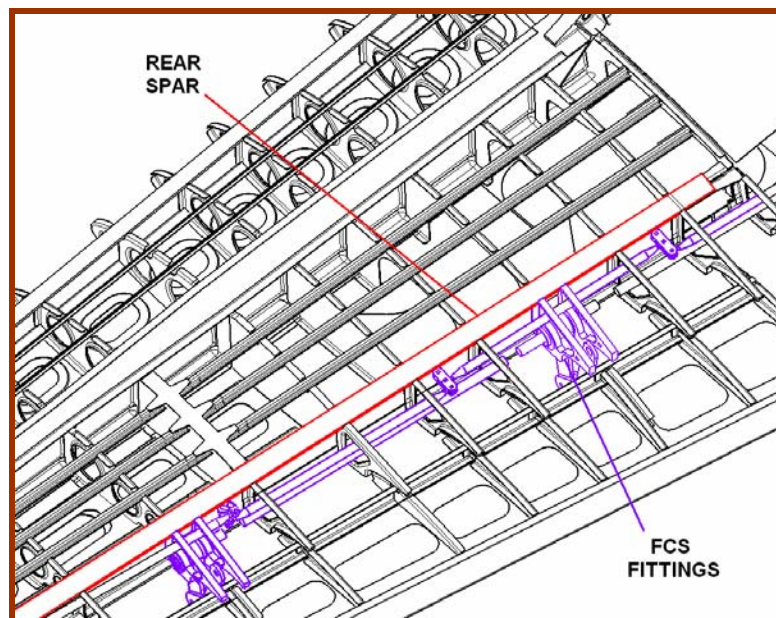


Figure 4.10 *Flight control system (FCS) installation on wing. Rear spar of the structure is located at 62% of the wing chord in order to provide sufficient space for FCS installation fittings*

4.4 Wing Finite Element Modeling

In this study finite element method is utilized as the analysis method for the optimization process. MSC/PATRAN[®] commercial package is used as the preprocessor and MSC.NASTRAN[®] is used as the solver for the analysis.

4.4.1 Material Properties

The material properties of sheet metal aluminum are Young modulus 71600 N/mm², mass density 2.7 10⁻⁶ Kg/mm³ and Poisson coefficient 0.33. In addition, 300 MPa has been used as tensile allowable for the maximum stress analysis.

4.4.2 FEM Elements Used in the Wing Members

In order to evaluate the design constraints and to model the wing structure, a finite element analysis is performed by using conventional finite element solvers (i.e. MSC/NASTRAN[®]). Also MSC/PATRAN[®] is used as preprocessor and postprocessor tool.

Because the FE model of the wing is very coarse (typically one element per frame/stringer pitch), it is more accurate to take the grid point forces from FE results for justification of frames instead of the stress values of the elements. Stress values have to be derivated (consideration of effective widths, distribution of loads to webs and caps, etc.). FE meshing procedure is described here. Every physical region on the wing skin panels bounded by two

stringers and two ribs are represented by using one element. In a similar manner each panel on the spar webs bounded by two ribs on left hand side and right hand side and bounded by spar caps on lower side and upper side are modeled using one shell element. Finally, each piece of stringer or spar cap separated by two ribs are modeled using one beam element. This FE modeling method is widely used in the finite element analyses performed in the aerospace industry. [26]

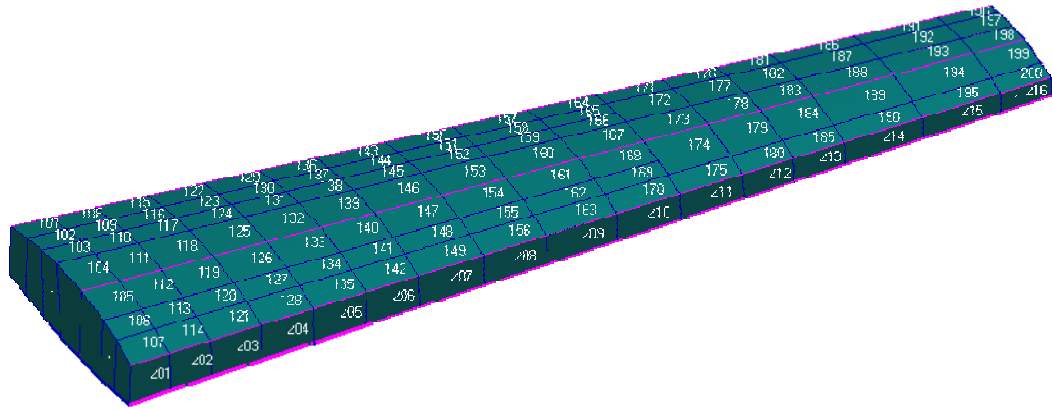


Figure 4.11 Complete wing FE model and element numbering

The total number of grid points (i.e. nodes) in the complete FE model is 2367. CQUAD elements have been utilized for modeling the skins, spar webs and rib webs. The element property associated to CQUAD element is PSHELL. The number of CQUAD elements in the model is 385. A total of 282 CAR elements have been used to model stringers and spar caps. The element property associated to CBAR element is PBAR. In addition, there are 13 point elements in the model in order to represent the inertia effects of the mass of the fuel in the cells of the integral fuel tank. These point elements, which have 0D elements properties, are connected to the main frame by means MPC elements. As a result, there are 13 MPC (RBE 3) elements.(Figure 4.12)

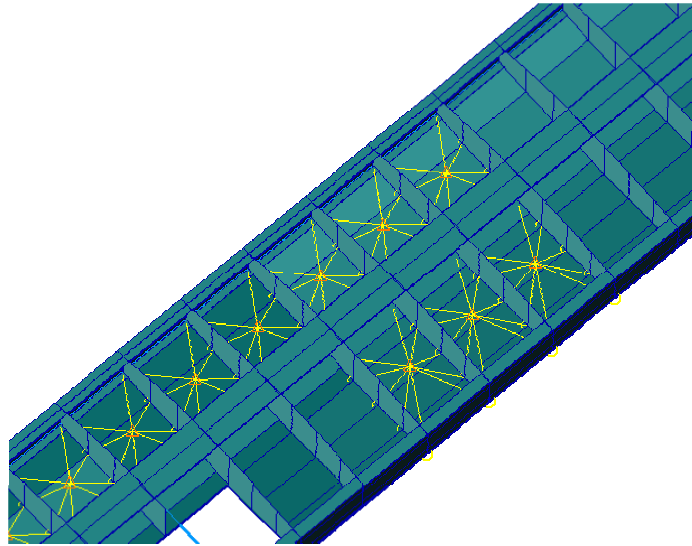


Figure 4.12 *Introducing the inertia effects of the fuel in the integral fuel tank*

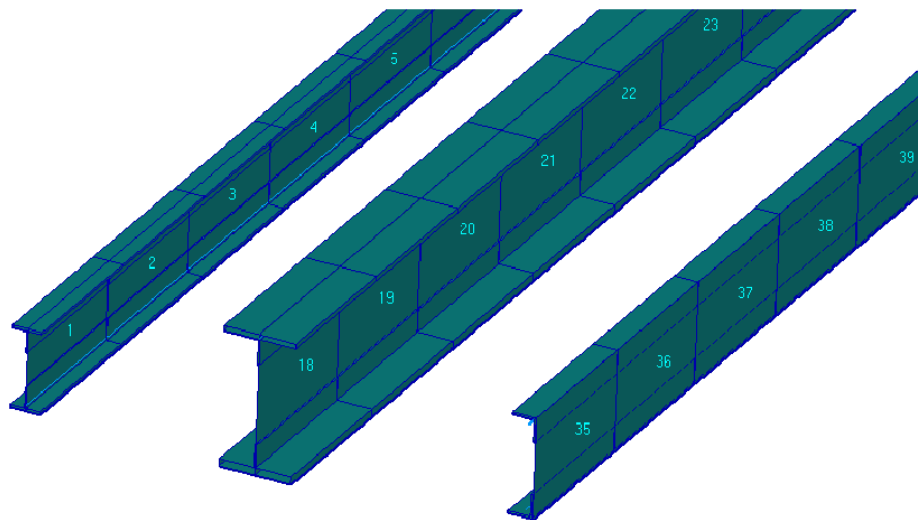


Figure 4.13 *FE model of wing spars*

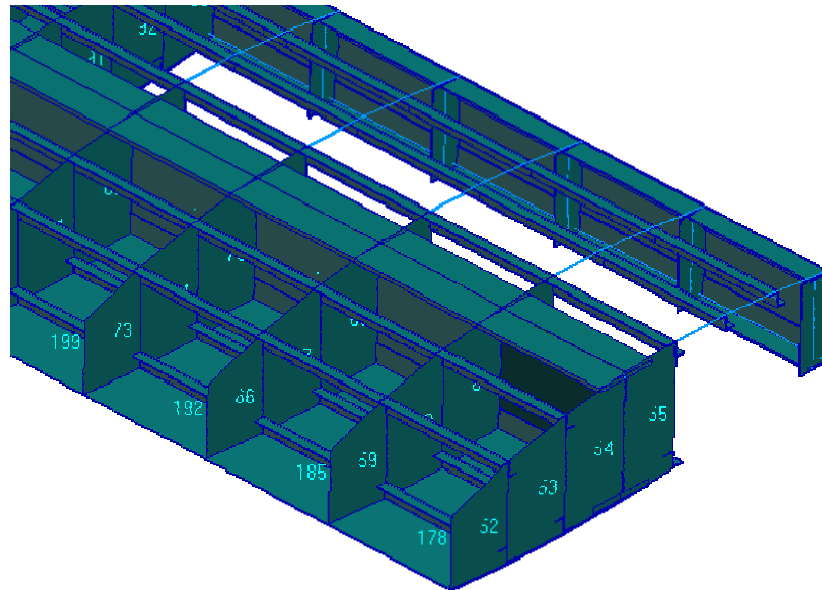


Figure 4.14 *FE model of ribs and stringers*

4.4.3 Loads and Boundary Conditions

4.4.3.1 Static Boundary Conditions

As previously discussed, the wing is assumed to be a cantilever structure. Therefore, it is clamped at the root section at spar locations only. (Figure 4.15). 6 DOF's are fixed in the clamped mode.

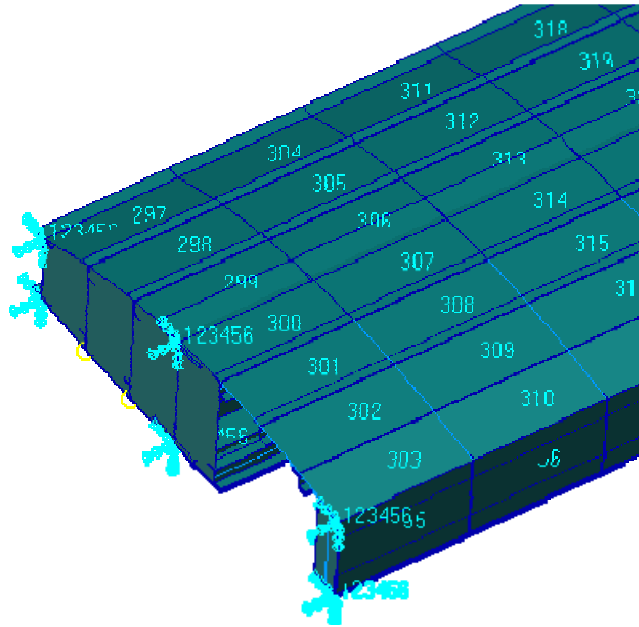


Figure 4.15 *Static boundary conditions on wing root section*

4.4.3.2 Flight Loads

The weight of the trainer aircraft to be examined is about 3000 kg. Maximum and minimum g levels of the aircraft are +7g and -3.5g since it is an acrobatic type aircraft. Among these loading conditions +7g is chosen as the design load case since it is the most critical load case. Since in normal straight and level flight the wing lift supports only the weight of the airplane the maximum positive lift on the aircraft is:

$$F=m \cdot a \quad \Rightarrow \quad F_{\text{lift}}=3000 \cdot 7 \cdot 9.81 \quad \Rightarrow \quad F_{\text{lift}}=206010 \text{ N} \quad (4.1)$$

Equation 4.1 describes the total lift force on wing surface on the wing surface. This load is also called the limit load. In addition, wing ultimate load can be calculated by multiplying the limit load by a safety factor. This safety factor is generally taken as 1.5 in aviation industry.

$$F_{\text{ultimate}} = F_{\text{limit}} \cdot 1.5 \Rightarrow F_{\text{ultimate}} = 206010 \cdot 1.5 \Rightarrow F_{\text{ultimate}} = 309015 \text{ N} \quad (4.2)$$

The load on one wing is half of the ultimate load which is 154507.5 N. Total wing load is distributed on the wing surfaces in a similar way as shown in Figure B.18 using the grid points in the FEM model. (Figure 4.16)

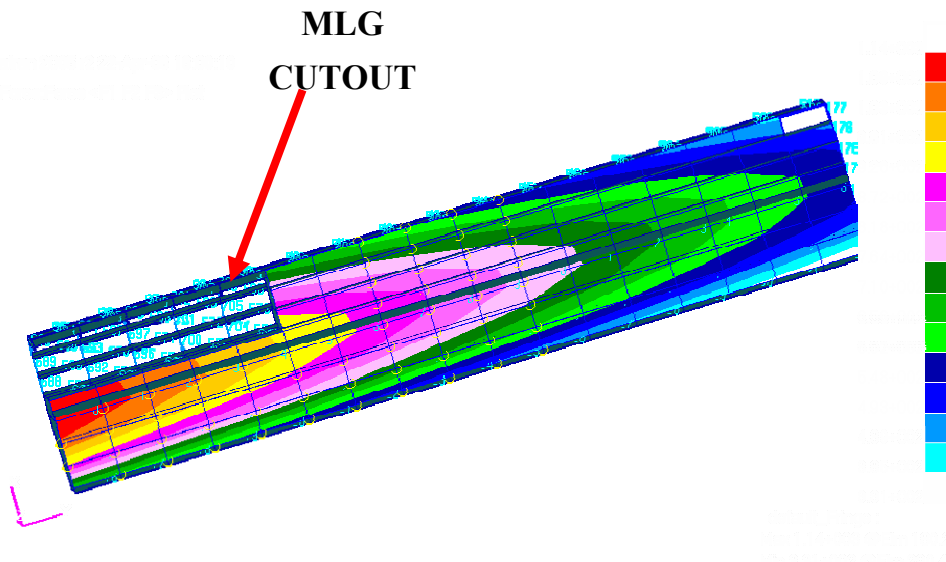


Figure 4.16 *Load distributions on the lower surface of wing FEM model in +7g load case*

4.5 Parameterization of Wing Structure

Since this is basically, an optimization problem, a set of unknowns or variables, which define the model and affect the value of the objective function, has to be determined. In this case, the set of unknowns are the parameters. MSC.Nastran commercial program can simultaneously solve both member dimension (sizing) and coordinate location (shape) optimization problems and a wide range of options are available to define the design variables. For example, design variables may be individual member dimensions and/or grid locations, or may be linear or nonlinear combinations of these.

A total of 53 design variables, including size and shape design variables, are defined for the wing model. These can be classified as follows:

1. Front spar web thickness
2. Main spar web thickness
3. Rear spar web thickness
4. Lower skin thickness
5. Upper skin thickness
6. Thickness properties of 18 ribs
7. Stringer thickness
8. Stringer geometric dimensions (Figure 4.17)
9. Spar cap geometric dimensions (Figure 4.18)
10. Spacing between each successive rib. (Figure 4.19 & Figure 4.20)

Table 4.1 Table of optimization design variables

| VARIABLE NUMBER | VARIABLES | DEFINITION |
|------------------------|------------------|---------------------------|
| 1 | SP1 | Front spar web thickness |
| 2 | SP2 | Main spar web thickness |
| 3 | SP3 | Rear spar web thickness |
| 4 | SK1 | Lower skin thickness |
| 5 | SK2 | Upper skin thickness |
| 6 | RB1 | 1. Rib thickness |
| 7 | RB2 | 2. Rib thickness |
| 8 | RB3 | 3. Rib thickness |
| 9 | RB4 | 4. Rib thickness |
| 10 | RB5 | 5. Rib thickness |
| 11 | RB6 | 6. Rib thickness |
| 12 | RB7 | 7. Rib thickness |
| 13 | RB8 | 8. Rib thickness |
| 14 | RB9 | 9. Rib thickness |
| 15 | RB10 | 10. Rib thickness |
| 16 | RB11 | 11. Rib thickness |
| 17 | RB12 | 12. Rib thickness |
| 18 | RB13 | 13. Rib thickness |
| 19 | RB14 | 14. Rib thickness |
| 20 | RB15 | 15. Rib thickness |
| 21 | RB16 | 16. Rib thickness |
| 22 | RB17 | 17. Rib thickness |
| 23 | RB18 | 18. Rib thickness |
| 24 | STR1 | Stringer thickness |
| 25 | STR2 | Stringer dimension 1 |
| 26 | STR3 | Stringer dimension 2 |
| 27 | STR4 | Stringer dimension 3 |
| 28 | STR5 | Stringer dimension 4 |
| 29 | CAP1 | Main Spar cap dimension 1 |
| 30 | CAP2 | Main Spar cap dimension 2 |
| 31 | CAP3 | Main Spar cap dimension 3 |

Table 4.1 *Table of optimization design variables (cont'd)*

| VARIABLE NUMBER | VARIABLES | DEFINITION |
|------------------------|------------------|----------------------------|
| 32 | CAP5 | Rear Spar cap dimension 1 |
| 33 | CAP6 | Rear Spar cap dimension 2 |
| 34 | CAP7 | Rear Spar cap dimension 3 |
| 35 | CAP9 | Front Spar cap dimension 1 |
| 36 | CAP10 | Front Spar cap dimension 2 |
| 37 | CAP11 | Front Spar cap dimension 3 |
| 38 | SPC1 | Rib Spacing 1 |
| 39 | SPC2 | Rib Spacing 2 |
| 40 | SPC3 | Rib Spacing 3 |
| 41 | SPC4 | Rib Spacing 4 |
| 42 | SPC5 | Rib Spacing 5 |
| 43 | SPC6 | Rib Spacing 6 |
| 44 | SPC7 | Rib Spacing 7 |
| 45 | SPC8 | Rib Spacing 8 |
| 46 | SPC9 | Rib Spacing 9 |
| 47 | SPC10 | Rib Spacing 10 |
| 48 | SPC11 | Rib Spacing 11 |
| 49 | SPC12 | Rib Spacing 12 |
| 50 | SPC13 | Rib Spacing 13 |
| 51 | SPC14 | Rib Spacing 14 |
| 52 | SPC15 | Rib Spacing 15 |
| 53 | SPC16 | Rib Spacing 16 |

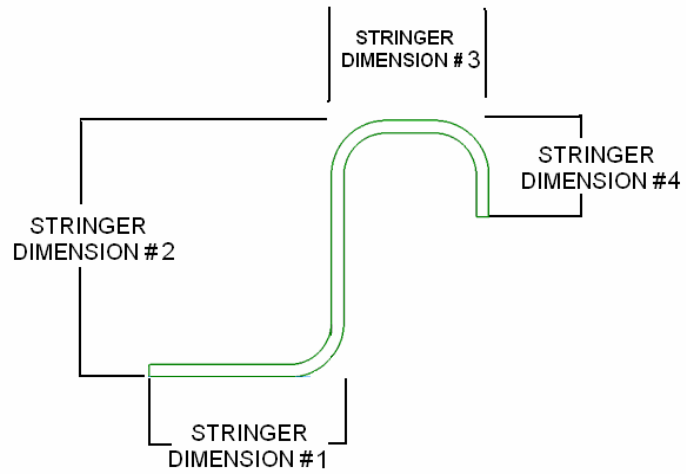


Figure 4.17 *Stringer geometric dimensions*

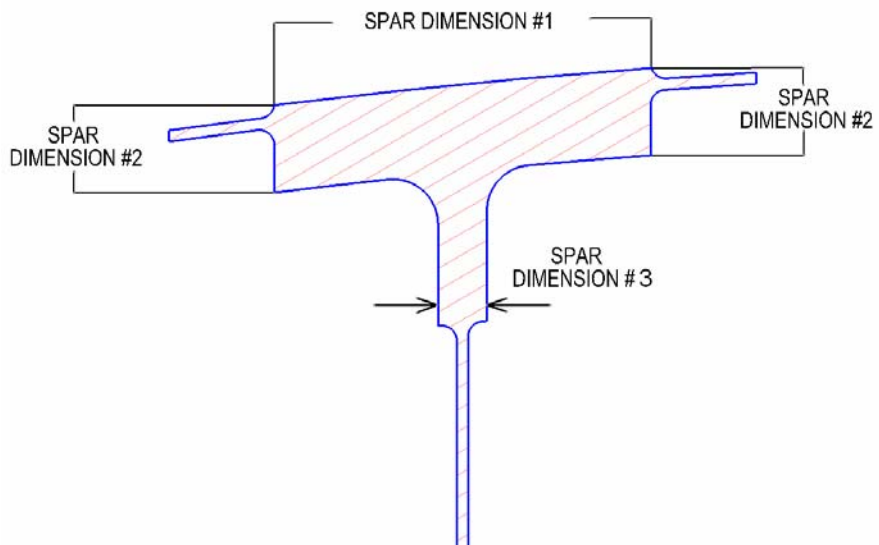


Figure 4.18 *Spar cap geometric dimensions*

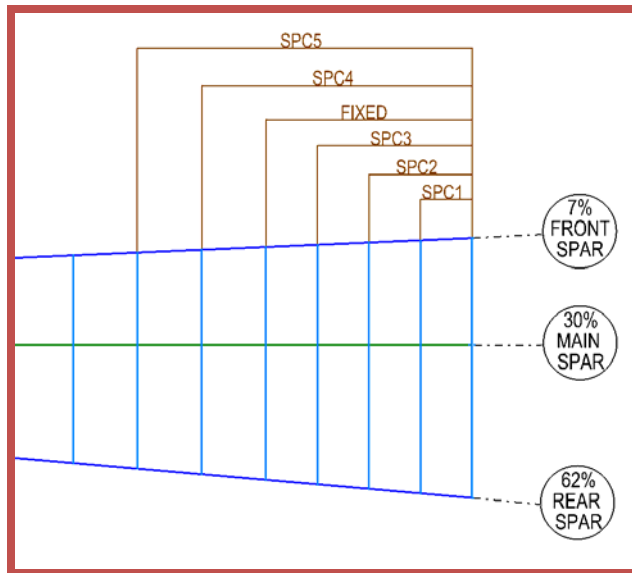


Figure 4.19 Rib reference planes (wing top view)

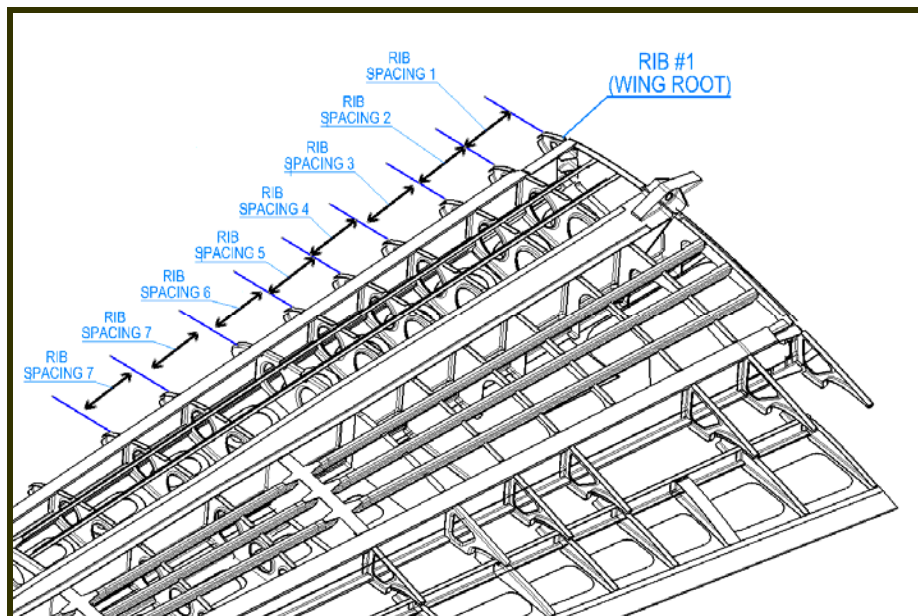


Figure 4.20 Rib spacings shown in 3D model

Genetic algorithm is a heuristic search method that is not guaranteed to find the optimum, but usually gives a very good solution though it cannot guarantee to do even that every time. The parameters previously discussed are utilized as the design variables of the genetic algorithm. Each parameter has a data set constituting of 15 values among which the most appropriate value leading to the best possible design is chosen. This means the genetic algorithm program utilized for this study works on discrete domain. The advantage of discrete domain against continuous domain is that working on continuous domain can take excessive time (and possibly computer memory) for problems that are larger and medium scale. The discrete data set values for the design parameters are presented in Table 4.2

Table 4.2 *Data sets for design parameters*

| | Stringer Dimensions | Rib Spacings | Front Spar Web Thickness | Main Spar Web Thickness | Rear Spar Web Thickness |
|-----------|----------------------------|---------------------|---------------------------------|--------------------------------|--------------------------------|
| 0 | 20 25 20 8 | 200 | 0,6 | 1 | 0,8 |
| 1 | 15 20 15 8 | 210 | 0,8 | 1,2 | 1 |
| 2 | 20 25 20 8 | 220 | 1 | 1,4 | 1,2 |
| 3 | 15 20 15 8 | 230 | 1,2 | 1,6 | 1,4 |
| 4 | 20 25 20 8 | 240 | 1,4 | 1,8 | 1,6 |
| 5 | 15 20 15 8 | 250 | 1,6 | 2 | 1,8 |
| 6 | 20 25 20 8 | 260 | 1,8 | 2,2 | 2 |
| 7 | 15 20 15 8 | 270 | 2 | 2,4 | 2,2 |
| 8 | 20 25 20 8 | 280 | 2,2 | 2,6 | 2,4 |
| 9 | 15 20 15 8 | 290 | 2,4 | 2,8 | 2,6 |
| 10 | 20 25 20 8 | 300 | 2,6 | 3 | 2,8 |
| 11 | 15 20 15 8 | 310 | 2,8 | 3,2 | 3 |
| 12 | 20 25 20 8 | 320 | 3 | 3,4 | 3,2 |
| 13 | 15 20 15 8 | 330 | 3,2 | 3,6 | 3,4 |
| 14 | 20 25 20 8 | 340 | 3,4 | 3,8 | 3,6 |
| 15 | 15 20 15 8 | 350 | 3,6 | 4 | 3,8 |

Table 4.2 Data sets for design parameters (cont'd)

| | Stringer Thickness | Rib Thickness | Skin Thickness | Spar Cap Dimension 1 | Spar Cap Dimension 2 | Spar Cap Dimension 3 |
|-----------|---------------------------|----------------------|-----------------------|-----------------------------|-----------------------------|-----------------------------|
| 0 | 1,2 | 0,6 | 0,8 | 30 | 2 | 1 |
| 1 | 1,2 | 0,8 | 1 | 40 | 3 | 2 |
| 2 | 1,2 | 1 | 1,2 | 50 | 4 | 3 |
| 3 | 1,2 | 1,2 | 1,4 | 60 | 5 | 4 |
| 4 | 1,2 | 1,6 | 1,6 | 70 | 6 | 5 |
| 5 | 1,2 | 1,8 | 1,8 | 80 | 7 | 6 |
| 6 | 1,2 | 2 | 2 | 90 | 8 | 7 |
| 7 | 1,2 | 2,2 | 2,2 | 100 | 10 | 8 |
| 8 | 1,2 | 2,4 | 2,4 | 110 | 12 | 9 |
| 9 | 1,2 | 3 | 2,6 | 120 | 14 | 10 |
| 10 | 1,2 | 3,2 | 2,8 | 130 | 16 | 11 |
| 11 | 1,2 | 3,4 | 3 | 140 | 18 | 12 |
| 12 | 1,2 | 4 | 3,2 | 150 | 20 | 13 |
| 13 | 1,2 | 4,2 | 3,4 | 160 | 22 | 14 |
| 14 | 1,2 | 4,6 | 3,6 | 170 | 24 | 15 |
| 15 | 1,2 | 5 | 3,8 | 180 | 26 | 16 |

4.3 Stress and Instability Analyses for Structural Members

Wing structural design optimization problem is actually a constrained minimization problem whose objective function is the mass of the wing. The solution for each population is graded according to its fitness. The fitness value of each population is certainly decided according to the mass of the whole wing structure in corresponding population. As discussed in the previous chapters, wing stress analysis mainly depends on instability of thin sheets and columns. Stress states of panels are decided according to the loading condition, which the sheet is subject to. As shown in Figure 4.22 , Figure 4.25 and Figure 4.28 under an external load of +7g the loading condition on upper skin and ribs is combined axial compression and in plane shear; the loading

condition on lower skin is axial tension; the loading condition on spar webs is combined bending and in plane shear. On the other hand, the loading condition on spar caps and stringers on the upper skin is axial compression and the loading condition on spar caps and stringers on the lower skin is axial tension. Depending on the loading conditions on the members, reserve factors (RF's) on each element can be calculated using the following interaction equations:

$(R_s^2 + R_c)$ interaction curve is used for the stress analyses of members under combined shear and compression (upper skin). RF is defined as $(R_s^2 + R_c)/1$ in this case. R_s and R_c are called the shear stress ratio and compression stress ratio respectively and defined by equations B.29 and B.28 in Appendix_B.

$(R_s^2 + R_b^2)$ interaction curve is used for the stress analysis of members under combined shear and bending (spar webs). RF is defined as $(R_s^2 + R_b^2)/1$ in this case. R_b is called the bending stress ratio and defined by equation B.30 in Appendix B.

Maximum stress failure case is considered for the stress analyses of members under axial tension. (lower skin and spar caps and stringers on the lower skin). In this case, RF is defined as maximum allowable tensile stress divided by actual tensile stress.

(i.e. $RF = \sigma_{all} / \sigma_{tensile}$)

For the stress analyses of members under axial compression load (SPAR CAPS AND STRINGERS ON THE UPPER SKIN) RF is defined as $F_{cr}/F_{compressive}$ where F_{cr} is defined by equation B.4 of Appendix B.

$$F_{cr} = \frac{\Pi^2 E}{\left(\frac{L'}{\rho}\right)^2} \quad (B.4)$$

4.3.1 Instability Analyses for Spar Webs

As mentioned before in this study MSC.PATRAN is used as the preprocessing and post processing tool and MSC.NASTRAN as the solver program. Furthermore MSC.NASTRAN is only used to obtain element nodal forces but not for Von Mises stress or shear stress calculations. Since, in this study structural optimization is performed according to instability analysis. For instance, The first element of the FEM model (i.e. CQUAD #1) is the element of the front spar at the root section. The node numbers of this element are; 1, 9, 17 and 25 as shown in Figure 4.21.

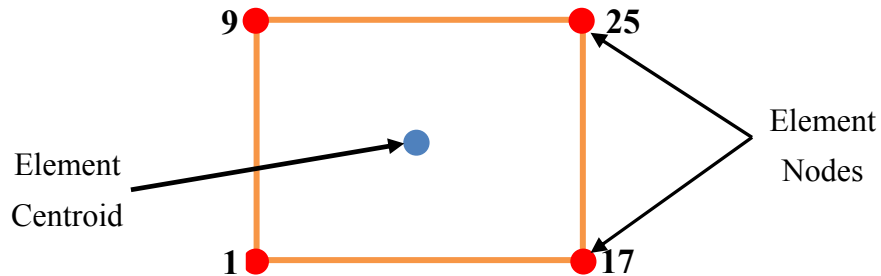


Figure 4.21 Nodes and centroid of the CQUAD #1 (i.e. front spar web first element)

As previously discussed spar web elements are under combined shear and bending load. Therefore the instability analysis for these elements are performed according to the interaction curve $R_s^2 + R_b^2 = 1.0$ for a RF of 1. The state of stress of spar web elements can be seen in Figure 4.22.

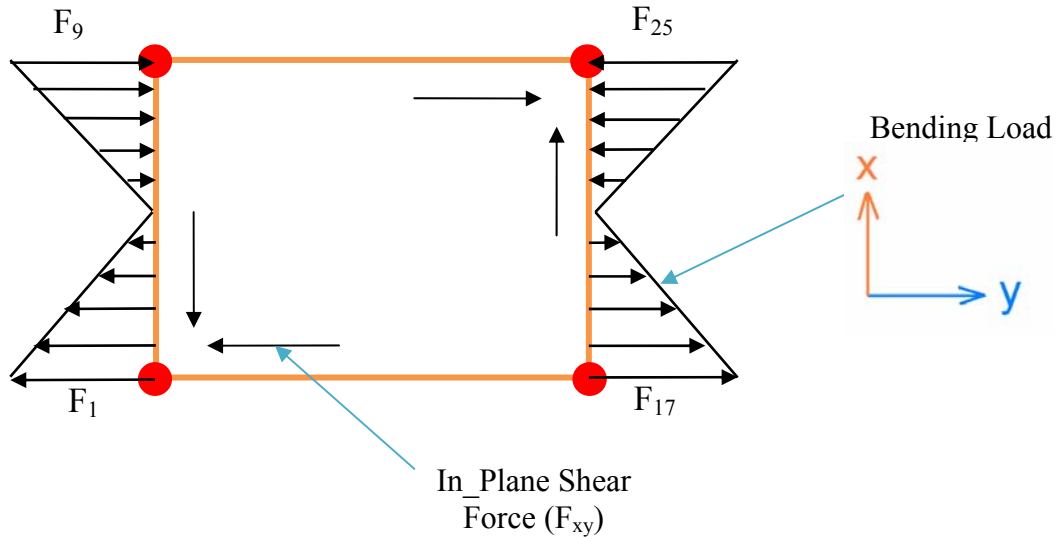


Figure 4.22 *Stress state of spar web element in the wing structure*

In order to calculate $R_s^2 + R_b^2$, both R_s and R_b must be determined first. In order to obtain R_s and R_b , applied loads must be calculated because R_b and R_s are both equal to applied stress divided by critical buckling stress as shown below.

$$R_b = \frac{f_b}{F_{b,cr}} \qquad R_s = \frac{f_s}{F_{s,cr}}$$

$F_{s,cr}$ and $F_{b,cr}$ can be calculated using the formulae A.23 and A.27 respectively.

In addition, f_s and f_b can be calculated using the element forces supplied by the output file of MSC.NASTRAN having an extension of F06. Centroidal and nodal element forces of CQUAD #1 can be seen in Figure 4.23.

| ELEMENT | | - MEMBRANE FORCES - | | | |
|---------|---------|---------------------|---------------|--------------|--|
| ID | GRID-ID | FX | FY | FGY | |
| 1 | CEN/4 | 8.567771E+00 | 3.383663E+01 | 1.328641E+02 | |
| | 1 | 1.116609E+01 | 6.477789E+02 | 1.328641E+02 | |
| | 9 | 1.116609E+01 | -5.801057E+02 | 1.328641E+02 | |
| | 25 | 5.969452E+00 | -5.801057E+02 | 1.328641E+02 | |
| | 17 | 5.969452E+00 | 6.477789E+02 | 1.328641E+02 | |
| 2 | CEN/4 | 1.377437E+00 | 2.066342E+01 | 5.250114E+01 | |
| | 17 | 1.622292E+00 | 2.891215E+02 | 5.250114E+01 | |
| | 25 | 1.622292E+00 | -2.477947E+02 | 5.250114E+01 | |
| | 41 | 1.132582E+00 | -2.477947E+02 | 5.250114E+01 | |
| | 33 | 1.132582E+00 | 2.891215E+02 | 5.250114E+01 | |

Figure 4.23 Element forces of front spar first element. Forces in blue frame are average element forces at the centroid of the element. Values in the yellow frame represent the in plane shear forces (i.e. F_{xy}). Finally, forces in the red frame represent the bending forces in y-direction. As a conservative approach, the force having the largest magnitude is taken as the bending force. In this case, $6.47E+02$ is taken as the bending load.

The unit of the force output of MSC.NASTRAN is N/m. In other words, MSC.NASTRAN supplies element forces per unit length. Therefore dividing the forces in Figure 4.23 by the thickness gives the applied stress value.

4.3.2 Instability Analyses for Upper Skin

In a similar manner, stress values in the upper skin elements can be calculated. The state of stress in the upper skin is in plane shear stress (τ_{xy}) and axial compression load. One of the elements of the upper skin at the root section is CQUAD #299. The nodes and the centroid of the element can be seen in Figure 4.24.

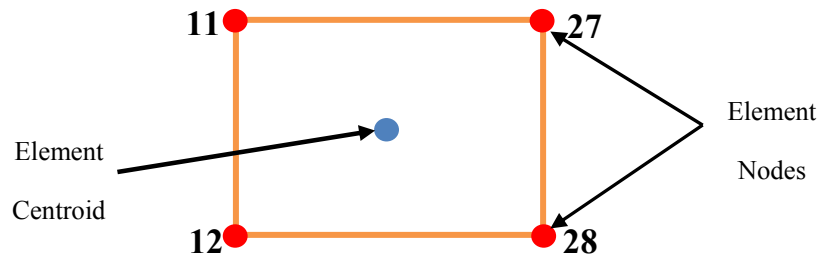


Figure 4.24 Nodes and centroid of the CQUAD #299 (i.e. upper skin element at the root section)

As previously discussed upper skin elements are under combined shear and compression load. Therefore the instability analysis for these elements are performed according to the interaction curve $R_s^2 + R_c = 1.0$ for a RF of 1 where R_s and R_c are the shear stress ratio and compression stress ratio and given in equations B.28 and B.29. The state of stress of upper skin elements can be seen in Figure 4.25.

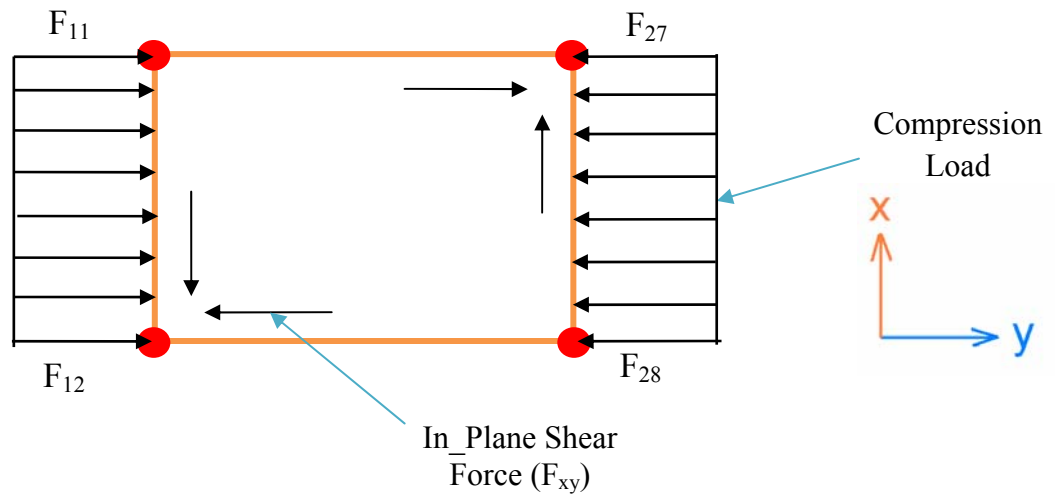


Figure 4.25 *Stress state of upper skin elements in the wing structure*

$F_{s,cr}$ and $F_{c,cr}$ can be calculated using the formulae B.23 and B.27 of Appendix B respectively.

In addition, f_s and f_c can be calculated using the element forces supplied by the output file of MSC.NASTRAN having an extension of F06. However, it should be noted that the element forces provided by the F06 file have a unit of N/m. Therefore dividing the element force by the element thickness gives the element stress. Centroidal and nodal element forces of CQUAD #299 can be seen in Figure 4.26

| ELEMENT | | - MEMBRANE FORCES - | | | |
|---------|---------|---------------------|---------------|---------------|-----|
| ID | GRID-ID | FX | FY | FX | FXY |
| | 26 | -3.975938E+01 | -1.314025E+02 | -2.204933E+02 | |
| | 25 | -3.975938E+01 | -5.988641E+02 | -2.204933E+02 | |
| 298 | CEN/4 | -2.814382E+01 | -1.258370E+02 | 2.194864E+01 | |
| | 10 | 2.141422E+01 | -1.135947E+02 | 2.194864E+01 | |
| | 11 | 2.141422E+01 | -1.380794E+02 | 2.194864E+01 | |
| | 27 | -7.770185E+01 | -1.380794E+02 | 2.194864E+01 | |
| | 26 | -7.770185E+01 | -1.135947E+02 | 2.194864E+01 | |
| 299 | CEN/4 | -1.264913E+02 | -5.810181E+02 | 3.543518E+02 | |
| | 11 | -2.428980E+02 | -1.705341E+02 | 3.543518E+02 | |
| | 12 | -2.428980E+02 | -9.915022E+02 | 3.543518E+02 | |
| | 28 | -1.008453E+01 | -9.915022E+02 | 3.543518E+02 | |
| | 27 | -1.008453E+01 | -1.705341E+02 | 3.543518E+02 | |

Figure 4.26 Element forces of upper skin element (CQUAD #299). Forces in blue frame are average element forces at the centroid of the element. Values in the yellow frame represent the in plane shear forces (i.e. F_{xy}). Finally, forces in the red frame represent the compression forces in y-direction. As a conservative approach, the force having the largest magnitude is taken as the bending force. In this case, the absolute value of $-9.91E+02$ is taken as the compression load.

The lift force in spanwise direction compresses upper skin. Therefore, F_y is accepted as the axial compression load. The orientation of the element can also be seen in the element local coordinate system in Figure 4.27.

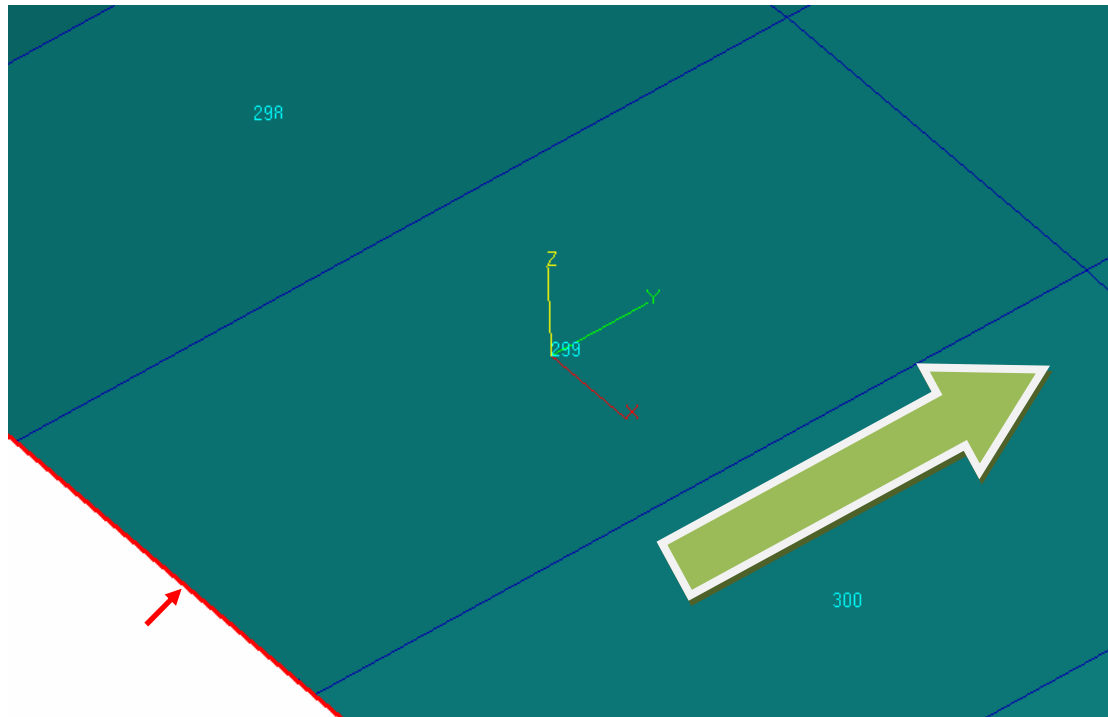


Figure 4.27 *Upper skin CQUAD element orientation. Red arrow indicates the wing root and green arrow indicates the wing tip.*

4.3.3 Instability Analyses for Rib Webs

Ribs utilized in the wing structure are under compression load because of wing crushing load, which tends to squeeze the wing from both the lower surface and the upper surface. In addition to the axial compression load there is also an in plane shear load carried by the rib webs. Therefore, it can be concluded that the stress state of the ribs is similar to that of upper skin. Loading on the first rib element (i.e. CQUAD #52) which is at the front root end of the wing can be seen in Figure 4.28.

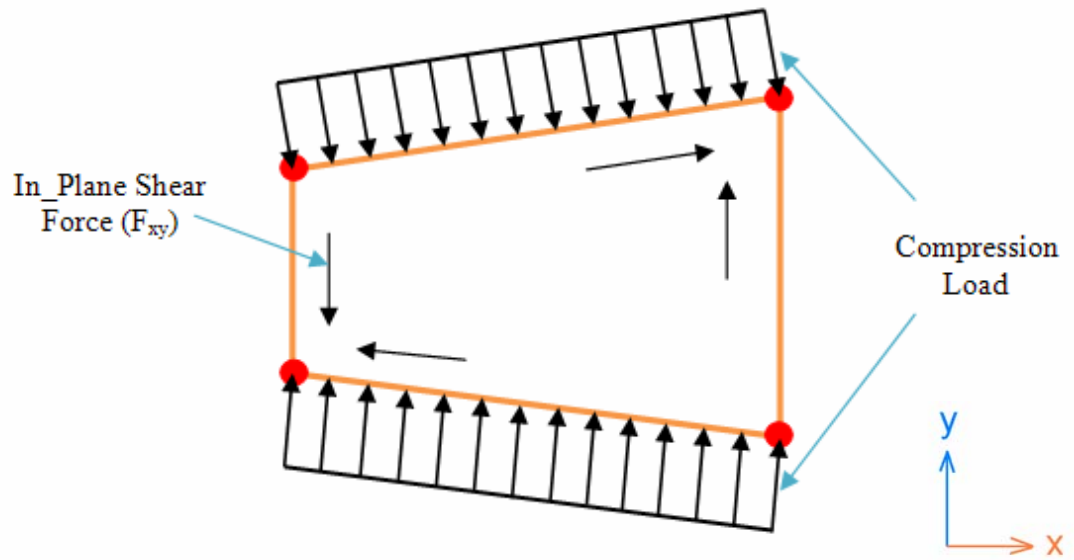


Figure 4.28 Loading on the first rib element (i.e. CQUAD #52)

As it can be seen from Figure 4.28 for the rib elements, the element local y-axis is in upward direction. Therefore, F_y is accepted as the rib compressive load. Centroidal and nodal element forces of CQUAD #52 can be seen in Figure 4.29.

| - MEMBRANE FORCES - | | | | | |
|---------------------|---------|---------------|---------------|--------------|-----|
| ELEMENT ID | GRID-ID | FX | FY | FX | FXY |
| 51 | CEN/4 | -6.785259E-03 | -1.813216E-01 | 3.726811E+00 | |
| | 264 | -7.236283E-01 | -7.807744E-01 | 3.726811E+00 | |
| | 272 | -7.236283E-01 | 4.181312E-01 | 3.726811E+00 | |
| | 288 | 7.100579E-01 | 4.181312E-01 | 3.726811E+00 | |
| | 280 | 7.100579E-01 | -7.807744E-01 | 3.726811E+00 | |
| 52 | CEN/4 | 4.481885E-01 | -3.690324E+00 | 1.220968E+01 | |
| | 1 | 1.776252E+01 | -1.972699E+00 | 1.366184E+01 | |
| | 2 | 1.283219E+01 | -5.050625E+00 | 1.312649E+01 | |
| | 10 | -1.205234E+01 | -5.242014E+00 | 1.114659E+01 | |
| | 9 | -1.696892E+01 | -2.158087E+00 | 1.090234E+01 | |

Figure 4.29 Element forces of rib element (CQUAD #52). Forces in blue frame are average element forces at the centroid of the element. Values in the yellow frame represent the in plane shear forces (i.e. F_{xy}). Finally, forces in the red frame represent the compression forces in y-direction. As a conservative approach, the force having the largest magnitude is taken as the bending force. In this case, the absolute value of $-5.24E+00$ is taken as the compression load. This time F_{xy} is not constant among the nodes of this element. Since the element has a trapezoidal shape rather than a rectangular shape. Therefore the maximum F_{xy} is taken as the in plane shear force.

4.3.4 Instability Analyses for Stringers and Spar Caps on the Upper Skin

Effective width concept in skin-stringer compression panels must be realized first, in order to better understand instability of stringers. The effective width of skin is that portion of skin supported by a stringer in a skin-stringer construction that does not buckle when subjected to axial compression load shown in Eq. (B.14)

$$F_{cr} = 3.62E \left(\frac{t}{L} \right)^2 \quad (\text{B.14})$$

Buckling of the skin alone does not constitute a panel failure; in fact, the panel will carry additional load up to the stress at which the stringer (or stiffener) starts to fail. As the stringer stress is increased beyond the skin buckling stress ($F_{cr,skin}$), the skin adjacent to the stringers will carry additional stress because of the support given by the stringers. It is noted that the stress at the center of the panel does not exceed the initial buckling stress no matter how high the stress becomes at the stringer.

It is seen that the skin is most effective at the stringers, where support against buckling exists. At a given stress, the effective width (b_e), as shown in Figure 4.14, is equal to the panel width at which buckling will just begin.

$$b_e = \left(\sqrt{\frac{K_c E}{F_{st}}} \right) \quad (4.1)$$

where: F_{st} is the stringer or stiffener allowable stress (generally the stringer crippling stress, F_{cc})

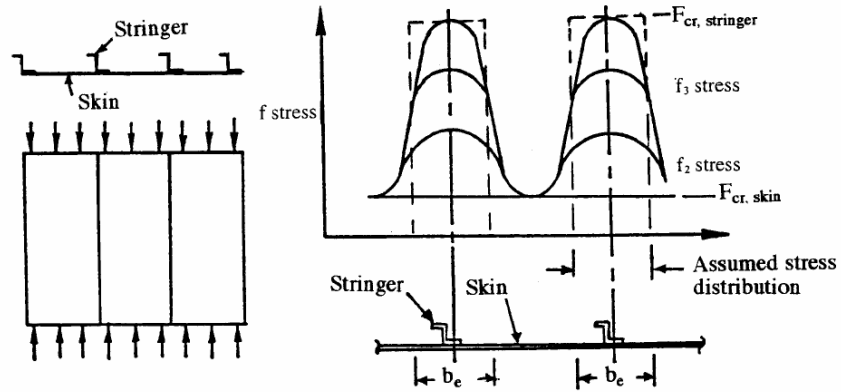


Figure 4.30 *Effective width of a skin stringer panel.* [22]

Because of the effective skin around a stiffener or stringer, one of the failure modes of a stringer is column buckling together with the skin around it having a width of b_e . Since this failure mode, case is generally more critical than the buckling of stringer alone, only calculation results for this failure mode is taken into account and going to be presented. Also sectional properties of the effective skin-stringer structure is calculated as if the structure acts like a single beam as shown in Figure 4.31.

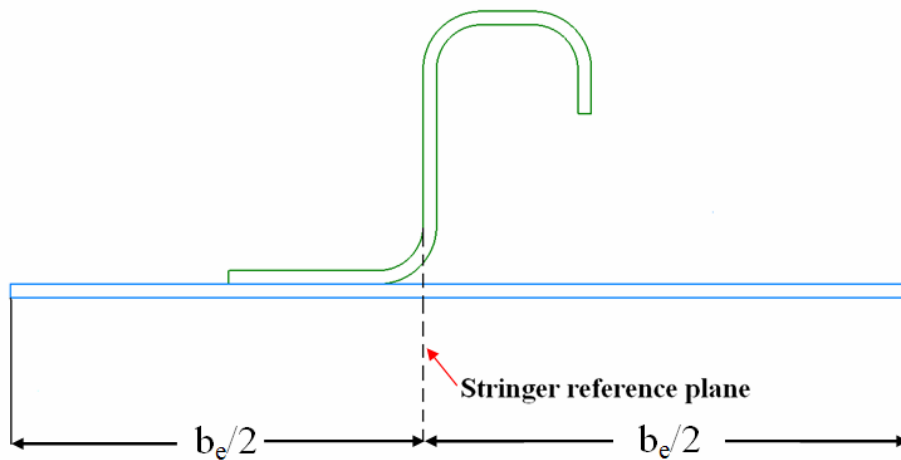


Figure 4.31 *Beam section constituting of stringer and effective skin*

Compression load on such a beam section is calculated by superposing the axial force on the stringer and a portion of the load on the skins adjacent to the stringer. The portion of the load on the skin, which is added to the force on the stringer, is proportional to effective width of the skin. In other words, force coming from the adjacent skin is equal to compression force on the skin at that node multiplied by the effective width of that skin panel divided by the whole width of that skin panel. The loading on the beams can be seen in Figure 4.32.

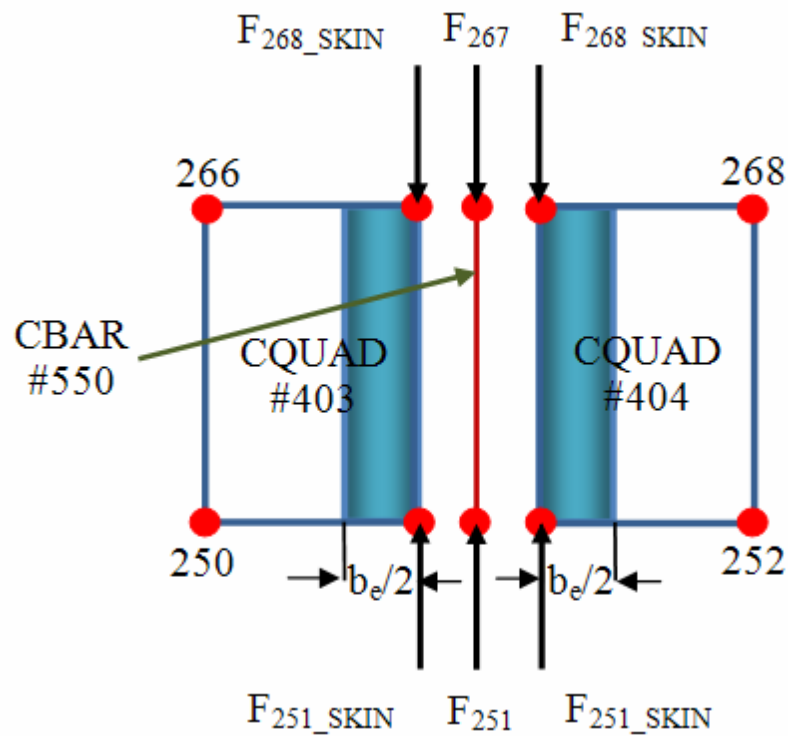


Figure 4.32 Loads on stringer (CBAR #550) and adjacent skin panels (CQUAD #403 and CQUAD #404). Red dots represent the nodes of elements and number next to dot is the number of that node.

4.3.5 Stress Analyses for Stringers and Spar Caps on the Lower Skin

Under a positive lift load on the wing spar caps and stringers on the lower skin are under tensile load. Therefore, for these elements, maximum stress analysis is performed instead of instability analysis.

The loading on the stringers and spar caps on the lower skin is shown in Figure 4.33.

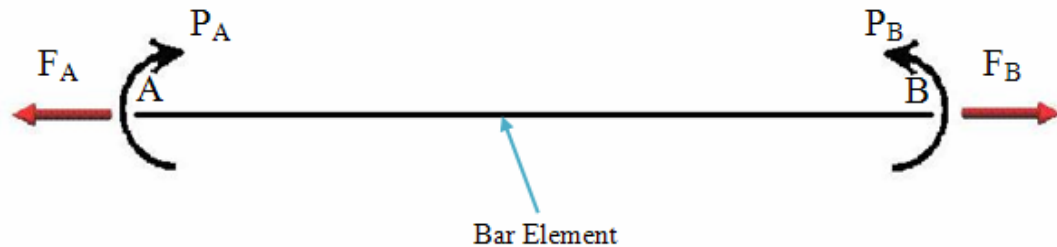


Figure 4.33 Primary loads on a stringer on the lower skin is axial tensile force and bending moment.

Because of the loading condition on these elements maximum stress value can be calculated using the following formulae;

$$\sigma_{\max} = \frac{Mc}{I} + \frac{F}{A} \quad (4.2)$$

Axial force is assumed to be constant along a stringer. Therefore, F_A is equal to F_B . P_A is the bending moment at end A and P_B is the bending moment at end B. Maximum of P_A or P_B is taken as the bending moment in equation 4.2.

Axial loads and bending moments on CBAR element 650 (i.e. one of the stringers on the lower skin) can be seen in F06 file output in figure 4.34.

| FORCES IN BAR ELEMENT | | | | |
|-----------------------|---------------------|---------------|---------------------|---------------|
| ELEMENT ID. | BEND-MOMENT PLANE 1 | END-A PLANE 2 | BEND-MOMENT PLANE 1 | END-B PLANE 2 |
| 650 | -3.552019E+03 | -5.368805E+02 | 4.877620E+03 | -3.248637E+02 |
| | - SHEAR - | | AXIAL FORCE | TORQUE |
| | PLANE 1 | PLANE 2 | | |
| | -3.180996E+01 | -8.000632E-01 | 1.319486E+03 | -3.052195E-01 |

Figure 4.34 Element forces on CBAR #650. Maximum of the bending moments in PLANE 1, which is $4.877E + 03$, is accepted as the bending moment value on this element.

Also for the members under tensile loading, a scatter factor of 1.5 is taken into account in order to count for fatigue failure. So maximum tensile allowable of the material is divided by 1.5 in this analysis.

4.3.5 Stress Analyses for Lower Skin

Maximum Von Mises stress values for lower skin elements are directly read from the F06 file since members constituting lower skin are under tension. In this analysis, again a scatter factor of 1.5 is used to take fatigue failure into account.

4.3.6 Reserve Factors of Wing Elements

RF value for all the elements in the FEM model should be greater than or equal to 1 for a convenient design. RF values getting larger than 1 are occurring as weight penalties in the optimization problem. Each population is graded according to RF values and genes having smallest but larger than 1 RF values gain the highest grades.

Buckling and von mises RF values for the elements in the FEM model are tabulated according to their locations on the wing.

| | | | | | | | | | | | | | | | | |
|--------|--------|--------|--------|--------|--------|--------|--------|--------|--------|--------|--------|--------|--------|---------|----------|--------|
| 826.81 | 679.05 | 442.63 | 347.13 | 323.73 | 300.34 | 276.94 | 253.55 | 230.16 | 206.76 | 183.37 | 159.98 | 136.58 | 113.19 | 89.7938 | 66.45 | 43.006 |
| 140.54 | 110.66 | 85.605 | 77.704 | 58.904 | 37.731 | 36.22 | 35.11 | 34021 | 32.89 | 31.78 | 28.67 | 25.56 | 22.45 | 19.34 | 16.23 | 13.12 |
| 25.358 | 24.002 | 22.645 | 21.289 | 19.932 | 18.575 | 17.219 | 16.031 | 14.295 | 13.066 | 11.919 | 13.413 | 16.422 | 16.887 | 18.12 | 12.067 | 4.068 |
| 171.93 | 132.15 | 87.52 | 66.934 | 47.15 | 43.679 | 38.63 | 30.89 | 24.156 | 17.329 | 11.55 | 14.061 | 22.846 | 24.513 | 17.816 | 10.44989 | 3.7181 |
| 100.21 | 72.4 | 48.66 | 35.231 | 19.125 | 10.176 | 7.932 | 18.2 | 15.346 | 11.746 | 9.512 | 9.3807 | 9.1443 | 8.0502 | 7.2526 | 5.980706 | 12.968 |
| 76.013 | 55.134 | 38.96 | 27.66 | 22.24 | 18.36 | 15.62 | 13.414 | 11.647 | 9.8952 | 8.3295 | 7.5944 | 7.0235 | 6.1363 | 5.51256 | 6.975374 | 11.789 |
| 54.816 | 39.051 | 27.43 | 24.356 | 17.68 | 13.45 | 9.17 | 7.8996 | 7.9704 | 7.8038 | 6.8899 | 5.9313 | 5.5916 | 4.8149 | 4.38719 | 5.260698 | 7.4143 |

Figure 4.35 Upper skin RF Map calculated according to combined shear and compression loading

| | | | | | | | | | | | | | | | | |
|---------|--------|--------|---------|--------|--------|--------|--------|--------|--------|--------|------------------------------|--------|--------|--------|--------|--------|
| 1293.28 | 637.64 | 467.15 | 296.649 | 126.15 | 61.126 | 42.131 | 76.139 | 59.377 | 48.721 | 40.319 | 25.699 | 20.5 | 18.648 | 17.556 | 17.241 | 16.706 |
| 892.31 | 355.78 | 225.67 | 120.342 | 65.890 | 44.321 | 33.452 | 55.785 | 39.421 | 32.145 | 27.96 | 18.097 | 15.48 | 13.56 | 12.43 | 9.84 | 8.27 |
| 231.342 | 110.28 | 80.731 | 51.1806 | 21.63 | 11.078 | 7.4858 | 8.9925 | 6.4506 | 5.2616 | 4.845 | 4.4572 | 4.007 | 3.7137 | 3.3224 | 3.039 | 3.0661 |
| 398.152 | 924.62 | 633.97 | 343.313 | 52.657 | 21.35 | 9.1126 | 9.2014 | 5.9753 | 3.9104 | 3.8999 | 5.1515 | 4.3453 | 3.6562 | 3.3461 | 3.0529 | 3.3227 |
| 266 | 117.48 | 85.821 | 54.1643 | 22.508 | 10.999 | 7.3843 | 9.1101 | 6.5477 | 6.3814 | 5.4139 | MAIN LANDING GEAR BAY | | | | | |
| 301.57 | 128.97 | 94.321 | 58.046 | 22.768 | 11.234 | 7.36 | 9.013 | 7.12 | 6.87 | 9.764 | | | | | | |
| 344.613 | 142.71 | 102.85 | 62.9861 | 23.124 | 11.859 | 7.3521 | 8.6438 | 7.431 | 7.9757 | 19.539 | | | | | | |

Figure 4.36 Wing lower skin RF map calculated according to maximum stress

| | | | | | | | | | | | | | | | | | | |
|---------|---------|---------|---------|---------|---------|---------|-------|--------|-------|-------|-------|-------|-------|-------|-------|-------|-------|-------------|
| 1293.28 | 789.789 | 587.453 | 445.776 | 61.4624 | 41.1043 | 12.9351 | 6.250 | 13.394 | 6.804 | 3.800 | 2.618 | 2.261 | 2.329 | 2.403 | 2.491 | 2.542 | 3.866 | Front spar |
| 1835.54 | 342.236 | 278.728 | 231.342 | 186.69 | 12.7222 | 6.25261 | 4.025 | 4.590 | 2.939 | 2.719 | 1.928 | 1.886 | 1.827 | 1.691 | 1.476 | 2.034 | 2.524 | 1. stringer |
| 678.456 | 285.457 | 224.098 | 189.234 | 66.733 | 10.92 | 5.023 | 3.270 | 3.720 | 2.377 | 2.248 | 1.700 | 1.621 | 1.466 | 1.252 | 1.020 | 1.567 | 1.635 | 2. stringer |
| 398.152 | 177.574 | 143.465 | 159.703 | 29.734 | 10.018 | 4.41099 | 1.818 | 4.452 | 3.056 | 1.981 | 3.363 | 3.679 | 2.853 | 2.369 | 1.972 | 1.585 | 2.160 | Main Spar |
| 532.223 | 288.103 | 232.108 | 266.002 | 37.3955 | 10.2971 | 4.38177 | 2.531 | 3.120 | 1.972 | 1.909 | 1.845 | 1.728 | 1.471 | 1.185 | 1.400 | 1.249 | 1.173 | 3. stringer |
| 404.2 | 234.5 | 223.31 | 201.566 | 32.114 | 11.023 | 5.056 | 4.045 | 4.418 | 3.235 | 3.363 | 2.580 | 2.405 | 2.151 | 1.795 | 1.382 | 1.591 | 1.607 | 4. stringer |
| 344.613 | 176.916 | 143.238 | 163.721 | 24.1682 | 12.7678 | 5.91016 | 4.462 | 4.481 | 3.440 | 3.674 | 3.078 | 3.134 | 2.955 | 2.563 | 2.037 | 1.910 | 1.694 | 5. stringer |
| 265.382 | 42.3976 | 79.2063 | 127.144 | 32.1957 | 11.234 | 5.81 | 4.350 | 4.21 | 3.68 | 3.56 | 3.21 | 3.014 | 2.708 | 2.034 | 2.11 | 1.89 | 1.191 | Rear spar |

Figure 4.37 Wing upper stringer and spar cap RF Map calculated according to axial compression loading

| | | | | | | | | | | | | | | | | | | |
|----------|----------|---------|---------|---------|--------|--------|-------|--------|-------|-------|-------|-----------------------|-------|-------|-------|-------|-------|--------------|
| 1875.255 | 1145.193 | 851.806 | 646.375 | 89.121 | 59.601 | 18.756 | 9.062 | 19.422 | 9.866 | 5.511 | 3.796 | 3.279 | 3.377 | 3.484 | 3.612 | 3.686 | 5.605 | Front spar |
| 2661.528 | 496.242 | 404.156 | 335.447 | 270.701 | 18.447 | 9.066 | 5.836 | 6.656 | 4.261 | 3.943 | 2.796 | 2.735 | 2.650 | 2.452 | 2.139 | 2.950 | 3.660 | 6. stringer |
| 983.765 | 413.918 | 324.915 | 274.358 | 96.76 | 15.834 | 7.283 | 4.741 | 5.394 | 3.446 | 3.260 | 2.465 | 2.351 | 2.125 | 1.815 | 1.479 | 2.273 | 2.371 | 7. stringer |
| 577.320 | 257.482 | 208.024 | 231.569 | 43.114 | 14.526 | 6.396 | 2.636 | 6.456 | 4.431 | 2.872 | 4.876 | 5.335 | 4.137 | 3.435 | 2.859 | 2.298 | 3.132 | Main Spar |
| 771.723 | 417.750 | 336.556 | 385.702 | 54.223 | 14.931 | 6.354 | 3.670 | 4.524 | 2.860 | 2.768 | 2.676 | MAIN LANDING GEAR BAY | | | | | | 8. stringer |
| 586.090 | 340.025 | 323.800 | 292.270 | 46.565 | 15.983 | 7.331 | 5.865 | 6.405 | 4.691 | 4.877 | 3.741 | | | | | | | 9. stringer |
| 499.689 | 256.528 | 207.695 | 237.395 | 35.044 | 18.513 | 8.570 | 6.470 | 6.498 | 4.987 | 5.328 | 4.463 | | | | | | | 10. stringer |
| 384.804 | 61.477 | 114.849 | 184.358 | 46.684 | 16.289 | 8.425 | 6.308 | 6.105 | 5.336 | 5.162 | 4.655 | 4.370 | 3.926 | 2.949 | 3.060 | 2.741 | 1.727 | Rear spar |

Figure 4.38 Wing lower stringer and spar cap RF Map calculated according to maximum stress

| | | | | | | | | | | | | | | | | | |
|---------|--------|--------|---------|--------|--------|--------|--------|--------|--------|--------|-----------------------|--------|--------|--------|--------|--------|--|
| 1138.09 | 561.12 | 411.09 | 261.051 | 111.01 | 53.791 | 37.075 | 67.002 | 52.251 | 42.875 | 35.481 | 22.615 | 18.04 | 16.41 | 15.449 | 15.172 | 14.701 | |
| 785.233 | 313.09 | 198.59 | 105901 | 57.983 | 39.002 | 29.438 | 49.091 | 34.690 | 28.266 | 24.605 | 15.925 | 13.622 | 11.933 | 10.938 | 8.6592 | 7.2776 | |
| 203.581 | 97.047 | 71.043 | 45.0389 | 19.035 | 9.7484 | 6.5875 | 7.9134 | 5.6765 | 4.6302 | 4.2636 | 3.9223 | 3.5262 | 3.2681 | 2.9237 | 2.6743 | 2.6981 | |
| 350.374 | 813.67 | 557.89 | 302.116 | 46.338 | 18.788 | 8.0191 | 8.0972 | 5.2582 | 3.4412 | 3.4319 | 4.5334 | 3.8238 | 3.2175 | 2.9445 | 2.6866 | 2.924 | |
| 234.08 | 103.38 | 75.522 | 47.6645 | 19.807 | 9.6793 | 6.4982 | 8.0169 | 5.762 | 5.6156 | 4.7642 | MAIN LANDING GEAR BAY | | | | | | |
| 265.382 | 113.49 | 83.002 | 51.080 | 20.036 | 9885.9 | 6.4768 | 7931.4 | 6.2656 | 6.0456 | 8.592 | | | | | | | |
| 303.26 | 125.59 | 90.507 | 55.4278 | 20.349 | 10.436 | 6.4699 | 7.6065 | 6.5393 | 7.0186 | 17.195 | | | | | | | |

Figure 4.39 Rib webs RF Map calculated according to combined in plane shear and axial compression load

| | | | | | | | | | | | | | | | | | | |
|----------|---------|---------|--------|--------|----------|--------|--------|--------|--------|--------|--------|--------|--------|--------|--------|--------|--------|----------------|
| 1590.734 | 971.44 | 722.567 | 548.3 | 75.599 | 50.55824 | 15.910 | 7.687 | 16.475 | 8.369 | 4.6745 | 3.22 | 2.7812 | 2.8646 | 2.9557 | 3.0644 | 3.1267 | 4.7549 | Front Spar Web |
| 489.7269 | 218.416 | 176.461 | 196.43 | 36.573 | 12.322 | 8.425 | 6.236 | 5.4765 | 3.7591 | 2.4367 | 4.136 | 4.5254 | 3.5094 | 2.9141 | 2.4251 | 1.949 | 2.6564 | Main Spar Web |
| 326.4198 | 52.149 | 97.4237 | 156.39 | 39.601 | 13.818 | 7.146 | 5.3505 | 5.1783 | 4.5264 | 4.3788 | 3.9483 | 3.707 | 3.331 | 2.502 | 2.5953 | 2.3247 | 1.465 | Rear Spar Web |

Figure 4.40 Spar webs RF Map calculated according to combined in plane shear and bending load

4.4 Interrelation of Genetic Algorithm and FEM Tools

The genetic algorithm software, which also utilizes MSC.PATRAN and MSC.NASTRAN as the FEM processor and solver respectively, is compiled in VISUAL FORTRAN program. Flow chart of interrelation of genetic algorithm and FEM building tools can be seen in Appendix A. This software can create and solve an individual FEM model at 30 seconds and a single iteration of a parameter set including 20 populations takes about 10 minutes. A total of 105 iterations are performed on a laptop computer and the duration of 1 run is about 17.5 hours. The computer utilized in this computation has a 1.73 GHz Intel Pentium M processor and the capacity of the RAM is 504 MB.

Optimization algorithm first performs a stress and instability check for FE model using the initial population. After this computation, each population is graded according to its fitness. The lower the mass of the wing in corresponding design, the higher the grade of that generation.. Then populations are ranked according to their grades and pair selection is

performed by using roulette-wheel selection. After pair selection, cross over operation is performed and some of the genes of populations, which are paired, are interchanged between these populations. In order to provide the variability of the solutions, some of the genes are mutated. In this case, 10% of the genes are mutated. During this process, elitist genes are kept constant and not mutated. Termination criteria of the loop is a certain convergence in the optimization objective function. If a 0,4% of improvement in the weight of the structure cannot be achieved in 5 successive iterations the flow of the program is terminated. Mass change of the structure during iterations is presented by a graph in Figure 4.41.

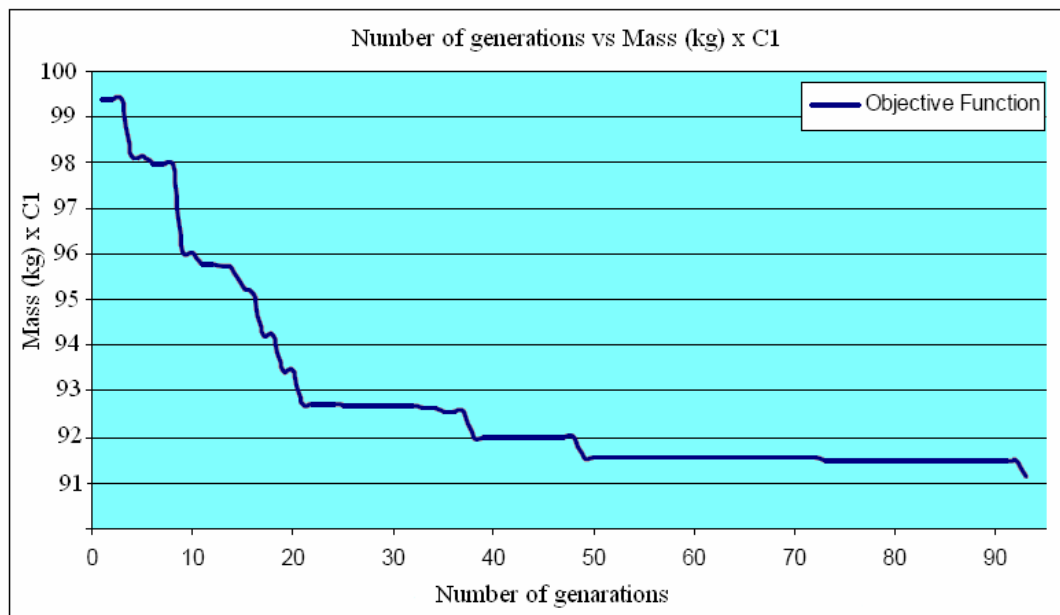


Figure 4.41 *Mass(kg) x C1 vs. generation number graph for optimization (C1: Scaling Constant)*

After 105 iterations of the optimization process, the mass of the wing structure decreased to 91% of its initial value and the stress distribution is uniform

compared to the initial model. Thickness map of the whole structure is redetermined and rib planes are modified as to give the optimum solution. Final dimensional properties of design variables of optimized model is given in Table 4.3. Modified rib planes vs. the initial rib planes geometry can be seen in Figure 4.42. In order to obtain more precise stress distribution views structure mesh is refined by remeshing the wing external surfaces by using the optimized parameters. Mesh refinement of the wing can be seen in figures 4.43 through 4.45.

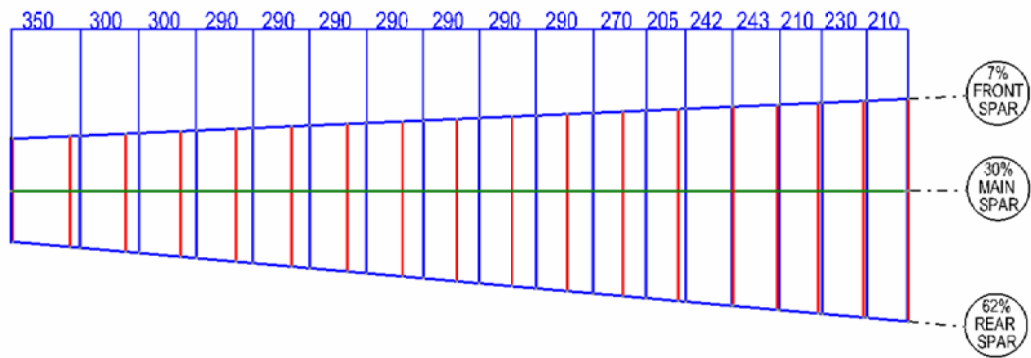


Figure 4.42 Comparison of initial rib planes and final rib planes
(Red lines are the initial rib planes whereas blue lines are the rib planes of finalized geometry)

Table 4.3 *Final values of the parameters in optimized model (All dimensions in [mm])*

| | | | | | | | | |
|-----------|-----------|-----------|-----------|-----------|-----------|-----------|-----------|-----------|
| 1 | 2 | 3 | 4 | 5 | 6 | 7 | 8 | 9 |
| 3,1 | 3,8 | 2,7 | 2,4 | 2,6 | 5 | 4,8 | 4,6 | 4,2 |
| 10 | 11 | 12 | 13 | 14 | 15 | 16 | 17 | 18 |
| 4 | 3,6 | 2,4 | 2,2 | 2 | 2 | 1,8 | 1,6 | 1,6 |
| 19 | 20 | 21 | 22 | 23 | 24 | 25 | 26 | 27 |
| 1,2 | 1 | 0,8 | 0,8 | 0,6 | 1,2 | 20 | 25 | 20 |
| 28 | 29 | 30 | 31 | 32 | 33 | 34 | 35 | 36 |
| 8 | 100 | 20 | 4 | 60 | 5 | 4 | 50 | 4 |
| 37 | 38 | 39 | 40 | 41 | 42 | 43 | 44 | 45 |
| 3 | 210 | 230 | 210 | 240 | 240 | 210 | 270 | 290 |
| 46 | 47 | 48 | 49 | 50 | 51 | 52 | 53 | |
| 290 | 290 | 290 | 290 | 290 | 300 | 300 | 350 | |

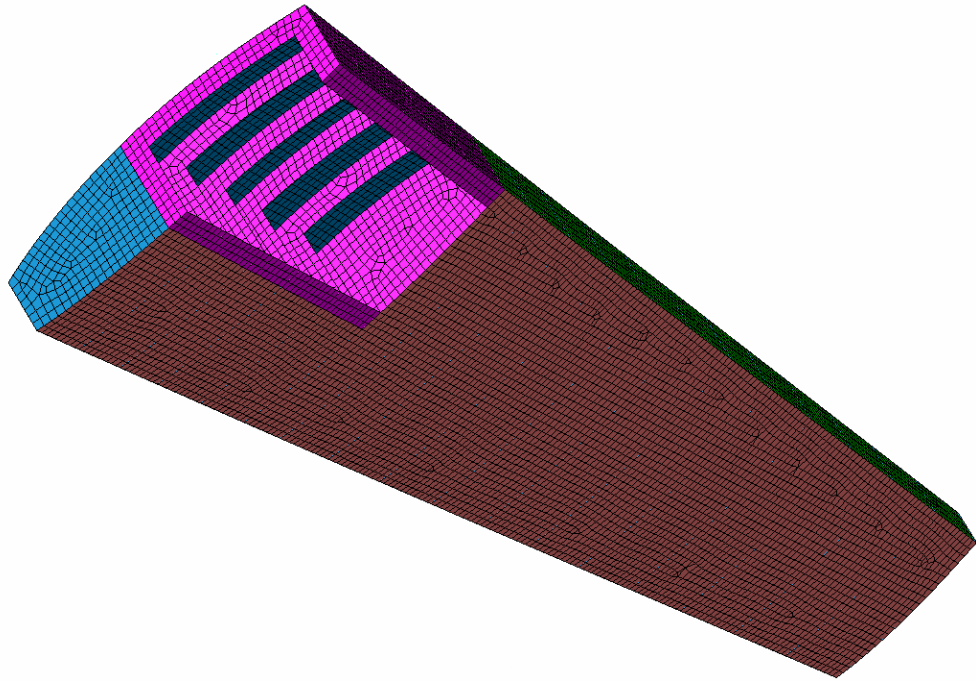


Figure 4.43 *Refined mesh of the wing according to optimization results. Main Landing Gear surround structure is seen in pink color.*

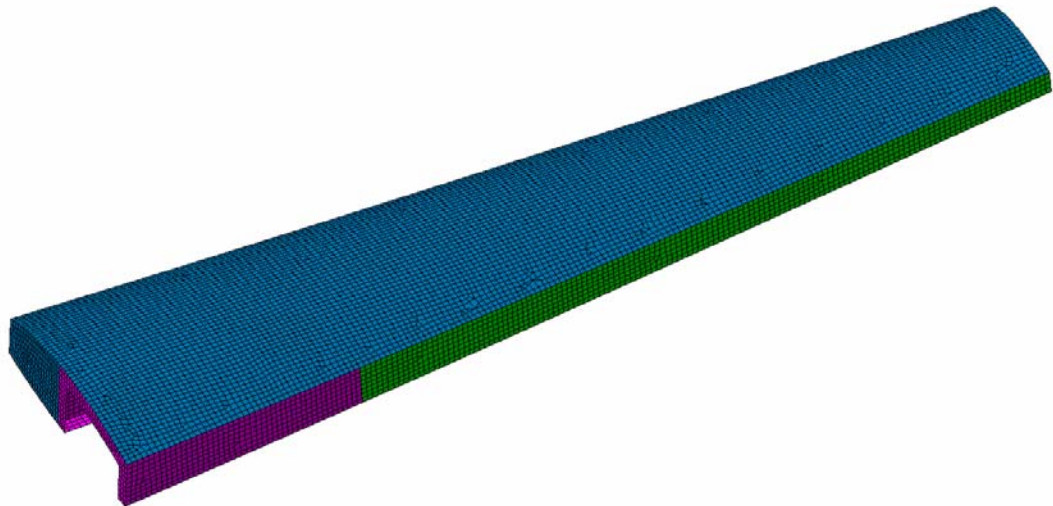


Figure 4.44 *Upper skin fine mesh*

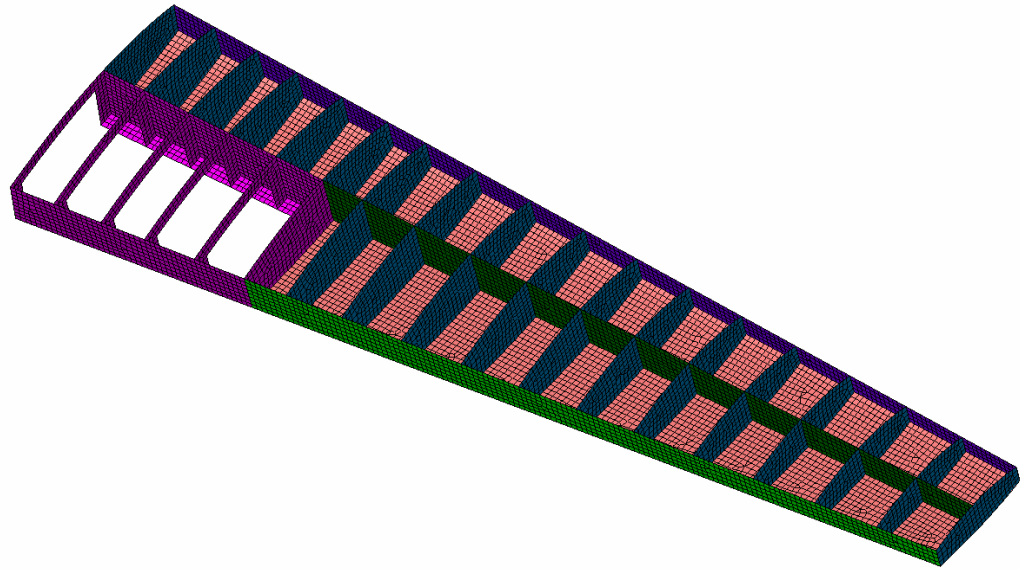


Figure 4.45 *Ribs and spars FEM model*

Distribution of Von Mises stress values on the initial and final (optimized) wing structures based on the refined FE model can be seen in Figure 4.46 through Figure 4.55.

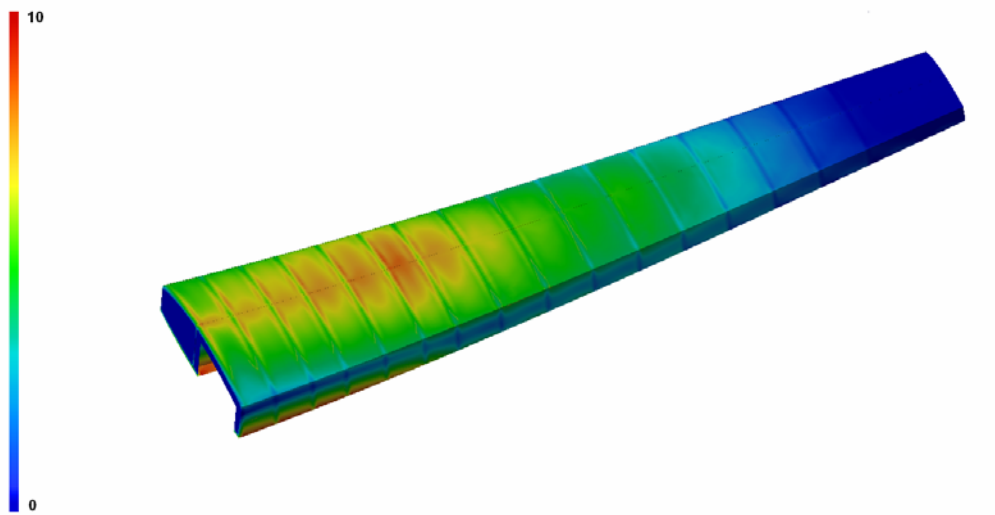


Figure 4.46 *Von Mises stress distribution of upper skin in optimized model*

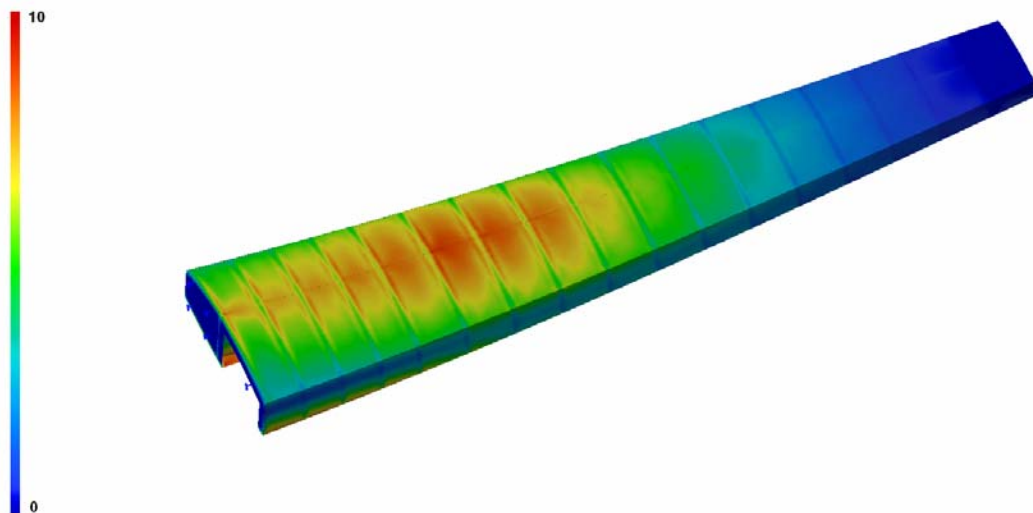


Figure 4.47 *Von Mises stress distribution of upper skin in initial model*

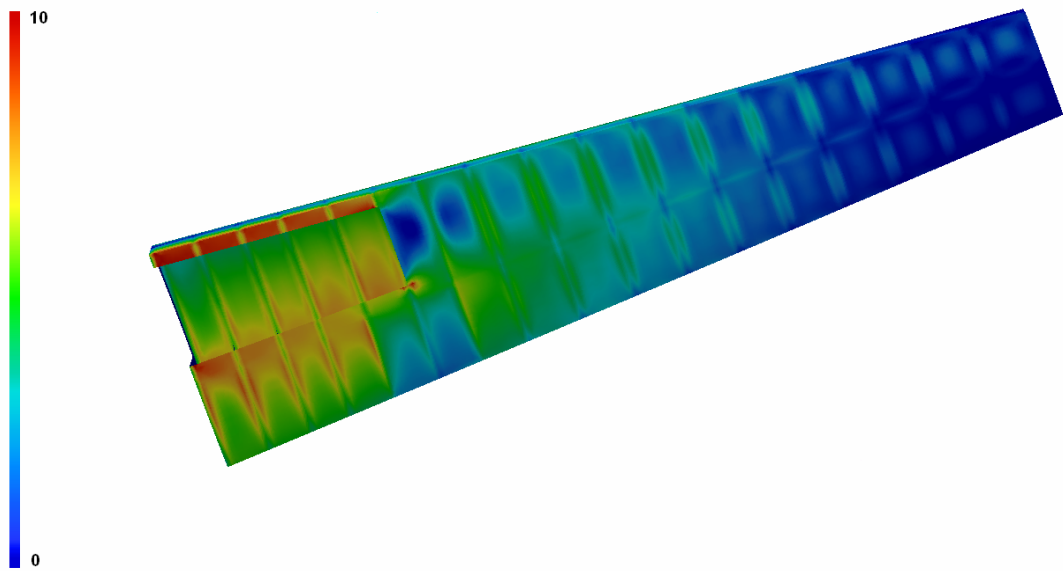


Figure 4.48 *Von Mises stress distribution of lower skin in initial model*

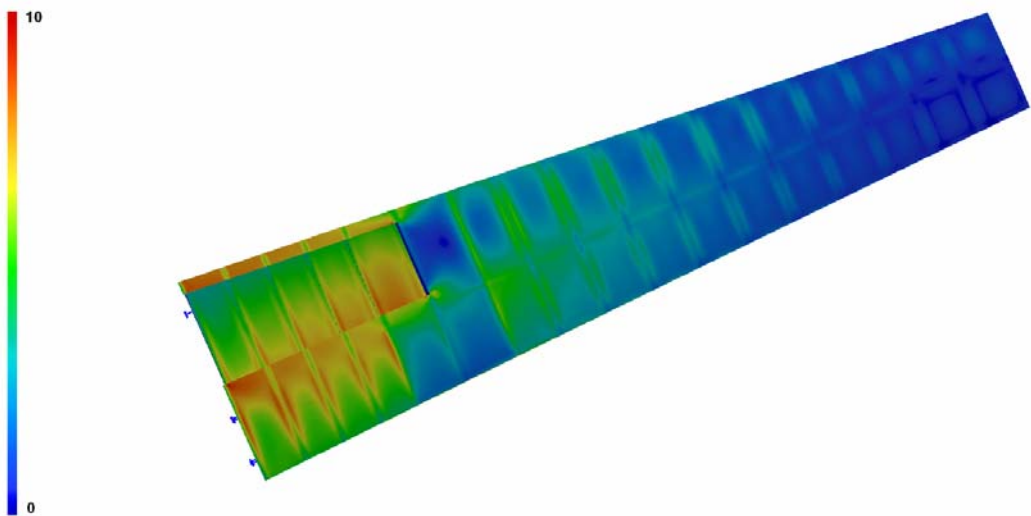


Figure 4.49 *Von Mises stress distribution of lower skin in optimized model*

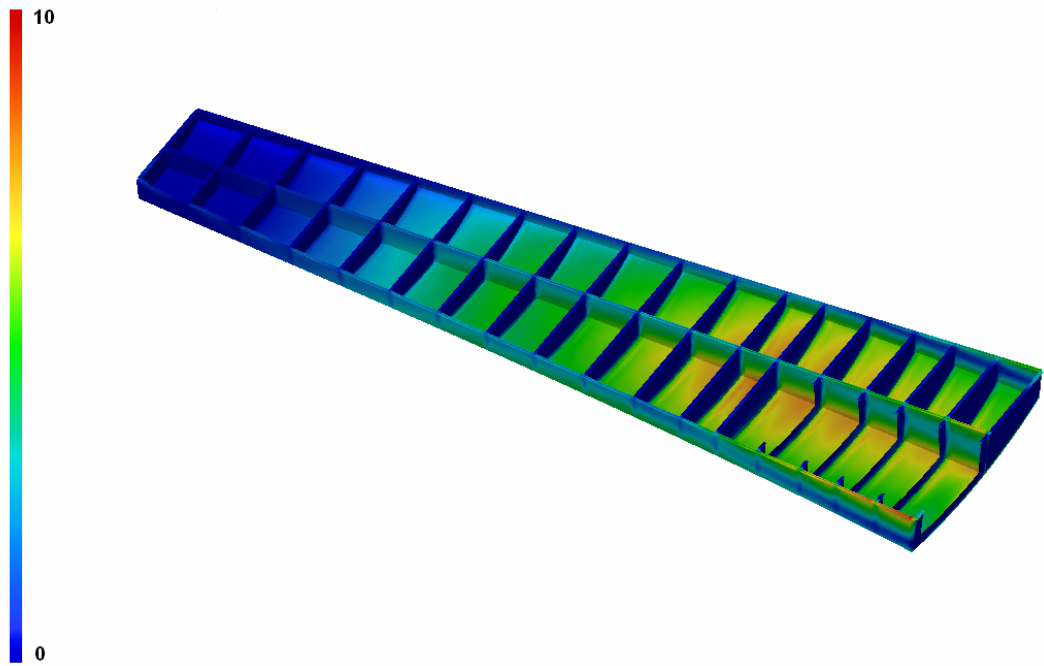


Figure 4.50 *Von Mises stress distribution at a section cutting wing structure spanwise looking up in optimized model*

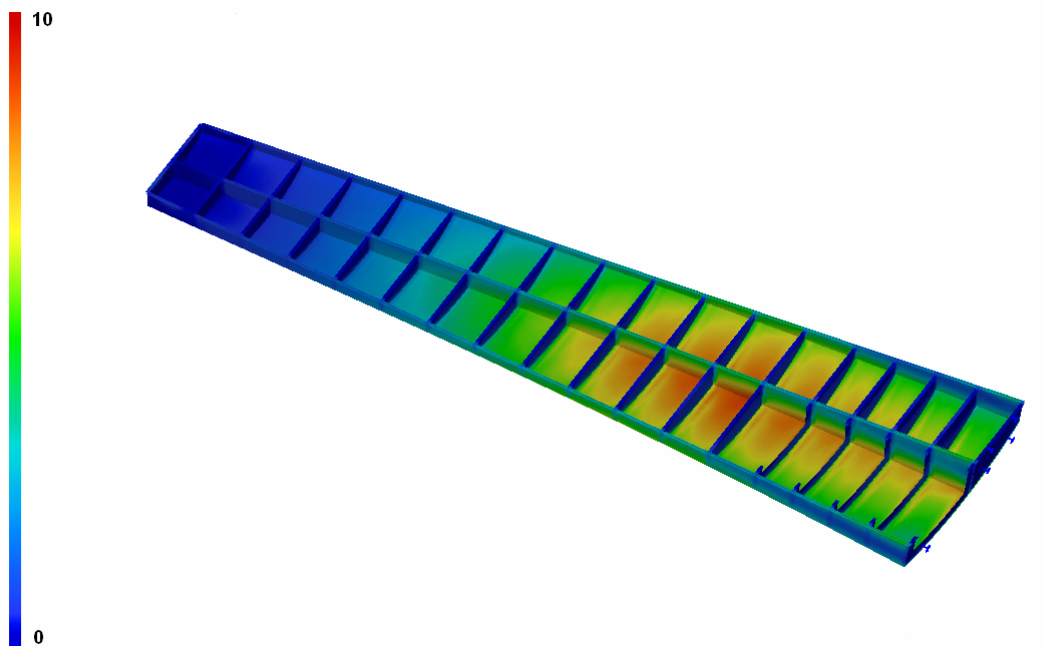


Figure 4.51 *Von Mises stress distribution at a section cutting wing structure spanwise looking up in initial model*

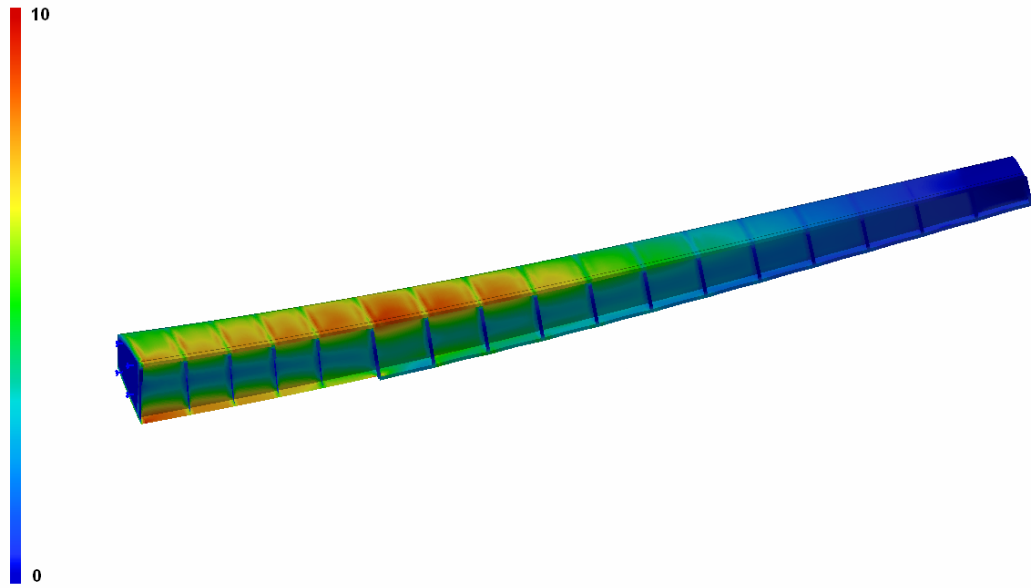


Figure 4.52 *Von Mises stress distribution at a section cutting wing structure chordwise near main spar plane looking forward in initial model*

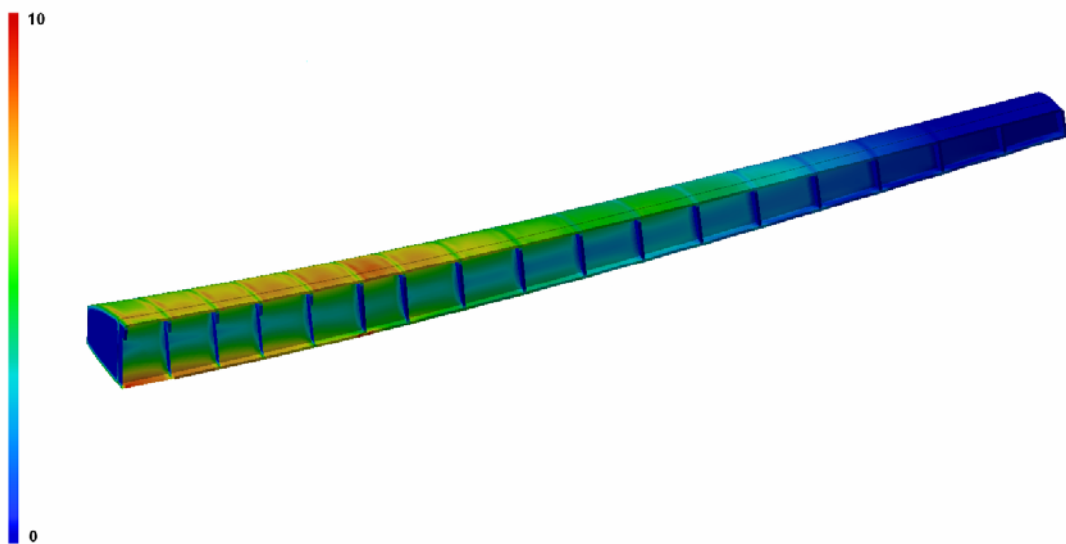


Figure 4.53 *Von Mises stress distribution at a section cutting wing structure chordwise near main spar plane looking forward in optimized model*

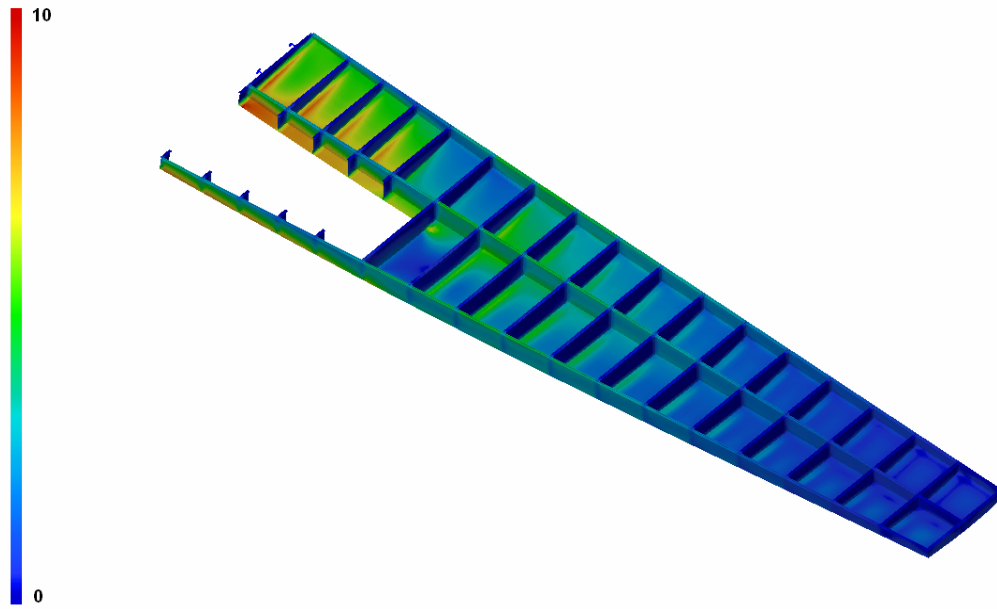


Figure 4.54 *Von Mises stress distribution at a section cutting wing structure spanwise looking down in initial model*

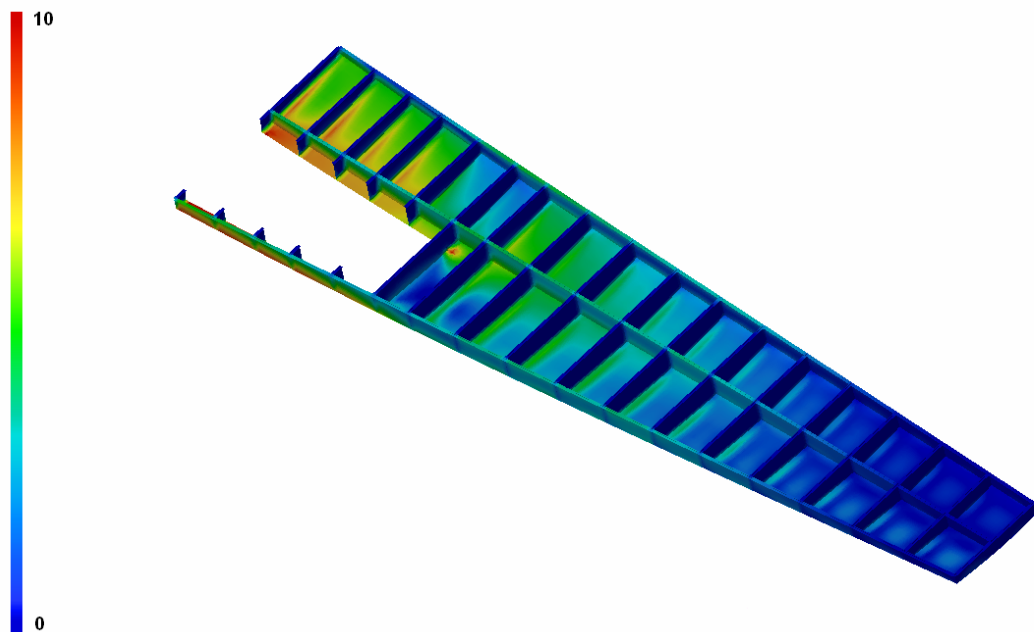


Figure 4.55 *Von Mises stress distribution at a section cutting wing structure spanwise looking down in initial model*

CHAPTER 5

DISCUSSION & CONCLUSION

In this study, structural design optimization of an acrobatic category trainer aircraft wing is performed by developing a Visual Fortran software including genetic algorithm.

Aircraft structures used in the aviation industry should be as light as possible in order to improve aircraft maneuver performance, decrease aircraft manufacturing and operational costs while keeping the stress levels under a certain value (static or fatigue allowables) in order to prevent fatigue or static failure.

Genetic algorithm is utilized as the optimization method in this study because it is one of the most popular optimization algorithms that is known for its robustness and ability to search complex and noisy search spaces. In addition, genetic algorithm searches for better solutions instead of searching exact optimum solution and this makes GA a more favorable optimization tool, since it lessens the computation time and becomes more cost effective.

After optimization process, the weight of the initial design was reduced to 91% of its value. In other words, a 9% of decrease is achieved in the mass of the wing. Also maximum design stress (Von Mises) in the global FE model was reduced to 85 % of its initial value. Furthermore, stress distribution was locally concentrated in some areas such as first 3 or 4 bays of the lower portions of the

spar webs, root section of the upper skin, ribs around the MLG surround, and skins around the MLG surround. After the optimization process, stress is more uniformly distributed around the members such as upper skin, which is under compression, spar web lower portions that are under combined bending and in plane shear and skin around the MLG surround.

Examining the RF tables for skins and stringer and spar caps, one can observe that the closer the member to the main spar plane the smaller the RF values of that member. The main reason for this is that main spar is the largest and stiffest structure in the wing. Therefore most of the shear load flows through the main spar web and most of the bending load flows through the main spar caps. Consequently other structural members such as skin pieces or axial members such as stringers close to the main spar web are loaded more than the structural members far from the main spar web are. In addition, RF values of these members are much smaller than other members.

The smallest RF value in the members is the RF of 3. stringer which is 1.173. In addition, the stringers and spar caps on the upper skin have the smallest RF values. So it can be concluded that the members in the wing structure driving the design are stringers and spar caps. In addition, these members carrying axial load are the most slender and weakest members in the wing structure.

The general tendency of the RF values is to increase around wing tip. Therefore, the smallest RF values are around the wing root. RF values are increasing from wing root to the wing tip, because stress values are decreasing from wing root to the wing tip. Also as previously discussed, RF values are decreasing as getting far from the main spar web. One obstacle disturbing this trend is the main landing gear (MLG) bay. Since the MLG is a retractable mechanism, there should be enough space in the wing root in order to provide

housing for the MLG. This means weakening of wing root around MLG. Therefore at some locations on the wing the trend of RF's getting larger from wing tip to the wing root is disturbed. For example, RF value of the upper skin decreases at the trailing edge at the 2. bay and starts to increase again from the 3. bay and so on. Similarly, in the lower skin there is large opening in order to provide access to the MLG. In the transition zone between the portions of the lower skin having the Access and full skin portion, RF values first start to decrease and then increase again.

The reason for providing RF maps instead of providing thickness maps in this study is that both the thickness of the upper skin and the lower skin is one parameter only. If the thickness of each skin bay in the upper skin were a design parameter there would be 119 design parameters for only upper skin, 101 design parameters for only lower skin. Therefore, the huge increase in the number of design parameters would cause the search domain to increase rapidly and the computation time would also increase in the same manner.

However, if enough computation power and time could be provided, by making the thickness of each skin bay a design parameter, a much more efficient design could be reached and the mass of the skin panels could be much lighter. The thickness value of the skin panels would decrease going from wing root to the wing tip.

As a manufacturing process, this could be achieved by chemical milling. Chemical milling also known as electro-chemical machining chemical (ECM) is a method of removing metal by an electrochemical process. It is used for working extremely hard materials or materials that are difficult to machine using conventional methods. Its use is limited to electrically conductive

materials; however, this includes all metals. ECM can cut small or odd-shaped angles, intricate contours or cavities.

As a result, by using ECM method it is possible to achieve different thickness values on different bays of the wing skins. This provides a lighter wing design.

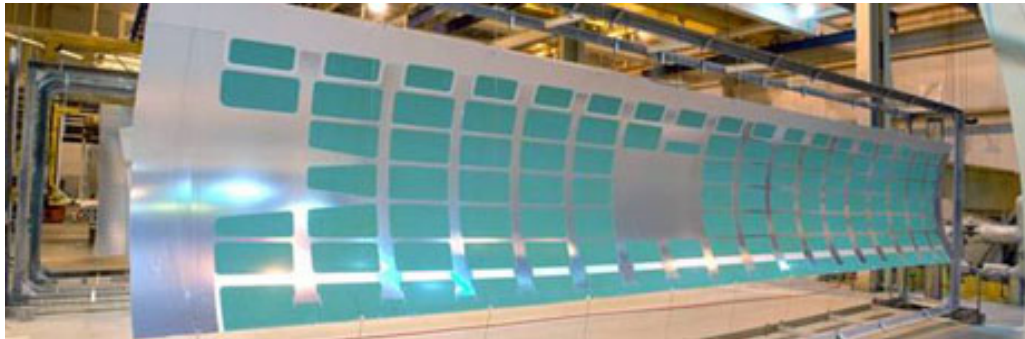


Figure 5.1 *An aircraft fuselage skin milled by ECM process.* [24]

REFERENCES

- [1] Belegundu A.D., Chandrupatla T.R. “Optimization Concepts and Applications in Engineering”, Prentice-Hall Inc., 1999
- [2] Kamat M.P., “Structural Optimization: Status and Promise”, Progress in Astronautics and Aeronautics, Volume 150, 1993
- [3] Haftka R.T., Gurdal Z., “Elements of Structural Optimization”, Kluwer Academic Publishers, 1990
- [4] Dianati M., Song I., Treiber M., “An Introduction to Genetic Algorithms and Evolution Strategies”, University of Waterloo, July 2002
- [5] Charbonneau P., “An Introduction to Genetic Algorithms for Numerical Optimization”, NCAR Technical Note, March 2002
- [6] Said Y.H., “On Genetic Algorithms and their Applications”, Handbook of Statistics, Vol. 24 ISSN: 0169-7161, 2005
- [7] Moore G.J., “MSC/NASTRAN^R Design Sensitivity and Optimization”, MSC.Corporation, 1994
- [8] Nanakorn P., Meesomklin K., “An Adaptive Penalty Function in Genetic Algorithms for Structural Design Optimization”, Computers and Structures 79 2527-2539, 2001
- [9] Pedersen P., “Optimal Designs- Structures and Materials - Problems and Tools” , Technical University of Denmark, Department of Mechanical Engineering, May 2003
- [10] “GENESIS User Manual Volume 4 Optimization Demonstration Problems”, VMA Engineering, 1998
- [11] Gantovnik V.B., Anderson-Cook C.M., Gurdal Z. and Watson L.T., "A Genetic

- Algorithm with Memory for Mixed Discrete–Continuous Design Optimization”, Computers and Structures, 81 2003-2009, 2003
- [12] Rajeev S, Krishnamoorthy C.S., “Discrete Optimization of Structures using Genetic Algorithms”, Journal of Structural Engineering ASCE 118(5): 1233-1250, 1992
- [13] Xicheng W, Guixu M., “A Parallel Iterative Algorithm for Structural Optimization”, Computer Methods in Applied Mechanics and Engineering 96:25-32, 1992
- [14] Yu X., Johnson E.H., Zhang S., “Discrete Optimization in MSC/NASTRAN[®]”, MSC Software Corporation, 2001
- [15] Wang D., Zhang W.H., Jiang J.S., “Truss Shape Optimization with Multiple Displacement Constraints”, Comput. Methods Appl. Mech. Eng., 191 3597-3612, 2002
- [16] Thanedar P.B., Vanderplaats G.N., “Survey of Discrete Variable Optimization For Structural Design”, Journal of Structural Engineering, Vol. 121. No: 6341, 1995
- [17] Gillman K.M., “Optimization of Shape, Size and Topology Design Variables In Trusses with a Genetic Algorithm”, Brigham Young University, April 2005 93
- [18] Rajan S.D., "Sizing, Shape and Topology Design Optimization of Trusses using Genetic Algorithm", Journal of Structural Engineering 121 1480-1487, 1995
- [19] McCALL J., "Genetic Algorithms for Modelling and Optimization”, Journal of Computational and Applied Mathematics, 184 205-222, 2005
- [20] “MSC Nastran Reference Manual” Version 68 The MacNeal-Schwindler Corporation
- [21] Airframe Structural Design, Second Edition, NIU, M.C.Y.
- [22] Airframe Stress Analysis Sizing, NIU, M.C.Y.

- [23] Analysis and Design of Flight Vehicle Structures, Bruhn, E.F.
- [24] WIKIMEDIA, http://en.wikipedia.org/wiki/Electro_chemical_machining, 20/08/2008.
- [25] Falco S.A., Faria A.R., “Optimization of a Simple Aircraft Wing”, Fibraforte Engenharia, São José dos Campos, SP, Brazil, February 2001.
- [26] Engineering experience formed by Turkish Aerospace Industries Inc. in the field of stress analysis work of airframe structures.

APPENDIX A

MODELING TOOLS USED IN THE STUDY

A.1 Introduction

Appendix A gives brief explanation about the finite element package programs MSC/PATRAN[®] and MSC/NASTRAN[®], which are used in the finite element modeling and analysis throughout this study.

A.2 MSC/PATRAN[®] and MSC/NASTRAN[®] Package Programs

MSC/PATRAN[®] is a software developed and maintained by Macneal-Schwendler Corporation (MSC) Software Corporation. Throughout this study MSC/PATRAN[®] version 9.0 is used as the pre and postprocessor. The major components of MSC/PATRAN[®] are graphical user interface (GUI), direct geometry integration, analysis preferences, engineering functionality and results visualization.

MSC/NASTRAN[®] developed by NASA in 1960's is a general-purpose finite element computer program for engineering analysis. "General purpose" means that MSC/NASTRAN[®] addresses a wide range of engineering problem-solving requirements such as statics, dynamics, nonlinear behavior, thermal analysis, or optimization as compared to specialty programs, which concentrate on particular types of analysis. MSC/NASTRAN[®] is also developed, supported, and maintained by Macneal-Schwendler Corporation (MSC) Software Corporation. [20]

MSC/NASTRAN[®] is written in FORTRAN programming language. MSC/NASTRAN[®] version 70.5 is used throughout this study.

MSC/NASTRAN[®] is composed of a large number of building blocks called modules. A module is a collection of FORTRAN subroutines designed to perform a specific task.

The engineering problems, which can be solved by MSC/NASTRAN[®], are:

- linear static analysis including inertia relief
- static analysis with geometric and material non-linearity
- transient analysis with geometric and material non-linearity
- normal modes and buckling analysis
- direct and modal complex eigenvalue analysis
- direct and modal frequency analysis and random response
- direct and modal transient analysis (including response spectrum analysis)
- linear static and vibration analysis with cyclic symmetry
- linear and nonlinear steady state heat transfer
- transient heat transfer
- aeroelasticity
- multilevel super elements
- design sensitivity and optimization
- acoustics
- composite analysis
- cyclic symmetry

- p-version elements and hp adaptivity

Linear static module of MSC/NASTRAN[®] is employed in this study.

A.3 Structural Elements Used in the Study

MSC/NASTRAN[®] offers an extensive variety of general purpose and special finite elements as shown in Table A-1.

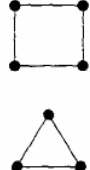
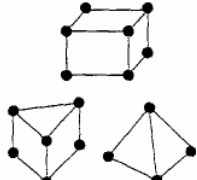
| Category | Spring Elements | Line Elements | Surface Elements | Solid Elements | Rigid Elements |
|---------------------------|---|---|---|---|---|
| Physical Behavior | Simple Spring | Rod, Bar, Beam | Membrane, Thin Plate | Thick Plate, Brick | Rigid Bar |
| MSC/NASTRAN Element Name | CELAS2* | CONROD* CROD CBAR | CQUAD4 CTRIA3 | CHEXA CPENTA CTETRA | RBE2* |
| Associated Property Entry | None Required | PROD PBAR | PSHELL | PSOLID | None Required |
| |  |  |  |  |  |

Figure A.1 *The basic MSC/NASTRAN[®] elements [20]*

A.3.1 1-D Elements

Bar elements are the 1-D elements used in the analysis. The CBAR element is a straight one-dimensional element that connects two grid points. The capabilities and limitations of the CBAR element are as summarized below:

- Extensional stiffness along the neutral axis and torsional stiffness about the neutral axis may be defined.
- Bending and transverse shear stiffness can be defined in the two perpendicular directions to the CBAR element's axial direction.
- The properties must be constant along the length of the CBAR element. This limitation is not present in the CBEAM element.
- The effect of out-of-plane cross-sectional warping is neglected. This limitation is not present in the CBEAM element.
- Transverse shear stiffness along the length of the CBAR can be included.

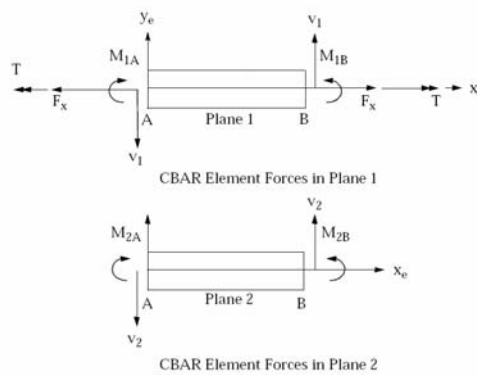


Figure A.2 *Demonstration of Beam Orientation* [20]

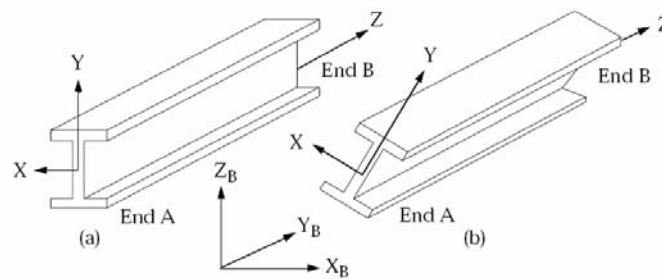


Figure A.3 *CBAR Element Forces* [20]

A.3.2 2-D Elements

Shell elements are 2-D elements and are used to represent a structure whose thickness is small compared to its other dimensions. Shell elements can model plates, which are flat, or shells, which have single curvature (like a cylinder) or double curvature (like a sphere). For grid points connected to plate elements, stiffness terms exist for five of the possible six degrees of freedom (DOF) where the rotational DOF about the normal to the plate is unconnected. This DOF must be constrained in order to prevent singularities. [20]

For linear analysis, MSC/NASTRAN® plate elements assume classical assumptions of thin plate behavior:

- A thin plate is the one in which the thickness is much less than the next larger dimension.
- The deflection of the plate's mid surface is much less compared to its thickness.
- The mid surface remains unstrained (neutral) during bending. This actually applies to lateral loads, not in plane loads.

The required structural mass of the shell elements are calculated from the membrane density and thickness.

MSC/NASTRAN® includes two different shapes of isoparametric shell elements (triangular and quadrilateral). QUAD4 elements have been used as shell elements in the modeling of the wing.

The QUAD4, which is the quadrilateral plate element, is MSC/NASTRAN®'s most commonly used element for modeling plates, shells and membranes. The QUAD4 can represent in-plane bending and transverse shear behavior. The

QUAD4 is a quadrilateral flat plate connecting four grid points as shown in Figure A.4.

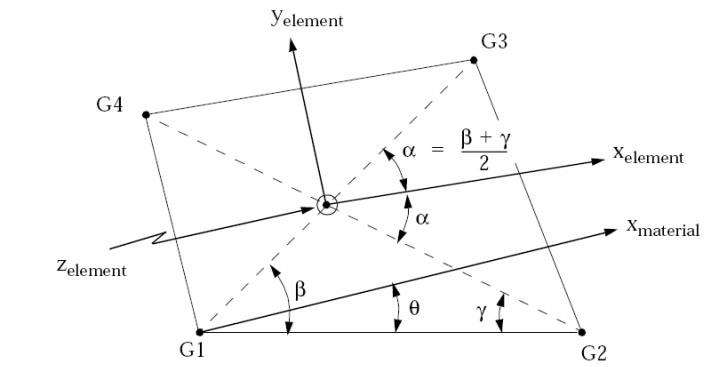


Figure A.4 QUAD4 element geometry and element coordinate system [20]

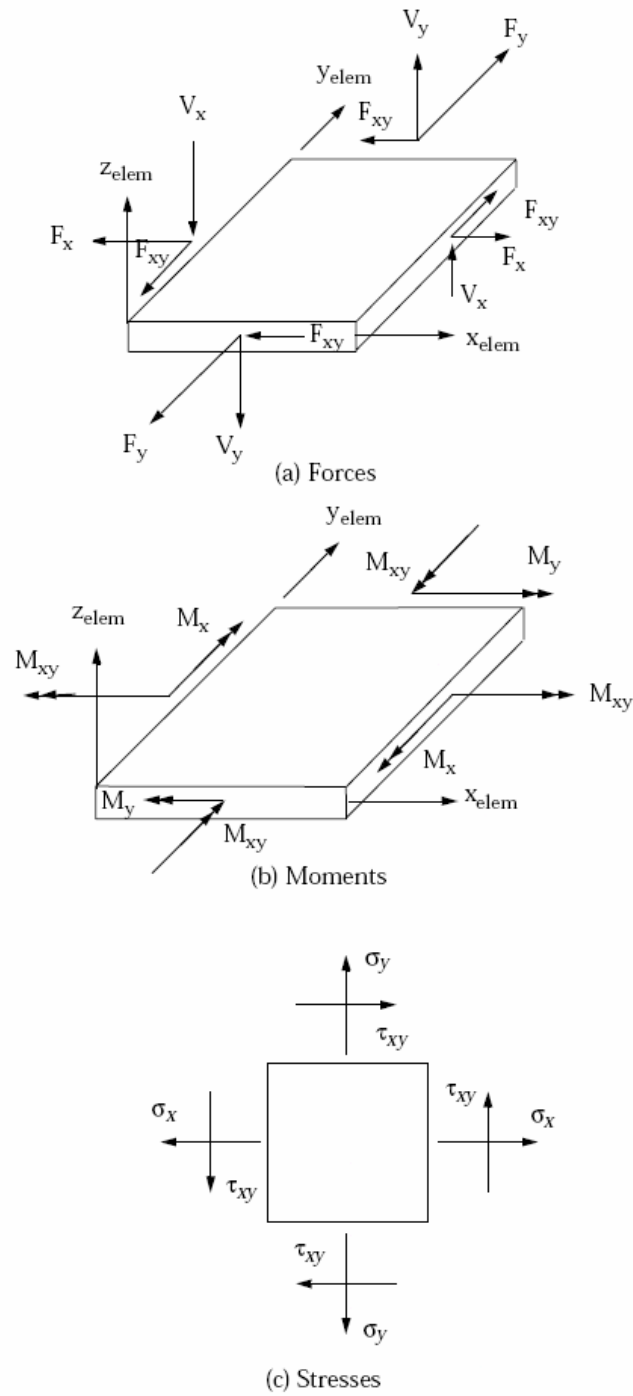


Figure A.5 Forces, Moments, and Stresses in Plate Elements [20]

A.3.3 0-D Elements

Lumped mass elements are 0-D scalar elements used in the analysis. The internal fuel is modeled by using lumped mass elements.

Scalar elements are connected between pairs of degrees of freedom (at either scalar or geometric grid points) or between one degree of freedom and ground. Scalar elements are available as springs, masses and viscous dampers.

Scalar masses are useful for selective representation of inertia properties, such as those, which occur when a concentrated mass is effectively isolated for motion in one direction only. The concentrated mass elements are used to define a concentrated mass at a grid point. [20]

APPENDIX B

STRUCTURAL ANALYSIS CRITERIA FOR INSTABILITY

B.1 Column Buckling

Since stringers and spar caps utilized in the wing structure act as column beams the sizing analysis of these parts are going to be performed according to column buckling theory. A column is a structural member subjected to a uniaxial compressive stress. Its normal failure mode is some form of instability.

(a) Primary column failure is defined as any type of failure in which the cross section is

- Translated
- Rotated
- Translated and rotated in its own plane.

(a) Secondary failure involves local distortion in the plane of the cross section of the column (crippling).

A perfectly straight, untwisted, and centrally loaded column will theoretically support an increasing load up to the critical load, P_{cr} , without translating or rotating. However, when P_{cr} is attained, the column experiences large deflections immediately with no corresponding increase in load as shown in Fig. B.1 below.

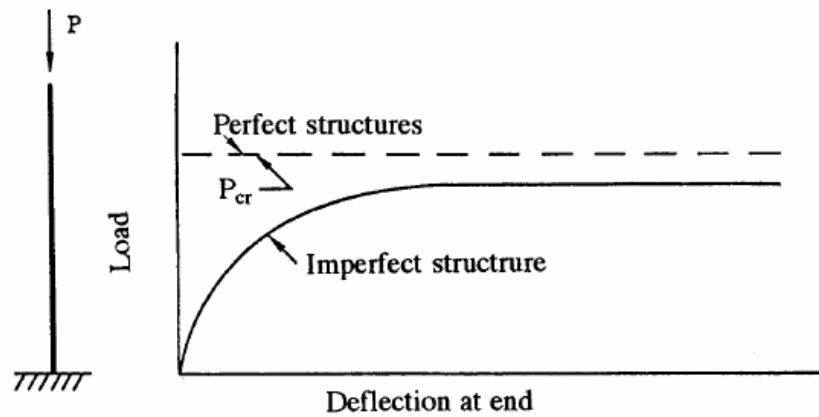


Figure B.1 *Perfect vs. Imperfect Structures of a Column* [22]

Actually, the geometrically perfect, centrally loaded column never occurs in practice. As a result, actual columns are not capable of sustaining the P_a associated with a perfect column. The difference between perfect and imperfect compression members must be recognized and the structural limitations imposed by these imperfections understood. Eccentrically loaded columns must be capable of carrying the compression load and the moment induced by the eccentricity and these members must be analyzed as beam columns, as will be discussed later.

A column may fail in one of the following modes and therefore the strength of a column is the lowest strength associated with any of the four failure modes:

- (a) Flexural instability - This mode is concerned with general buckling of the column and is dependent on the end fixity, cross section, and material.

- (b) Crippling stress - Crippling or local buckling of the cross sectional shape, occurs mainly in extrusions, formed sheet metal shapes, and thin walled tubes. It is dependent upon the material and cross section geometry and dimensions.
- (c) Interaction between local crippling and flexural instability - When the critical buckling stress reaches a value of one half local crippling stress, some interaction between flexural instability and crippling may occur.
- (d) Torsional instability - Torsional failure is relatively rare in columns, but it is to be expected in the following sections:
- I - sections of short length and very wide flanges or webs
 - T - sections of short and intermediate length
 - L - sections with equal and unequal legs of all lengths
 - In general, torsional buckling is critical in sections having wide flanges and short column lengths

The theoretical buckling load for various types of columns frequently encountered in airframe practical design and sizing can be obtained from the formulas, curves, and tabular forms given in this chapter. Furthermore, the methods given apply only to perfectly straight columns without side load, whereas in most practical cases eccentricities due to manufacturing tolerances introduce such severe bending moments as to reduce the strength of the member. In such cases, the member would have to be treated as a beam-column.

B.1.1 Euler Equation

Column failures by lateral translation are well known. Below the proportional limit of the material, the critical buckling load, P_E , is given by the Euler formula and still remains the basis of all buckling phenomena including the buckling of thin sheets. In terms of load, the Euler equation for the buckling load of a simple pin-ended column can be written as follows:

$$P_E = \frac{\Pi^2 EI}{L^2} \quad (B.1)$$

where: P_E - Euler buckling load.

E - Modulus of elasticity (in elastic range).

I - Smallest moment of inertia for the column cross-section.

L - Length of the column.

B.1.1.1 Effective Column Length

By inspecting this equation, it is readily seen that it actually describes the bending stiffness of the column. The quantities affecting the bending stiffness of a column members are:

- Material modulus of elasticity
- Moment of inertia
- Length of the column

Eq. B.1 can be rewritten for any other end-fixity by:

$$P_E = \frac{\Pi^2 EI}{L'^2} \quad (B.2)$$

where: c - Column end-fixity (values of 'c' for various column end-fixity and loading conditions are shown in Table B.1.

$$L' = \frac{L}{\sqrt{c}} \quad (B.3)$$

L' is the effective column length, use smallest moment of inertia for the column cross section

Rewriting the Euler equation in terms of stress by:

- Dividing the Euler load, P_E by the column area (A)
- And introducing the slenderness ratio term $\left(\frac{L'}{\rho}\right)$

$$F_{cr} = \frac{\Pi^2 E}{\left(\frac{L'}{\rho}\right)^2} \quad (B.4)$$

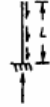
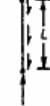
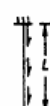
where: $\rho = \sqrt{\frac{I}{A}}$ is the least radius of gyration of cross-section

When the critical stress in a column is above the proportional limit, it is necessary to substitute the tangent modulus of elasticity (E_t) for the modulus of elasticity (E). The resultant formula is known as the Euler-Engesser equation: [22]

$$F_{cr} = \frac{\Pi^2 E_t}{\left(\frac{L'}{\rho}\right)^2} \quad (B.5)$$

where: E_t is the tangent modulus of elasticity of the column material

Table B.1 Column End-Fixity Coefficients [22]

| Column shape and end fixity | | End fixity coefficient | Column shape and end fixity | | End fixity coefficient |
|---|---|--|---|--|--|
|  | Uniform column, axially loaded, pinned ends | $c = 1$ $\frac{1}{\sqrt{c}} = 1$ |  | Uniform column, distributed axis load, one end fixed, one end free | $c = 0.794$ $\frac{1}{\sqrt{c}} = 1.12$ |
|  | Uniform column, axially loaded, fixed ends | $c = 4$ $\frac{1}{\sqrt{c}} = 0.5$ |  | Uniform column, distributed axis load, pinned ends | $c = 1.87$ $\frac{1}{\sqrt{c}} = 0.732$ |
|  | Uniform column, axially loaded, one end fixed, one pinned end | $c = 2.05$ $\frac{1}{\sqrt{c}} = 0.7$ |  | Uniform column, distributed axis load, fixed ends | $c = 7.5$ (Approx.) $\frac{1}{\sqrt{c}} = 0.365$ |
|  | Uniform column, axially loaded, one end fixed, one end free | $c = 0.25$ $\frac{1}{\sqrt{c}} = 2$ |  | Uniform column, distributed axis load, one end fixed, one end pinned | $c = 6.08$ $\frac{1}{\sqrt{c}} = 0.406$ |

$$P_{cr} = \frac{c \pi^2 EI}{L^2}$$

B.1.1.2 Crippling Stress

Compression in airframe members can be considered as instability problems and may be classified as:

- Column failure
- Local instability failure (usually referred to as crippling)

A perfect column is a member that is initially straight and has zero deflection up to a load P_{cr} at which point the member becomes unstable, as shown in Fig. B.2. In an airframe, the structural members are very seldom initially straight.

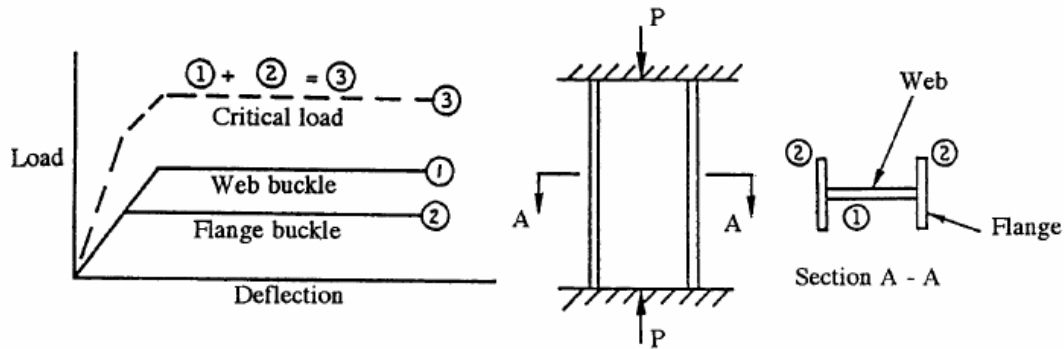


Figure B.2 *Deflection vs. Load* [22]

When a crippling failure, as shown in Fig. B.3, occurs on a formed section it appears as a local distortion. The more stable parts of the section continue to carry load and support the buckled parts until failure of the total section takes place. The initial buckling stress of the various elements of a section can be calculated, but the determination of the failing stress of the section is impossible to calculate mathematically.

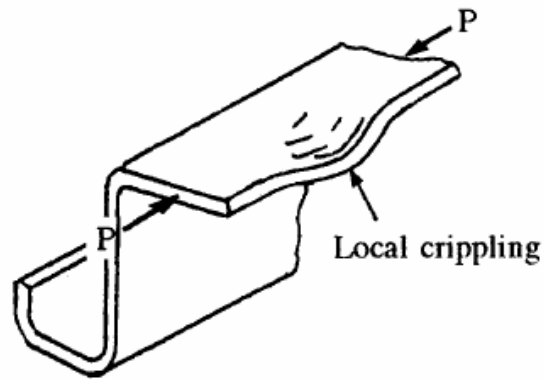


Figure B.3 *Flange Crippling* [22]

Compressive crippling also referred to as local buckling, is defined as an inelasticity of the cross section of a structural member in its own plane rather than, along its longitudinal axis, as in column buckling. The maximum crippling stress of a member is a function of its cross section rather than its length.

The crippling stress for a given section is calculated as if the stress were uniform over the entire section. In reality, the stress is not uniform over the entire section; parts of the section buckle at a stress below the crippling stress with the result that the more stable areas, such as intersections and corners, reach a higher stress than the buckled members as shown in Fig. B.4.

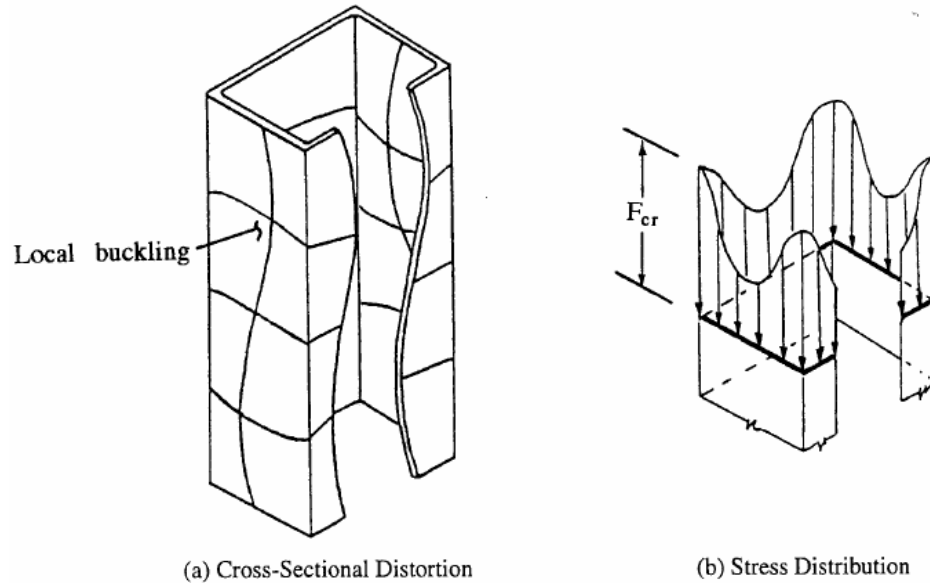


Figure B.4 *A Cross Section Subjected to Crippling Stress [22]*

Formed and extruded sections are analyzed in the same manner, although different values are used for each.

- (a) The section is broken down into individual segments, as shown in Fig. B.4, and each segment has a width 'b' and a thickness 't' and will have either one or no edge free.
- (b) The allowable crippling stress for each segment is found from the applicable material test curve of which can be selected from the typical curves shown in Fig. B.7 and Fig. B.8 for aluminum alloys that are commonly used in airframe structures.

The allowable crippling stress for the entire section is computed by taking a weighted average of the allowables for each segment:

$$F_{cc} = \frac{(b_1 t_1 F_{cc1} + b_2 t_2 F_{cc2} + \dots)}{(b_1 t_1 + b_2 t_2 + \dots)} \quad (B.6)$$

$$F_{cc} = \frac{\sum b_n t_n F_{ccn}}{\sum b_n t_n} \quad (B.7)$$

where: $b_1, b_2,$ - Lengths of the individual segments

$t_1, t_2,$ - Individual segment thicknesses

$F_{cc1}, F_{cc2},$ - Allowable crippling stresses of individual segments (see Fig. B.7 and Fig. B.8)

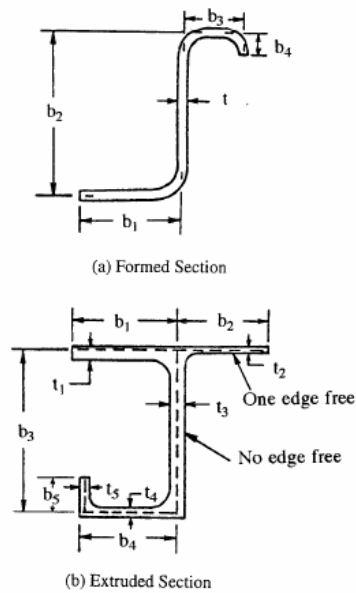


Figure B.5 *Formed vs. Extruded Sections* [22]

The following Fig. B.6 provides sufficient stability to adjacent formed flange segment of b_L .

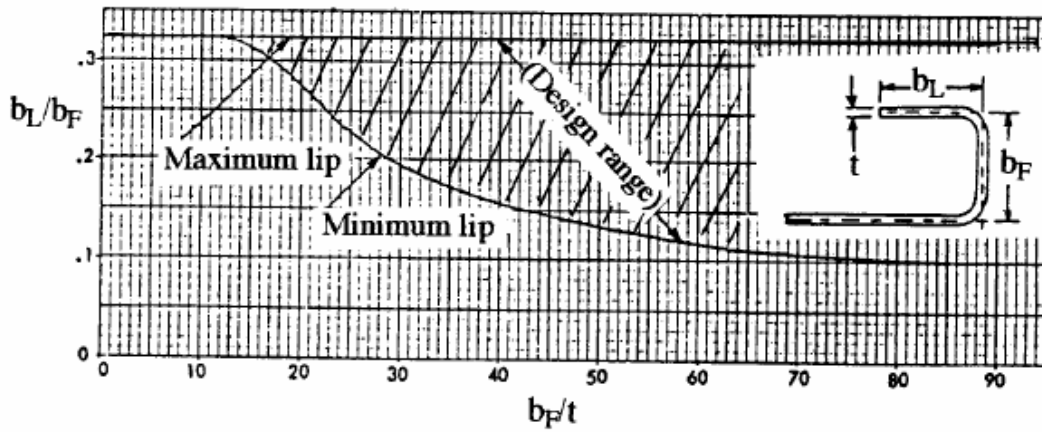


Figure B.6 Lip Criteria for Formed Sections [22]

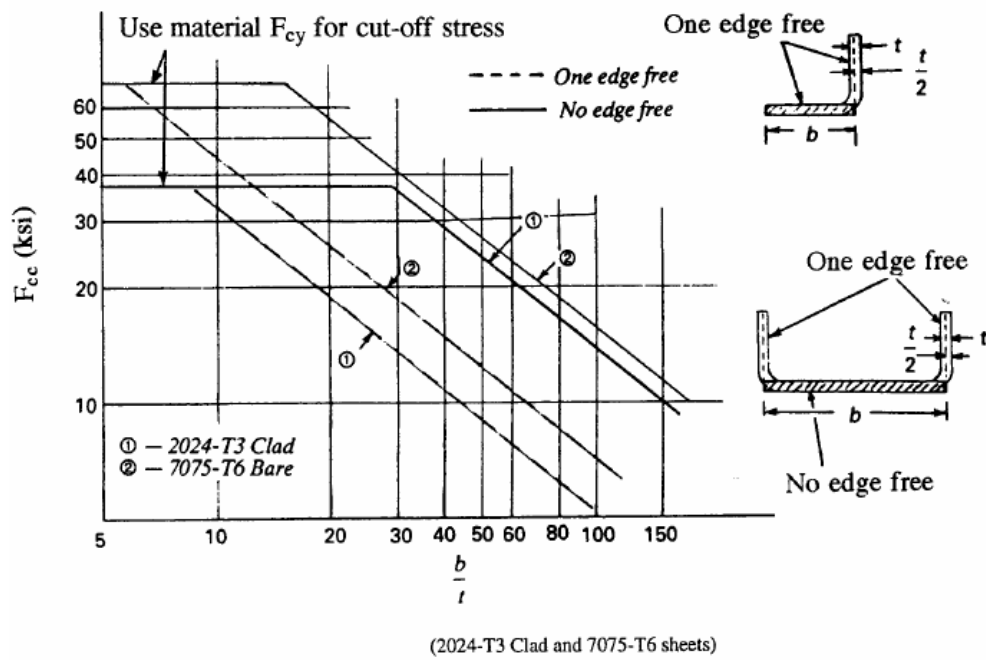
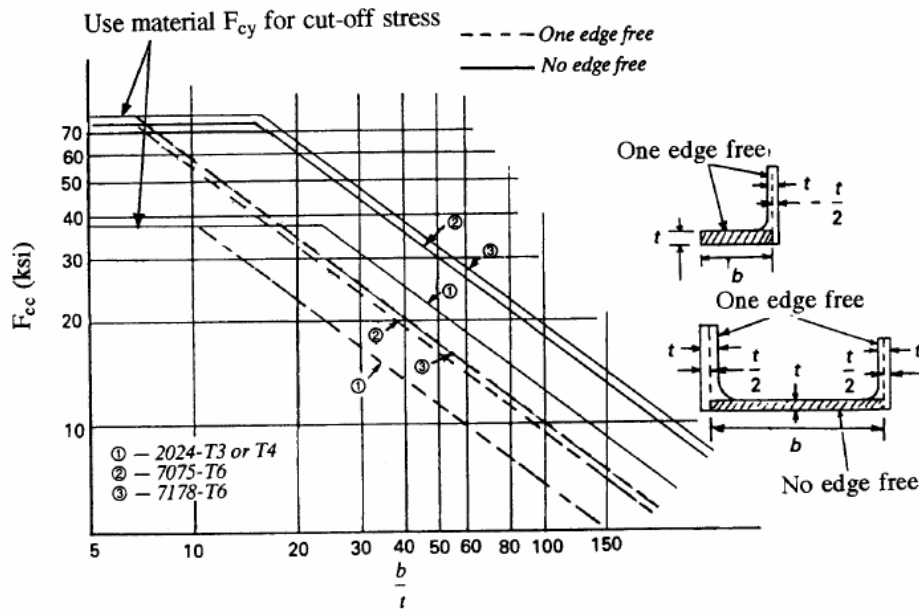


Figure B.7 Crippling Stress of Formed Sections [22]



(2024-T3511, T4, T42, T81 and 7075-T6511 extrusions)

Figure B.8 Crippling Stress of Extruded Sections [22]

B.2 Buckling of Thin Sheets

Skins, spar webs and rib webs utilized in the wing structure are thin walled plates. The stability of a plate supported on its edges and loaded by various types of in-plane loads has been solved for many types of boundary conditions. This chapter presents design data and curves for the determination of initial buckling stresses for flat and curved plates subjected to in-plane compression, shear, bending, and combinations of these stresses, for materials commonly used in airframe structures. It should be remembered that the practical skin-stringer panel constructions after the initial buckling of the plate would not take additional loads. Although the adjacent stringers will still withstand additional loads until the stringers reach their crippling stress.

The basic equation of plate buckling is derived from the Euler column equation, which is

$$F_{cr} = \frac{\Pi^2 E}{\left(\frac{L'}{\rho}\right)^2} \quad (B.8)$$

or

$$F_{cr} = \frac{c\Pi^2 EI}{AL^2} \quad (B.9)$$

The unit elongation (ϵ) of a flat plate loaded in two directions (x, y) is shown in Fig. 6.21

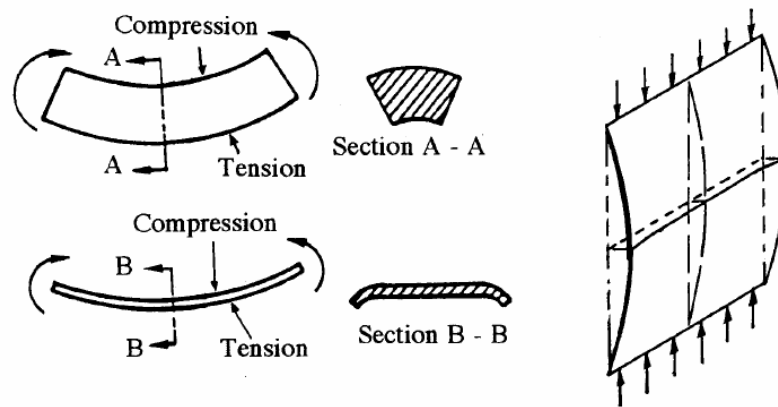


Figure B.9 *Effect of Poisson's Ratio on a Flat Plate* [22]

The strain in the y-direction due to the effect of Poisson's ratio (μ) is:

$$e_y = \left(\frac{f_y}{E} \right) - \mu \left(\frac{f_x}{E} \right) \quad (B.10)$$

The stress in x-direction is:

$$f_x = \mu f_y \quad (B.11)$$

So that the strain in y-direction becomes:

$$e_y = \left(\frac{f_y}{E} \right) - \mu^2 \left(\frac{f_y}{E} \right) \quad (B.12)$$

or

$$e_y = \frac{f_y(1 - \mu^2)}{E} \quad (B.13)$$

The Euler column equation of Eq. B.8 for flat plate becomes:

$$F_{cr} = \frac{c\Pi^2 EI}{(1 - \mu^2)(AL^2)} \quad (B.14)$$

Since the moment of inertia of a plate is $I = \frac{bt^3}{12}$ and plate area is $A = bt$, when these two values are substituted into the equation above it becomes:

$$F_{cr} = \frac{k\Pi^2 E}{12(1 - \mu^2)} \left(\frac{t}{L} \right)^2 \quad (B.15)$$

or

$$F_{cr} = KE \left(\frac{t}{L} \right)^2 \quad (B.16)$$

where: L - Plate length (parallel to the load direction)

E - Modulus of elasticity

k - Buckling coefficient

c - End-fixity coefficient

$$K = \frac{k\Pi^2}{12(1-\mu^2)} = 0.904k \quad (6.17)$$

Modified buckling coefficient for $\mu \sim 0.3$ (e.g., aluminum, steel alloys) [22]

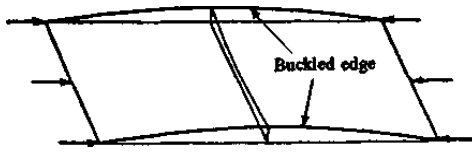
The two equations above are still the Euler equation, but they apply to a plate loaded as a column. For instance, a flat plate subjected to load on two ends which are hinged and the other two edges are free, as shown in Fig. B.9:

$K = 0.9$ approximately

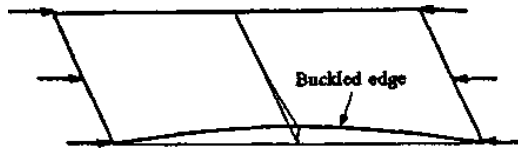
or $K = 0.82$ (without effect of Poisson's ratio)

When in-plane loads are applied to the edge of a flat plate, it will buckle at some critical load depending on the plate aspect ratio, plate thickness, and edge conditions, as shown in Fig. B.9:

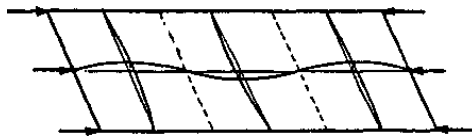
- Fig. B.9 (a) shows both that the unloaded side is free and that the plate acts as a column
- Fig. B.9 (b) shows that one unloaded side is free and the other side is restrained; this is referred to as a free flange
- Fig. B.9 (c) shows that both unloaded sides are restrained and this is referred to as a plate



(a) Column



(b) Free flange



(c) Plate

Figure B.10 *Plates with Various Edge Supports* [22]

Let the vertical edges of a flat plate be supported by vee grooves so that they can rotate but must remain straight lines, as shown in Fig. B.10. If the panel is to buckle, it must bend in two directions and the resistance to buckling is greatly increased; in fact, the panel will now sustain four times the load previously carried when no edge support was provided. The buckling equation for a square plate with hinged supports on all four edges is: [22]

$$F_{cr} = 3.62E \left(\frac{t}{L} \right)^2 \quad (B.18)$$

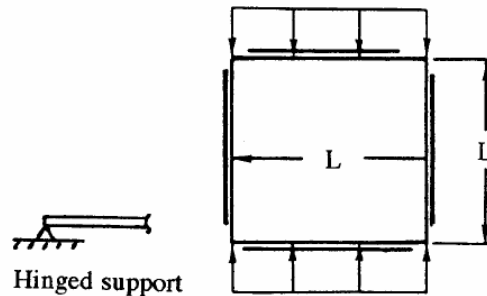


Figure B.11 *Square Plate with Hinged Support on Four Edges* [22]

When the plate is lengthened in the direction of loading (L), the principal restraint against buckling is the bending of the plate across the minimum panel dimension 'b'. Fig. B.11 shows the plate under in-plane compression loading buckles into three waves, each of them being square and acting in the same manner as the plate in Fig. B.10. [22]

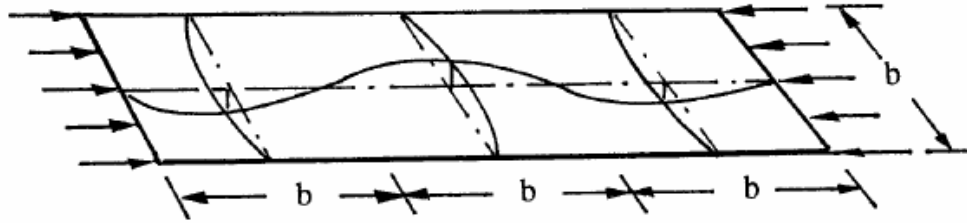


Figure B.12 *Long Rectangular Plate with Four Hinged Support Edges* [22]

B.2.1 Loading and Edge Conditions

It is seen that the minimum dimension or short side 'b' of the plate is the most important parameter in the buckling formula. The buckling equation for the rectangular plate shown in Fig. B.22 is:

$$F_{cr} = 3.62E \left(\frac{t}{b} \right)^2 \quad (B.15)$$

Therefore, the general buckling equation for both flat and curved plates is:

$$F_{cr} = \frac{k\eta_p \Pi^2 E}{12(1-\mu^2)} \left(\frac{t}{b} \right)^2 \quad (B.16)$$

or

$$F_{cr} = K\eta_p E \left(\frac{t}{b} \right)^2 \quad (B.17)$$

The buckling coefficients (k and K) depend upon:

(b) Plate size (aspect ratio)

(c) Edge restraint (free, hinged, fixed, or rotational restraints) is shown in Fig. B.25:

- Free edge (F) - Entirely free to deflect and rotate
- Hinged edge (H) - Simply supported (SS) where the plate cannot deflect, but can freely rotate
- Clamped edge (C) - Fixed support so that the plate cannot deflect or rotate
- Edge rotational restraint (ϵ) having a degree of restraint between that of a hinged edge and a fixed edge

(c) Type of loading (in-plane compression, shear, or bending)

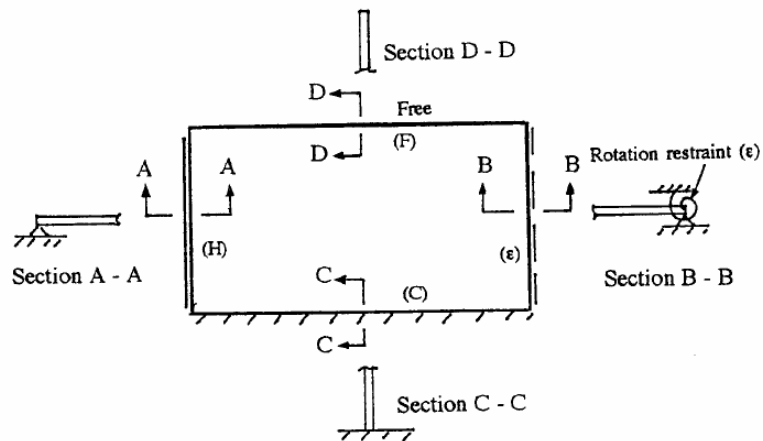


Figure B.13 *Rectangular Plate with Various Edge Supports* [22]

For Eq. B.16 and Eq. B.17, where t (thickness) and b (width or short side) are dimensions of the plate it is established that these are general formulas and are valid with the selection of the proper buckling coefficients:

- k_c or K_c - Compression load
- k_s or K_s - Shear load
- k_b or K_b - bending load
- η_p - plasticity reduction factor

B.2 Buckling of Flat Plates

B.2.1 Compression Load

The initial buckling stress for a flat plate under an in-plane compression load is:

$$F_{c,cr} = \frac{k_c \eta_c \Pi^2 E}{12(1 - \mu^2)} \left(\frac{t}{b} \right)^2 \quad (\text{B.18})$$

or

$$F_{c,cr} = K_c \eta_c E \left(\frac{t}{b} \right)^2 \quad (\text{B.19})$$

where: η_p - Plasticity reduction factor in compression load

Fig. B.13 shows flat plate buckling coefficients (K_c) for in-plane compression loads for Eq. B.19.

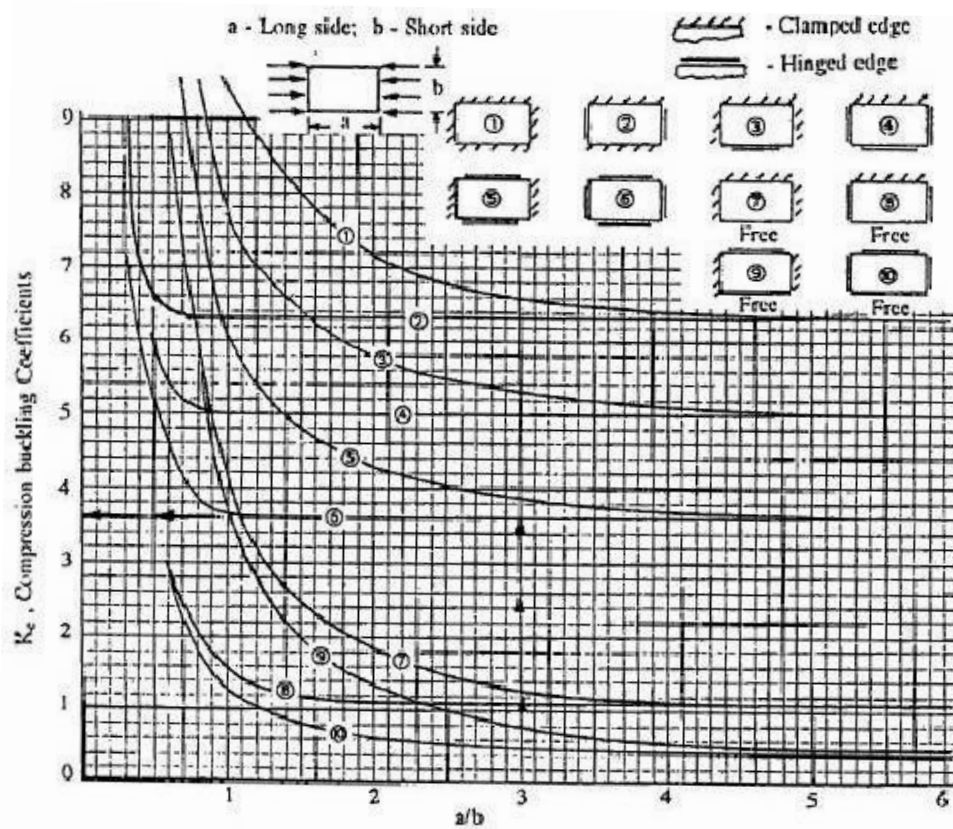


Figure B.14 K_c Coefficients (Compression) [22]

In this study, the edge conditions for flat panels such as skins, spar webs and rib webs are neither clamped nor simply supported conditions but a special edge rotational restraint, which is in between. Because these flat panels are riveted to the surrounding structure. Therefore, K_c coefficient is calculated for both clamped and simply supported edge conditions and the average of these two values is taken as K_c . [26]

Curves in Fig. B.13 is digitized using CurveExpert 1.3[®] software and a MMF model type curve is fitted for each curve. Related curve fit data and point coordinates can be found in Appendix A.

The equation of the fitted curve of K_c for clamped edge case is:

$$y = \frac{ab + cx^d}{b + x^d} \quad (B.20)$$

where; a=6.36 b=0.53 c=11.1 d=-3.16

The equation of the fitted curve of K_c for free edge case is:

$$y = \frac{ab + cx^d}{b + x^d} \quad (B.21)$$

where; a=3.58 b=28.15 c=7.56 d=-4.22

B.2.2 Shear Load

The initial buckling stress for a flat plate under in-plane shear load is

$$F_{s,cr} = \frac{k_s \eta_s \Pi^2 E}{12(1-\mu^2)} \left(\frac{t}{b}\right)^2 \quad (B.22)$$

or

$$F_{s,cr} = K_s \eta_s E \left(\frac{t}{b}\right)^2 \quad (B.23)$$

Fig. B.14 shows flat plate buckling coefficients (K_s) for in-plane shear.

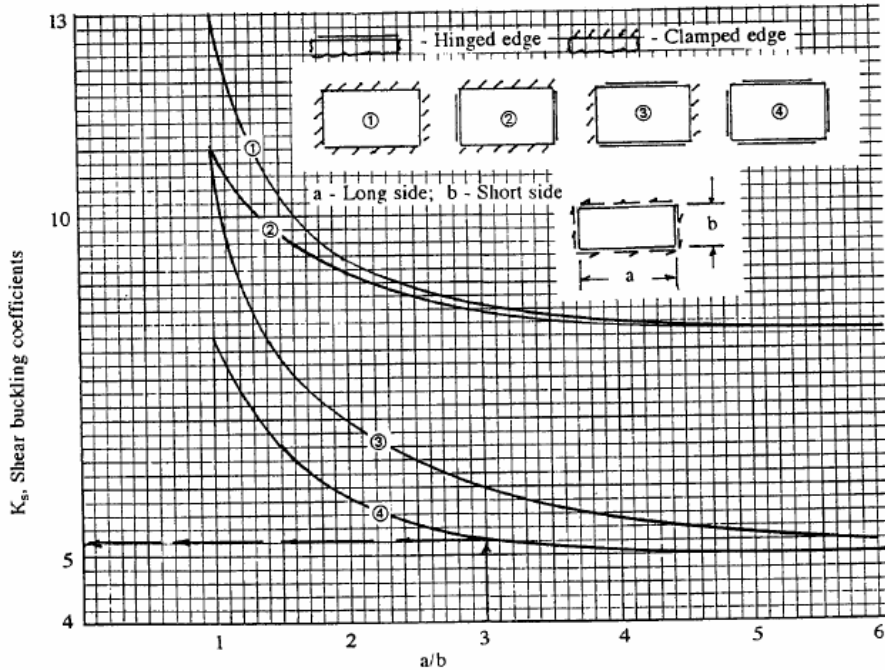


Figure B.15 K_s Coefficients (Shear) [22]

The equation of the fitted curve of K_s for clamped edge case is:

$$y = \frac{ab + cx^d}{b + x^d} \quad (B.24)$$

where; $a=8.19$ $b=5.21$ $c=37.65$ $d=2.26$

The equation of the fitted curve of K_s for free edge case is:

$$y = \frac{a + bx}{1 + cx + dx^2} \quad (B.25)$$

where; $a=10^9$ $b=5.46 \cdot 10^8$ $c=2 \cdot 10^8$ $d=-9.6 \cdot 10^6$

B.2.3 Bending Load

The initial buckling stress for a flat plate under in-plane bending load is

$$F_{b,cr} = \frac{k_b \eta_b \Pi^2 E}{12(1 - \mu^2)} \left(\frac{t}{b} \right)^2 \quad (B.26)$$

or

$$F_{b,cr} = K_b \eta_b E \left(\frac{t}{b} \right)^2 \quad (B.27)$$

Fig. B.15 shows flat plate buckling coefficients (K_s) for in-plane shear.

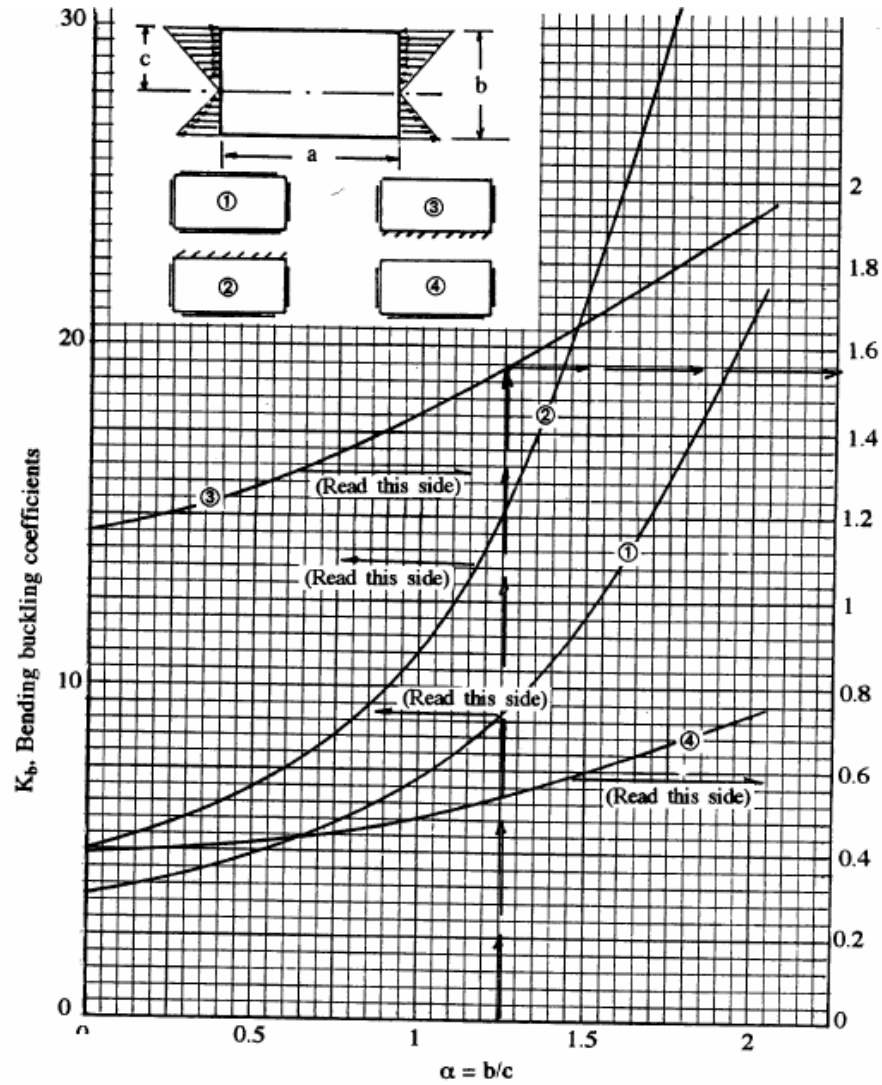


Figure B.16 K_b Coefficients (Bending) [22]

B.2.4 Combined Loadings

An example of the interaction curves of combinations of various types of loadings is shown in Fig. B.17. The more frequently used interaction curves are given in Fig. B.17 through Fig. B.18. Interaction curves for buckling conditions

can be constructed based on the stress ratio 'R', which is the ratio of the actual stress (f) to the allowable stress (F_{cr}):

$$R_c = \frac{f_c}{F_{c,cr}} \quad (B.28)$$

(compression stress ratio)

$$R_s = \frac{f_s}{F_{s,cr}} \quad (B.29)$$

(shear stress ratio)

$$R_b = \frac{f_b}{F_{b,cr}} \quad (B.30)$$

(bending stress ratio)

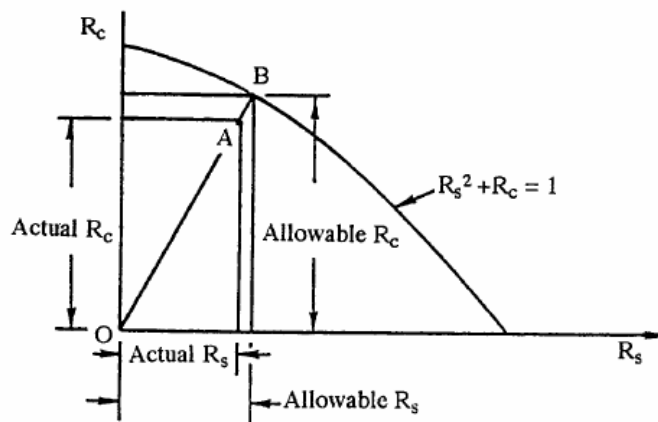


Figure B.17 Example of an Interaction Curve for Combined Compression (R_c) and Shear (R_s) Loadings [22]

The margin of safety for a combination of various buckling stresses can be determined using an interaction curve:

$$MS = \frac{O - B}{O - A} - 1 \quad (B.31)$$

Following interaction equations can be used when calculating critical buckling load under combined loading [22]

Table B.2 Interaction equations for shear, compression and bending loads

| Type of combined loadings | Equation | Fig. No |
|---------------------------|-----------------------|---------|
| Shear and compression | $R_s^2 + R_c = 1.0$ | B.30 |
| Shear and bending | $R_s^2 + R_b^2 = 1.0$ | B.31 |

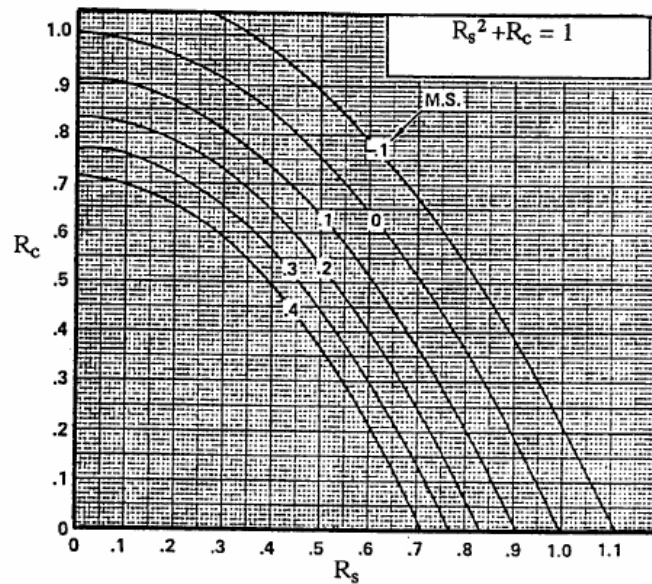


Figure B.18 Interaction Curves For Combined Shear and Compression loading ($R_s^2 + R_c = 1$) [22]

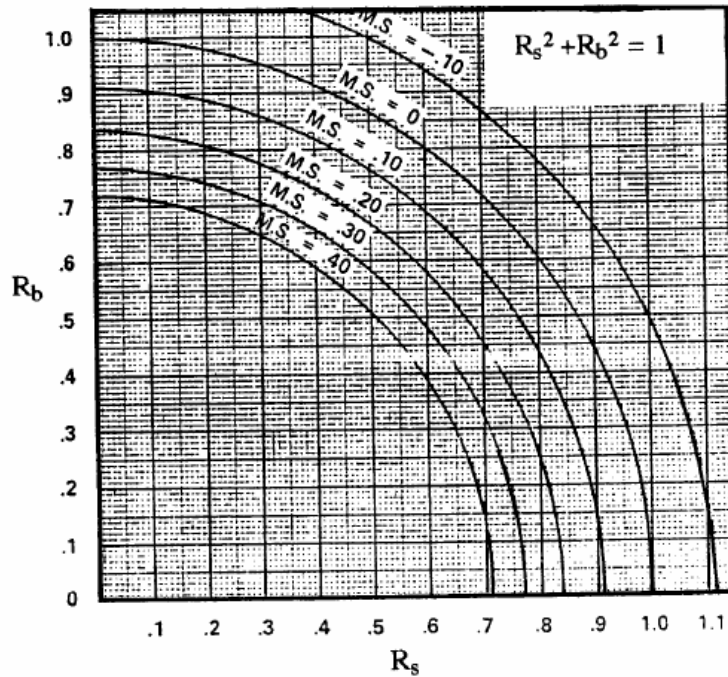


Figure B.19 *Interaction Curves For Combined Shear and Bending Loading*
[22]

B.3 Wing External & Inertial Loads

Aircraft loads are those forces and loadings applied to the airplane structural components to establish the strength level of the complete airplane. These loadings may be caused by air pressure, inertia forces, or ground reactions during landing. The determination of design loads involves a study of the air pressures and inertia forces during certain prescribed maneuvers, either in the air or on the ground. In normal straight and level flight, the wing lift supports the weight of the airplane. [22]

Limit loads are the maximum loads anticipated on the aircraft during its service life. The aircraft structure shall be capable of supporting the limit loads without suffering detrimental permanent deformation. For all loads up to "limit", the deformation of the structure shall be such as not to interfere with the safe operation of the aircraft.

Ultimate loads (or design loads) are equal to the limit loads multiplied by a factor of safety,

$$\text{Ultimate load} = \text{Limit load} \times \text{Factor of safety} [22]$$

In general, the ultimate factor of safety is 1.5. The requirements also specify that these ultimate loads be carried by the structure without failure.

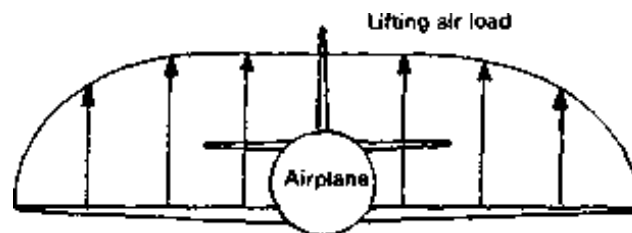


Figure B.20 *Airplane weight and lifting air loads* [22]

In the stress analysis of a conventional wing, it will be necessary to investigate each cross section for each of the four conditions shown in Fig. B.20. Each stringer or spar flange will then be designed for the maximum tension and the maximum compression obtained in any of the conditions.

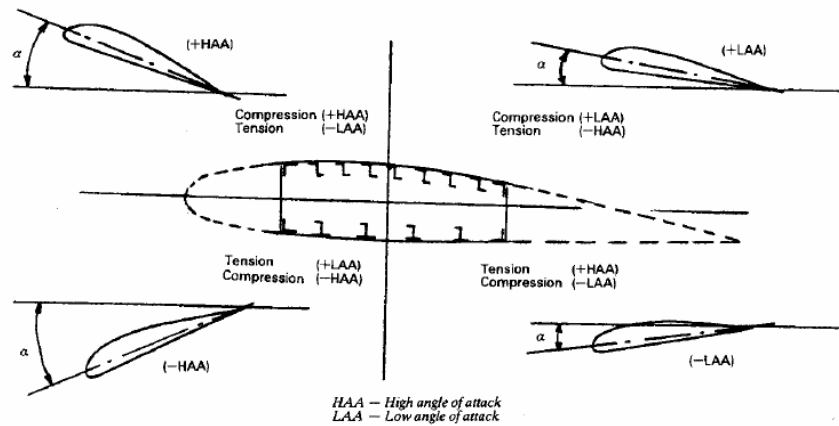


Figure B.21 *Critical conditions for wing box structure [22]*

B.3.1 Wing Design Loads

Design wing loads consist of the shears, bending moments, and torsions, which result from air pressures and inertia loadings. Flight loads are those experienced when maneuvering to the limits of the V-n diagram (Figure B.21) or those caused by gusts. Other flight conditions are those associated with control surface deflections. In addition, wing design loads must be determined for the landing and taxi conditions.

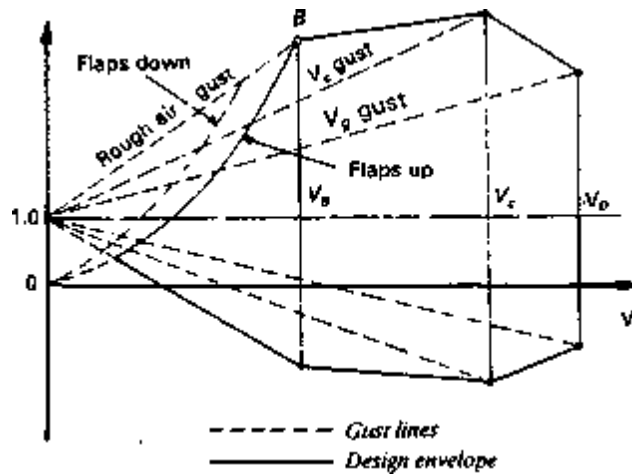


Figure B.22 *V-n Diagram (Gust Envelope)* [22]

Clean configuration: The air loading on a wing consists of two parts, additional loading and basic loading. The additional air loading is caused by angle of attack. On normal aspect ratio wings (> 3) this lift and its distribution varies directly with angle of attack. The basic loading is that distribution of air load on the wing when the total lift is zero. This type of loading is caused by wing twist. The lift load on a wing surface takes the form of a parabola as shown in Figure B.22. [22]

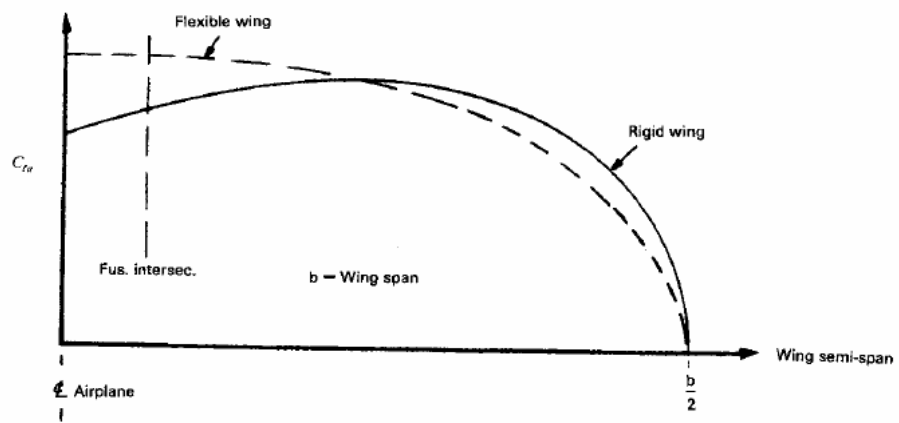


Figure B.23 *Wing additional lift distribution* [22]

APPENDIX C

FLOW CHARTS

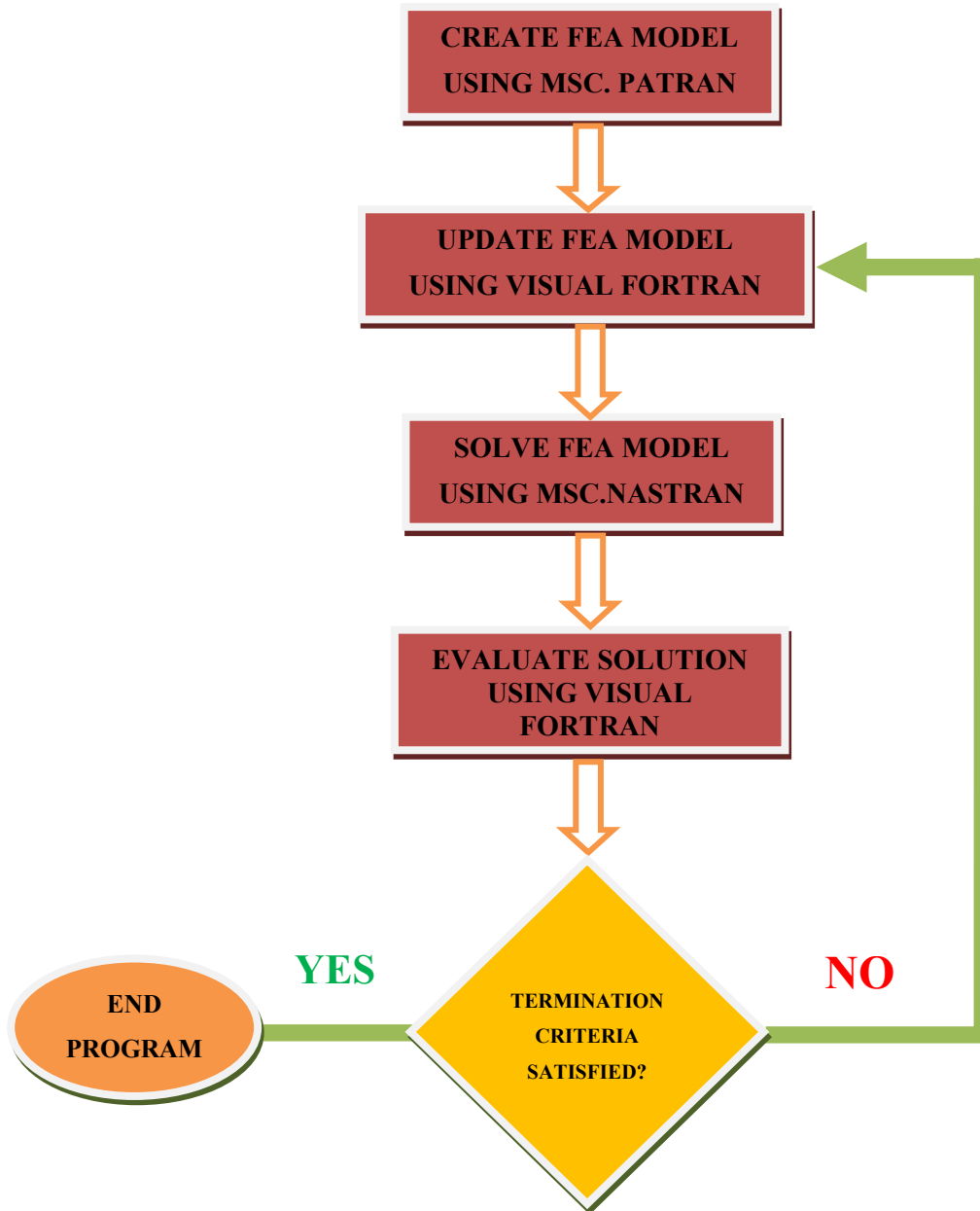


Figure C.1 Flow chart of interrelation of genetic algorithm and FEM building tools